

Contribution of mesoderm to the developing dental papilla

MICHAELA ROTHOVÁ^{1,2,3}, JIFAN FENG¹, PAUL T. SHARPE¹, RENATA PETERKOVÁ²
and ABIGAIL S. TUCKER^{*,1}

¹Department of Craniofacial Development and Orthodontics, King's College London, London, UK,
²Institute of Experimental Medicine, Academy of Sciences of the Czech Republic, v.v.i., Prague and
³Department of Cell Biology, Faculty of Science, Charles University, Prague, Czech Republic

ABSTRACT Teeth develop from epithelium and neural crest-derived mesenchyme via a series of reciprocal epithelial-mesenchymal interactions. The majority of the dental papilla of the tooth has been demonstrated to be of neural crest origin. However, non-neural crest cells have also been observed in this region from the bud stage of tooth development onwards. The number of these non-neural crest-derived cells rises as the dental papilla develops. However, their origin is unknown. We have followed migration of cells into the tooth *in vitro* using Dil to fate map regions surrounding the developing tooth. To identify the contribution of mesodermally-derived cells, we have utilised *Mesp1cre/R26R* transgenic reporter mice. We document that cells outside the early tooth primordium migrate into the developing dental papilla from the late cap stage of development. Here, we show that migrating cells are mesodermally-derived and create a network of endothelial cells, forming the blood vessels of the tooth. No cells of mesodermal origin were present in the condensed mesenchyme surrounding the dental epithelium until the cap stage of tooth development. Mesodermally-derived cells start invading the dental papilla at the late cap stage, providing the blood supply to the dental pulp. Endothelial cells are able to invade the developing dental papilla *in vitro* using the slice culture method. Understanding the origin and timing of migration of the mesodermally-derived cells is an important advance in our understanding of how a tooth develops and is particularly relevant to studies which aim to create bioengineered teeth.

KEY WORDS: tooth, dental papilla, *Mesp1cre*, mesoderm, endothelial cells

Introduction

Teeth develop from dental epithelium and neural crest-derived mesenchyme driven by reciprocal interactions. The dental epithelium invaginates into the surrounding dental mesenchyme to form a tooth bud. The dental epithelium starts to fold to produce a cap shape, with the mesenchymal dental papilla forming between the extending epithelial cervical loops. The dental papilla goes on to form the dental pulp at the centre of the tooth. The dental mesenchyme has been shown to be of neural crest cell origin, by using a *Wnt1cre/R26R* reporter mouse (Chai *et al.* 2000). However, these authors also reported the presence of some non-neural crest cells from the bud stage of tooth development onwards. As the tooth develops to the cap and bell stages, an

increasing number of non-neural crest cells were observed in the dental papilla. This dynamic distribution of neural crest cell-derived tissue was attributed to differential proliferation of non-neural crest derived cells and/or possible apoptosis of neural crest cells (Chai *et al.* 2000). The number of non-neural crest cells

Abbreviations used in this paper: E, embryonic day; IDE, inner dental epithelium; M1, first lower molar; *Mesp1cre/R26R*, Cre-recombinase expressed under the control of the *Mesp1* promoter as a transgene crossed with the ROSA26 conditional reporter (R26R); ODE, outer dental epithelium; P, postnatal; VEGF, vascular endothelial growth factor; *Wnt1cre/R26R*, cre-recombinase expressed under the control of the *Wnt1* promoter as a transgene crossed with the ROSA26 conditional reporter (R26R); X-Gal, β substrate (bromo-chloro-indolyl-galactopyranoside).

*Address correspondence to: Abigail S. Tucker, Dept. Craniofacial Development, King's College London, Floor 27, Guy's Tower, Guy's Hospital, London Bridge, SE1 9RT, London, UK. Tel: +44-207-1887384. Fax: +44-207-1881674. e-mail: Abigail.tucker@kcl.ac.uk - web: <http://www.kcl.ac.uk/schools/dentistry/research/cell/tucker>

Accepted: 23 June 2010. Final author corrected PDF published online: 21 January 2011

in the dental papilla can also increase as a result of immigration of cells. In support of this, when wild-type tooth germs were dissected at the cap stage and implanted into *LacZ* (β -galactosidase) or *GFP* (*Green Fluorescent Protein*) reporter host mice, an influx of host derived cells into the dental papilla was observed after a week to two weeks of development (Cho *et al.* 2003; Nait Lechguer *et al.* 2008).

During tooth development blood vessels and nerves move into the developing dental papilla (the prospective tooth pulp) to provide nutrients, oxygen and innervation. The non-neural crest derived cells in the early bell stage papilla might therefore represent endothelial or neuronal cell types. Nerves are found within the branchial (pharyngeal) arches at the earliest stages of tooth development but remain far from the tooth region itself (Mohamed and Atkinson 1983). At the cap stage a network of nerves forms under the tooth with fibres moving into the dental follicle which surrounds the tooth. Nerve fibres do not enter the papilla however, until cytodifferentiation is well underway, which for the first molar occurs a few days after birth (Mohamed and Atkinson 1983). The non-neural crest cells in the papilla at the bell stage are therefore unlikely to be due to the influx of neuronal cell types. Blood vessels, in contrast, are present in the papilla at a much earlier stage. In mouse embryo the endothelial cell markers are expressed in the central part of the future pulp from the early bell stage (E16.0) of the first lower molar (M1) (Nait Lechguer *et al.* 2008). There is thus a correlation between the expression of endothelial cell markers and the increase in non-neural crest cells in the papilla (Chai *et al.* 2000). It therefore seems likely that at least some of the non-neural crest derived cells in the dental papilla can be accounted for by an influx of endothelial cells.

In summary these data suggest that non-neural crest cells are present in the mouse dental mesenchyme at the bud stage (E13.5) and blood vessels are present in the dental papilla at the early bell stage (E16.0). However, it has not been proven whether the first capillary network rises *de novo* (vasculogenesis) or by an invasion of pre-existing capillaries (angiogenesis). We have therefore focused on the development of blood vessels in the dental tissue to verify the hypothesis that the cells of non-neural crest origin in the dental papilla are endothelial cells of mesodermal origin, which have migrated into the tooth.

The migration of cells into the dental papilla during tooth development was investigated using Dil to label the cells adjacent to the dental papilla *in vitro*. Previous studies have shown that no blood vessel-like structures could be detected in the dental pulp in tooth germs cultured *in vitro* (Nait Lechguer *et al.* 2008). This represents a serious problem for studying long-term tooth development *in vitro* as the health of the tooth germ is compromised. We therefore took advantage of the slice culture technique, in order to include the tissue that normally surrounds the tooth germ, thereby providing a more natural environment (Matalova *et al.* 2005; Cho *et al.* 2007; Diep *et al.* 2009).

To determine the nature of the non-neural crest cells in the dental papilla, we investigated the contribution of mesodermally-derived cells to the tooth using the *Mesp1cre/R26R* reporter mouse. *Mesp1* is an early marker of mesoderm expressed from the onset of gastrulation (Saga *et al.* 1996). The *Mesp1cre/R26R* mouse allows the contribution of cells of mesodermal origin to be followed at any stage of mouse development (Saga *et al.* 1999) and has previously been used to describe the contribution of

mesoderm to craniofacial development (McBratney-Owen *et al.* 2008; Yoshida *et al.* 2008). However, the contribution of mesodermally-derived cells to tooth development has not yet been described. Finally we investigated the identity of the mesodermally-derived cells using immunohistochemistry.

Results

Movement of cells into the dental papilla in vitro

Tissue slices have been shown to provide a good method of visualising tooth germs as they develop *in vitro* (Matalova *et al.* 2005; Cho *et al.* 2007; Diep *et al.* 2009) (Fig. 1 A,B). Here we show that this culture method also allows vascularisation of the developing dental papilla. For this we used 250 μ m slices of E14.5 mouse embryonic mandibles comprising the M1 tooth germ at the cap stage and cultured them for 4 days *in vitro*. To follow the blood vessel development during culture we used CD31 (PECAM-1) antibody as a specific endothelial marker (Newman *et al.* 1990). At the cap stage, the CD31 positive cells were present in the dental follicle surrounding the forming dental papilla (Fig. 1C). After 4 days in culture, the CD31 positive cells had entered the dental papilla, mimicking the expression observed *in vivo* (Fig. 1D) (Nait Lechguer *et al.* 2008).

To follow the fate of cells we labelled small groups of cells at the periphery of the condensed mesenchyme with a lipophilic dye – Dil (Diekwisch 2002; Diep *et al.* 2009) on the tissue slices as described above (Fig. 2A). No movement of the labelled cells into the dental papilla was observed over the first 24 hours in culture but after 2 to 3 days, as the tooth germ reached the late cap/early bell stage, Dil labelled cells were observed delaminating from the

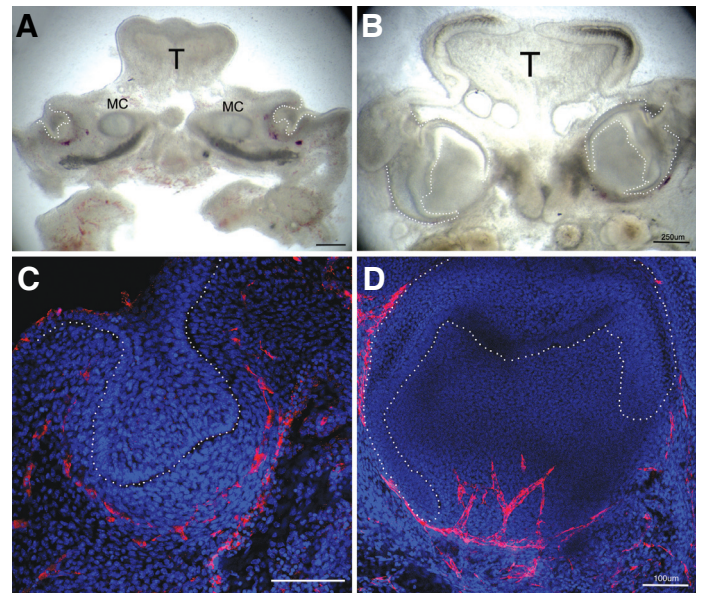


Fig. 1. Slice culture *in vitro* technique and the blood vessel invasion *in vitro*. (A) Slice of the E14.5 mouse mandible. (B) The same slice after 4 days *in vitro* culture. MC, Meckel cartilage; T, Tongue. (C,D) Sliced molar tooth germs. Nuclei stained in blue with Hoechst, CD31 positive cells in red. (C) E14.5. At this stage there are no CD31 positive endothelial cells in the forming dental papilla. (D) Molar tooth germ after 4 days *in vitro* culture. The CD31 positive cells have invaded the dental papilla. The dental epithelium is highlighted by the white dotted line.

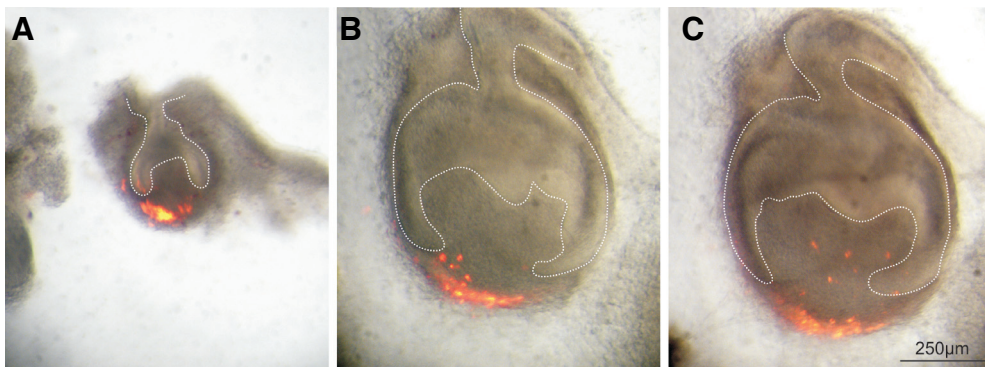


Fig. 2. Cell migration into the dental papilla. (A) E14.5 molar tooth germ. Cells at the periphery of the condensed mesenchyme labelled in red with Dil. (B) The same molar tooth germ after 3 days in vitro culture. A few Dil labelled cells have separated from the main Dil labelled region and have started to migrate towards the dental papilla. (C) The same molar tooth germ after 4 days in vitro culture. The separated Dil labelled cells have migrated further into the dental papilla. The dental epithelium is highlighted by the white dotted line.

main Dil labelled area (Fig. 2B). After 4 days in culture Dil labelled cells moved further into the developing dental papilla in a dispersed manner (Fig. 2C) (migration into dental papilla observed in N=48 cultures). This finding documents that some cells which contribute to the dental papilla at the bell stage are originally located in the periphery of the condensed dental mesenchyme at the cap stage.

Mesodermal cell contribution to the developing tooth

To analyze the origin of the Dil labelled cells migrating into the developing dental papilla *in vitro* we performed the same experiment as described above, using a *Mesp1cre/R26R* reporter mouse. The Dil labelled cells which invaded into the dental papilla overlapped with the X-Gal labelled mesodermally-derived cells (Fig. 3 A,B). On histological sections it is clear that the Dil labelled cells are linked to the mesodermally-derived cells, with the Dil label located along the blue labelled tracts of the mesodermally-derived tissue (Fig. 3 C,D).

To trace the mesodermal contribution to the tooth germ *in vivo* we looked at histological sections of the *Mesp1cre/R26R* reporter mouse during various stages of tooth development. At the bud to cap transition stage there were no cells of mesodermal origin in the forming dental papilla. Mesodermally-derived cells were however located in the dental follicle (i.e. in the condensed mesenchyme adjacent to the papilla and outer dental epithelium – ODE – of the enamel organ) and in surrounding tissue (Fig. 4A). A few hours later at E15.0, a few blue cells were observed in the dental papilla as the tooth germ progressed to the late cap stage (Fig. 4B). At the early bell stage (E 16.5) mesodermally-derived cells were noted not only throughout the dental follicle but also in the dental papilla, reaching up to the odontoblast layer (Fig. 4C). At postnatal stage (P)5 mesodermally-derived cells were found scattered throughout the dental pulp (Fig. 4D). At P18, when the first molars have started to erupt and roots are formed, the blue

stained mesodermally-derived cells marked out a crisscrossing network of cells in the dental pulp, with high concentrations located at the apex of the roots (Fig. 4E). Cells of mesodermal origin therefore enter the developing dental papilla at E15.0 and then spread throughout the forming dental pulp.

Endothelial cells in the developing tooth

The pattern of the mesodermally-derived cells at E14.5 and E16.5 (see Fig. 4 A,C) closely matched that of the endothelial cells labelled with the CD31 antibody (see Fig. 1 C,D and Fig. 5 A,B). In keeping with this, the *Mesp1cre/R26R* reporter has been shown to label endothelial cells which migrate throughout the head during development forming the blood vessel network (Yoshida *et al.* 2008). To confirm that the mesodermally-derived cells moving into the dental papilla were endothelial cells, CD31 immunohistochemistry was performed on *Mesp1cre/R26R* stained sections. A clear co-localisation of CD31 and mesodermally-derived cells was detected in the dental pulp (Fig. 5C), document-

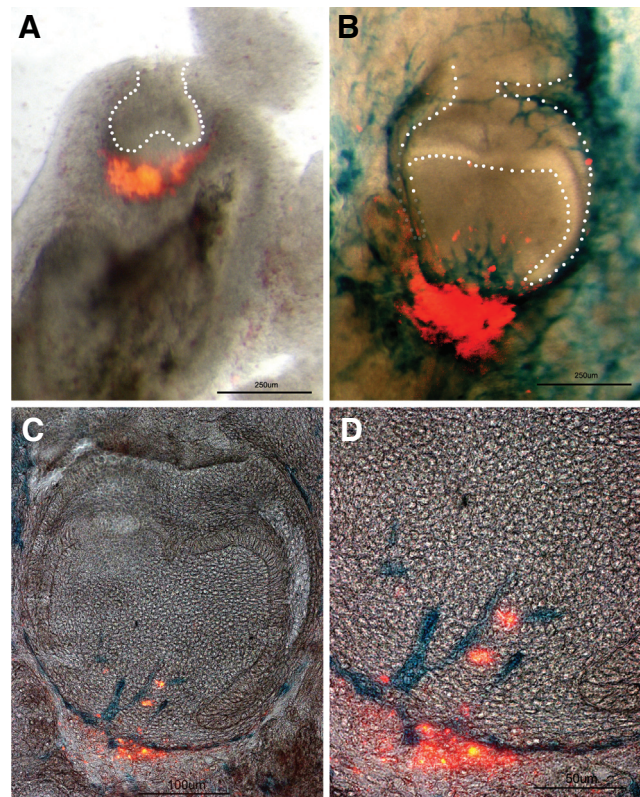


Fig. 3. Migration of mesodermally-derived cells into the dental papilla. (A) E14.5 molar tooth germ of *Mesp1cre/R26R* embryo. Cells at the periphery of the condensed mesenchyme labelled in red with Dil. (B) The same molar tooth germ after 4 days in culture and X-Gal staining. The Dil labelled cells (in red) entered the dental papilla. The mesodermally-derived cells are stained in blue with X-Gal. (C) Histological section of the same X-Gal stained molar tooth germ. Dil in red, mesodermally-derived cells in blue. (D) Higher magnification of the same molar tooth germ showing the Dil labelled cells linked to the blue mesodermally-derived cells in the dental papilla. The dental epithelium is highlighted by the white dotted line.

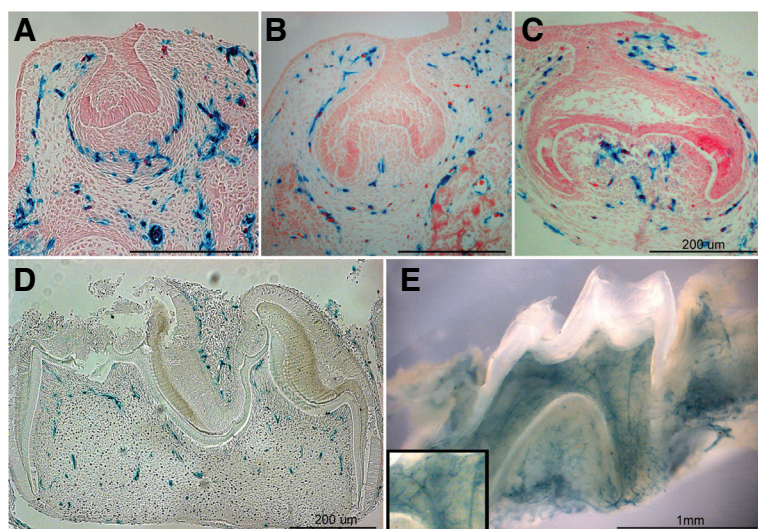


Fig. 4. Contribution of mesodermally-derived cells to molar development. The mesodermally-derived cells are stained with X-gal in blue. (A) Frontal section of molar tooth germ of E14.5 *Mesp1cre/R26R* embryo. There are no cells of mesodermal origin present in the dental epithelium or the adjacent condensed mesenchyme. (B) Frontal section of molar tooth germ of E15.0 *Mesp1cre/R26R* embryo. Single mesodermally-derived cells are found in the tooth papilla. (C) Frontal section of molar tooth germ of E16.5 *Mesp1cre/R26R* embryo. The mesodermally-derived cells are present in the dental papilla and the forming dental follicle. (D) Sagittal section of the first molar of *Mesp1cre/R26R* mouse at P5. (E) Sagittal view of the first molar of *Mesp1cre/R26R* mouse at P18, showing large numbers of mesodermally-derived cells in the dental pulp and at the roots with closer look at the capillary network in the frame.

ing the immigration of endothelial cells of mesodermal origin into the dental papilla.

Discussion

By culturing the *Mesp1cre/R26R* tooth germs in slice culture we have shown that mesodermally-derived blood vessels were able to successfully invade the dental papilla *in vitro*. This finding is in contrast to the lack of blood vessel invasion observed in isolated tooth germs after *in vitro* culture (Nait Lechguer *et al.* 2008). The difference between these two *in vitro* culture methods probably lies in the amount of tissue left surrounding the tooth germ, which is a prerequisite for the blood capillaries to invade the

dental papilla. This is supported by the fact that well-formed blood vessels invaded the papilla of dissected tooth germs after subcutaneous implantation, where the implanted tooth germ is surrounded by the host connective tissue rich in blood vessels (Nait Lechguer *et al.* 2008). These differences also suggest that the blood vessels in the dental papilla originate by angiogenesis (generation of vessels by sprouting from pre-existing capillaries) rather than vasculogenesis (de novo formation of a vascular network from endothelial precursors) (reviewed in Byrd and Grabel 2004).

The majority of the mesodermally-derived cells appear to be CD31 positive endothelial cells which move into the tooth to provide the blood supply. Endothelial cells have been shown to be a highly invasive cell population throughout the head (Yoshida *et al.* 2008). During the bell stage of tooth development, the endothelial cells rapidly colonise the dental papilla reaching up to the odontoblast layer. The close relationship between the odontoblasts and peripheral capillaries of the tooth has been related to the secretory activity of the odontoblasts (Yoshida and Ohshima 1996).

At the early cap stage a network of mesodermally-derived endothelial cells sits adjacent to the dental papilla but does not enter the papilla until the late cap stage. What controls the movement of the endothelial cells into the papilla? Blood vessels growth is regulated by the Vascular Endothelial Growth Factor (VEGF) (Mustonen and Alitalo 1995). Interestingly, one of the receptors for VEGF is Neuropilin, which was first discovered as a receptor for the semaphorin family of axon guidance molecules (reviewed in Geretti *et al.* 2008). Semaphorin-3a is expressed in the dental mesenchyme and has been shown to have a repulsive role: by defining where axons can migrate in the tooth by inhibiting axon growth into the regions where the sema3a is expressed (Loes *et al.* 2001). Semaphorin members may therefore act as guidance cues for both nerves and blood vessels. Other molecular cascades involved in angiogenesis include Notch and Hedgehog signalling which can target endothelial cells directly or can stimulate blood vessel support cells to produce VEGFs. For example, addition of Sonic hedgehog promotes expression of VEGF ligands (reviewed in Byrd and Grabel 2004). In the developing tooth, low levels of VEGF have been observed in the epithelium and dental papilla at the cap stage, with levels increasing in the inner dental

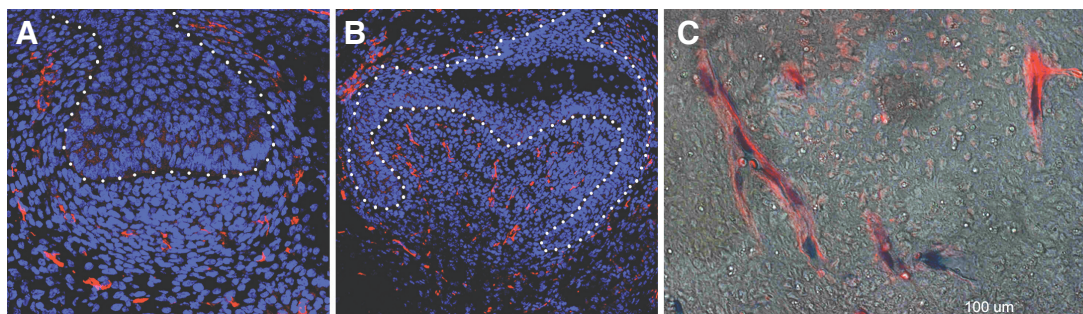


Fig. 5. Endothelial cells in the dental papilla. (A,B) Frontal section of WT embryo at (A) E14.5 (B) E16.5. CD31 positive endothelial cells are stained in red, nuclei with DAPI in blue. The CD31 pattern corresponds with the *Mesp1-Cre/R26R* X-gal stained molar tooth germ shown in Fig. 4. (C) CD31 staining on *Mesp1-Cre/R26R* X-gal stained sections of molar tooth germ at P5. CD31 positive endothelial cells are stained in red and are co-localized with X-gal stained blue mesodermally-derived cells.

epithelium (IDE) at the bell stage (Aida *et al.* 2005). The increase in VEGF level coincides with the movement of endothelial cells into the papilla, and may play a stimulating role. The molecular mechanisms regulating blood vessels entering the dental papilla is an important question for future studies.

In conclusion, the increase of non-neural crest derived cells in the dental papilla during development is caused by the immigration of mesodermally-derived endothelial cells, which start to infiltrate the dental papilla at E15.0. No mesodermally-derived cells are present in the condensed mesenchyme before this time point. Our findings open an interesting question regarding the origin of the non-neural crest cells found at earlier stages of tooth development (Chai *et al.* 2000). From the *Wnt1cre/R26R* and *Mesp1cre/R26R* analysis these cells appear to be neither of neural crest nor of mesodermal origin. Thus either some other cell population contributes to the tooth mesenchyme at these early stages, or perhaps not all mesodermally or neural crest derived cells are labelled by the above-mentioned reporters.

Vascularisation of the tooth is an important process to ensure gas and metabolite exchange and therefore good vascularisation is an essential step for any attempts to bioengineer teeth (Nait Lechguer *et al.* 2008). Our study shows that migration of cells that will form the blood network of the tooth occurs relatively early during tooth development. Importantly blood vessel invasion can occur *in vitro* if the tissue surrounding the tooth germ is included in the explant. Knowledge of the timing and position of blood vessel precursors has a bearing on the health of tooth explants and the timing of implantation of bioengineered tooth germs. Our study also indicates that the *Mesp1cre/R26R* mice line could be an important tool in analysing the success of vascularisation in such studies.

Material and Methods

CD1 mice, *Mesp1cre/R26R* mice

All animals were killed using a schedule 1 method as approved by the Home Office and King's College London. The females were mated overnight and noon after the detection of the vaginal plug was considered as embryonic day (E) 0.5. For *in vitro* experiments and cryo-sections CD1 mice were used. The *Mesp1cre* heterozygous male was mated with homozygous *Rosa26R* female to generate the reporter line (Saga *et al.* 1999). Positive embryos were selected using a quick X-gal staining procedure on the embryonic bodies (20 minutes in X-Gal solution at 37°C).

Slice culture

E14.5 mouse mandibles of CD1 embryos were dissected out and sliced using a McIlwain tissue chopper (Mickle Laboratory Engineering Co., Ltd. UK) into frontal slices 250 µm thick (Matalova *et al.* 2005; Diep *et al.* 2009). Slices showing a clear molar tooth cap were then selected and cultured. Slices were cultured on transparent nucleopore filters (VWR) supported on metal grids over medium. Medium consisted of DMEM F12 (Invitrogen) supplemented with 1% penicillin/streptomycin and 1% Glutamax (Invitrogen) and 10% fetal calf serum. Matrigel basement membrane matrix (7 µl) (BD Biosciences) was added on top of the slice. Slices were cultured at 37°C / 5% CO₂ for 4-5 days.

Dil Labeling

Dil is a lipophilic dye, which intercalates in the cell membrane, marking groups of cells. Dil (Molecular probes cell tracker CM-Dil, C-7000) was dissolved in 100% EtOH. Small amounts of Dil were injected into the

slices before culture using a mouth pipette (Diep *et al.* 2009). The slices were then placed on filters and cultured. The position of the Dil was recorded using fluorescent Leica dissecting microscope every 24 hours.

X-Gal staining

Mesp1-Cre/R26R positive embryo heads were dissected to remove the lower jaws at a range of stages (E14.5, E15.0, E16.5). Excess tissue was removed prior to staining. At postnatal stages (P5 and P18) it was necessary to remove the bone and the P18 molar was cut in half to allow the X-Gal staining solution to penetrate. The tooth germs were fixed in 4% PFA for 45 minutes, washed in PBS and stained in X-Gal staining solution for 42 hours at 37°C. The tooth germs were then post-fixed in 4% PFA O/N and then processed through a methanol series, isopropanol and tetrahydro-naphthalene to wax. Then the tooth germs were sectioned for 10 µm thickness for frontal and sagittal sections.

Immuno-fluorescent staining

For embryonic stages, the immuno-staining of CD31 antibody was performed on 10 µm thick frozen sections. The heads were dissected from CD1 mouse embryos at E14.5 and E16.5 and frozen immediately in O.C.T. Tissue Tek (Sakura) diluted 1:1 with Hank's balanced solution (Sigma). Frozen sections were post-fixed in 4% PFA and processed by a Citric acid epitope retrieval method (boil in 10 mM citric acid pH 6.5). The sections were then incubated at 4°C O/N with primary antibody CD31 (Rabbit polyclonal IgG to CD31, Abcam, #Ab28364) diluted 1:150 in 1% BSA. The secondary antibody (Alexa Fluor® 568 goat anti-rabbit IgG, Invitrogen, #A11036) was diluted 1:500 in 1% BSA and incubated at RT for 1 hour. Nuclei were stained with Prolong® Gold anti-fade reagent with DAPI (Invitrogen).

For the postnatal stage P5, the *Mesp1cre/R26R* molars were embedded into wax and then sectioned for 5 µm thickness. The same staining protocol as described for frozen sections was then performed.

The slices of CD1 mandibles were fixed in 4% PFA 3 hours at RT prior or after the *in vitro* culture, blocked in 10% goat serum in 0.1% Tween20 (Sigma) O/N. The slices were then incubated with CD31 primary antibody (1:150 in 1%BSA) for 6 hours, with the Alexa Fluor 568 (1:300 in 1%BSA) secondary antibody O/N and then stained with Hoechst (Sigma #H6024) for 4 hours. The images were taken using Leica SP5 confocal microscope.

Acknowledgements

We thank Karen Liu and Albert Basson for the *Mesp1cre* and *Rosa26R* mice. Michaela Rothova and Renata Peterkova are funded by the Grant Agency of the Czech republic (grant CZ:GACR:GA304/07/0223) and by ÚEM AV CR - AV0Z50390512, AV0Z50390703.

Michaela Rothova performed this work during an Erasmus exchange programme with King's College London. Abigail Tucker is funded by a Royal Society international joint grant with the Czech Republic (RS 2009/R1).

References

- AIDA M, IRIÉ T, AIDA T and TACHIKAWA T (2005). Expression of protein kinases C beta1, beta11, and VEGF during the differentiation of enamel epithelium in tooth development. *J Dent Res* 84(3): 234-239.
- BYRD N, GRABEL L (2004). Hedgehog signaling in murine vasculogenesis and angiogenesis. *Trends Cardiovasc Med* 14(8): 308-313.
- CHAI Y, JIANG X, ITO Y, BRINGAS P JR, HAN J, ROWITCH DH, SORIANO P, MCMAHON AP and SUCOV HM (2000). Fate of the mammalian cranial neural crest during tooth and mandibular morphogenesis. *Development* 127(8): 1671-1679.
- CHO SW, HWANG HJ, KIM JY, SONG WC, SONG SJ, YAMAMOTO H and JUNG HS (2003). Lineage of non-cranial neural crest cell in the dental mesenchyme: using a lacZ reporter gene during early tooth development. *J Electron Microsc*

- (Tokyo) 52(6): 567-571.
- CHO SW, LEE HA, CA J, LEE MJ, KIM JY, OHSHIMA H and JUNG HS (2007). The primary enamel knot determines the position of the first buccal cusp in developing mice molars. *Differentiation* 75: 441-451.
- DIEP L, MATALOVA E, MITSIADIS TA and TUCKER AS (2009). Contribution of the tooth bud mesenchyme to alveolar bone. *J Exp Zool B Mol Dev Evol* 312B(5): 510-517.
- DIEKWISCH TGH (2002). Pathways and fate of migratory cells during late tooth organogenesis. *Connect Tissue Res* 43: 245-256.
- GERETTI E, SHIMIZU A and KLAGSBRUN M (2008). Neuropilin structure governs VEGF and semaphorin binding and regulates angiogenesis. *Angiogenesis* 11: 31-39.
- LOES S, KETTUNEN P, KVINNSLAND IH, TANIGUCHI M, FUJISAWA H and LUUKKO K (2001). Expression of class 3 semaphorins and neuropilin receptors in the developing mouse tooth. *Mech Dev* 101: 191-194.
- MATALOVA E, ANTONARAKIS GS, SHARPE PT and TUCKER AS (2005). Cell lineage of primary and secondary enamel knots. *Dev Dynamics* 233: 754-759.
- MCBRATNEY-OWEN B, ISEKI S, BAMFORTH SD, OLSEN BR and MORRIS-KAY GM (2008). Development and tissue origins of the mammalian cranial base. *Dev Biol* 322: 121-132.
- MOHAMED SS, ATKINSON ME (1983). A histological study of the innervation of developing mouse teeth. *J Anat* 136: 735-749.
- MUSTONEN T, ALITALO K (1995). Endothelial receptor tyrosine kinases involved in angiogenesis. *J Cell Biol* 129: 895-898.
- NAIT LECHGUER A, KUCLER-BOPP S, HU B, HAIKEL Y and LESOT H (2008). Vascularization of engineered teeth. *J Dent Res* 87(12): 1138-1143.
- NEWMAN PJ, BERNDT MC, GORSKI J, WHITE GC 2ND, LYMAN S, PADDOCK C and MULLER WA (1990). PECAM-1 (CD31) cloning and relation to adhesion molecules of the immunoglobulin gene superfamily. *Science* 247(4947): 1219-1222.
- SAGA Y, HATA N, KOBAYASHI S, MAGNUSON T, SELDIN MF and TAKETO MM (1996). MesP1: a novel basic helix-loop-helix protein expressed in the nascent mesodermal cells during mouse gastrulation. *Development* 122: 2769-2778.
- SAGA Y, MIYAGAWA-TOMITA S, TAKAGI A, KITAJIMA S, MIYAZAKI J and INOUE T (1999). Mesp1 is expressed in the heart precursor cells and required for the formation of a single heart tube. *Development* 126: 3437-3447.
- YOSHIDA S, OHSHIMA H (1996). Distribution and organization of peripheral capillaries in dental pulp and their relationship to odontoblasts. *Anat Rec* 245: 313-326.
- YOSHIDA T, VIVATBUTSIRI P, MORRIS-KAY G, SAGA Y and ISEKI S (2008). Cell lineage in mammalian craniofacial mesenchyme. *Mech Dev* 125: 797-808.

Further Related Reading, published previously in the *Int. J. Dev. Biol.*

See our recent Special Issue **Placenta** edited by Joan S. Hunt and Kent L. Thornburg at:
<http://www.ijdb.ehu.es/web/contents.php?vol=54&issue=2-3>

Coexpression of Notch3 and Rgs5 in the pericyte-vascular smooth muscle cell axis in response to pulp injury

Henrik Lovschall, Thimios A. Mitsiadis, Knud Poulsen, Kristina H. Jensen and Annette L. Kjeldsen
Int. J. Dev. Biol. (2007) 51: 715-721

Formation of a successional dental lamina in the zebrafish (*Danio rerio*): support for a local control of replacement tooth initiation

Ann Huisseune
Int. J. Dev. Biol. (2006) 50: 637-643

BMP signalling in craniofacial development

Xuguang Nie, Keijo Luukko and Paivi Kettunen
Int. J. Dev. Biol. (2006) 50: 511-521

Molar tooth development in caspase-3 deficient mice

Eva Matalova, Paul T. Sharpe, Saquib A. Lakhani, Kevin A. Roth, Richard A. Flavell, Jana Setkova, Ivan Misek and Abigail S. Tucker
Int. J. Dev. Biol. (2006) 50: 491-497

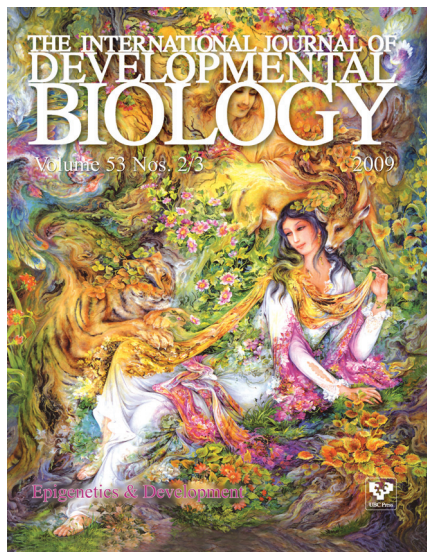
Detection of differentially expressed genes in the early developmental stage of the mouse mandible

H Yamaza, K Matsuo, T Kiyoshima, N Shigemura, I Kobayashi, H Wada, A Akamime and H Sakai
Int. J. Dev. Biol. (2001) 45: 675-680

A mouse mandibular culture model permits the study of neural crest cell migration and tooth development

Y Chai, P Bringas, C Shuler, E Devaney, R Grosschedl and H C Slavkin
Int. J. Dev. Biol. (1998) 42: 87-94

5 yr ISI Impact Factor (2008) = 3.271



Patterning by heritage in mouse molar row development

Jan Prochazka^{a,b,1,2}, Sophie Pantalacci^{c,1}, Svatava Churava^{a,d}, Michaela Rothova^{a,b}, Anne Lambert^c, Hervé Lesot^e, Ophir Klein^f, Miroslav Peterka^{a,d}, Vincent Laudet^c, and Renata Peterkova^a

^aInstitute of Experimental Medicine, Academy of Sciences of the Czech Republic, 142 20 Prague, Czech Republic; ^bDepartment of Cell Biology, Faculty of Science, Charles University, CZ 128 00 Prague, Czech Republic; ^cDepartment of Anthropology and Human Genetics, Faculty of Science, Charles University, CZ 128 43 Prague, Czech Republic; ^dInstitut de Génomique Fonctionnelle de Lyon, Université de Lyon, Centre National de la Recherche Scientifique, Institut National de la Recherche Agronomique, F 69394 Lyon Cedex 07, France; ^eInstitut National de la Santé et de la Recherche Médicale and Dental School, University of Strasbourg, F 67085 Strasbourg, France; and ^fProgram in Craniofacial and Mesenchymal Biology, Departments of Orofacial Sciences and Pediatrics, Institute of Human Genetics, University of California, San Francisco, CA 94143-0442

Edited* by Nicole M. Le Douarin, Centre National de la Recherche Scientifique, Gif-sur-Yvette, France, and approved July 22, 2010 (received for review March 17, 2010)

It is known from paleontology studies that two premolars have been lost during mouse evolution. During mouse mandible development, two bud-like structures transiently form that may represent rudimentary precursors of the lost premolars. However, the interpretation of these structures and their significance for mouse molar development are highly controversial because of a lack of molecular data. Here, we searched for typical tooth signaling centers in these two bud-like structures, and followed their fate using molecular markers, 3D reconstructions, and lineage tracing *in vitro*. Transient signaling centers were indeed found to be located at the tips of both the anterior and posterior rudimentary buds. These centers expressed a similar set of molecular markers as the “primary enamel knot” (pEK), the signaling center of the first molar (M1). These two transient signaling centers were sequentially patterned before and anterior to the M1 pEK. We also determined the dynamics of the M1 pEK, which, slightly later during development, spread up to the field formerly occupied by the posterior transient signaling center. It can be concluded that two rudimentary tooth buds initiate the sequential development of the mouse molars and these have previously been mistaken for early stages of M1 development. Although neither rudiment progresses to form an adult tooth, the posterior one merges with the adjacent M1, which may explain the anterior enlargement of the M1 during mouse family evolution. This study highlights how rudiments of lost structures can stay integrated and participate in morphogenesis of functional organs and help in understanding their evolution, as Darwin suspected long ago.

rudiment | signaling center | tooth evolution | SHH | molar development

Adult vestiges and embryonic rudiments are defined as traces of ancestral structures lost during evolution (1, 2). These evolutionary remnants are present in many species, including humans, and have fascinated scientists since Aristotle and have been at the heart of evolutionary thought since Darwin (3), who first suggested that they can help to reveal ancestry. These residual structures may represent key intermediates in morphological innovation (2). Indeed, once a body part loses functionality following a change in lifestyle, it will degenerate in a neutral manner, and this neutral evolution makes it prone to assume new functions. To our knowledge, however, very few examples have been described yet (1, 4).

If they are not identified, rudiments can obscure the developmental studies of prospective functional structures. However, consideration of the evolutionary history of species can help to draw attention to the possible presence of rudiments. For example, mouse dentition is strongly reduced compared with other mammals. In each jaw quadrant, one incisor is separated from three molars by a gap (diastema), where incisor, canine, and premolar teeth are present in other species (Fig. 1A). The common ancestor of lagomorphs (e.g., rabbits) and early rodents in the mouse lineage had premolars, and these were maintained in some extant rodent or lagomorph families (Fig. 1C and D), where they

develop earlier than and anterior to molars (5). Despite the lack of premolars in the adult mouse, there is morphological evidence for bud-like structures that develop earlier than and anterior to the upper and lower first molar (M1), and which have been interpreted as rudimentary (vestigial) premolar buds (6, 7). In the lower jaw these buds (called MS and R2) develop transiently at embryonic day (ED) 12 and 13, respectively, and then they regress (Fig. 1E). The M1 becomes a distinct structure posteriorly by day 14, and the R2 is thought to be integrated into it (8, 9).

However, the existence of the two premolar rudimentary buds has been poorly recognized in the literature, mainly because of a lack of molecular data correlated with their development. As a consequence, the morphological changes, molecular events, and tooth-specific signaling centers evident at ED 12 and 13 are generally thought to reflect M1 development (Fig. 1F) (e.g., ref. 10, <http://bite-it.helsinki.fi/>). Interestingly, a supernumerary tooth occurs in front of the M1 in some mouse mutants (11–23), and this has been considered as an extra molar (19, 20, 23) or related to the lost premolar (13–16, 18, 21, 22). In the latter case, some authors explicitly proposed the continued development of a rudimentary premolar (diastemal) bud as a possible origin for this supernumerary tooth in mutants (8, 12–16). However, the “rudimentary bud hypothesis” (Fig. 1E) has not yet been experimentally tested or validated on the basis of molecular data.

To clarify whether the prominent bud-like structures detected in WT mouse mandible at ED 12 and 13 reflect the rudimentary tooth primordia (Fig. 1E) or the M1 anlage (Fig. 1F), we set out to test these two concepts by correlating morphological and molecular aspects of tooth development in the mouse embryonic mandible. By studying the dynamics of molecular markers of tooth development and performing lineage tracing during early cheek tooth formation, we validated the vestigial bud hypothesis. Our studies provide a unique understanding of molar row development and first molar morphogenesis. They also provide a clear example of participation by a rudiment in development and evolution of a functional organ.

Results and Discussion

Three *Shh* Signaling Centers Are Sequentially Patterned in the Cheek Region of Mandible and Colocalized, Respectively, with MS, R2, and M1 Tooth Buds. To investigate the dynamics of tooth development

Author contributions: J.P., S.P., H.L., M.P., V.L., and R.P. designed research; J.P., S.P., S.C., and A.L. performed research; J.P., S.P., S.C., M.R., H.L., O.K., M.P., and R.P. analyzed data; and J.P., S.P., O.K., M.P., V.L., and R.P. wrote the paper.

The authors declare no conflict of interest.

*This Direct Submission article had a prearranged editor.

¹J.P. and S.P. contributed equally to this work.

²To whom correspondence should be addressed. E-mail: janproch@biomed.cas.cz.

This article contains supporting information online at www.pnas.org/lookup/suppl/doi:10.1073/pnas.1002784107/-DCSupplemental.

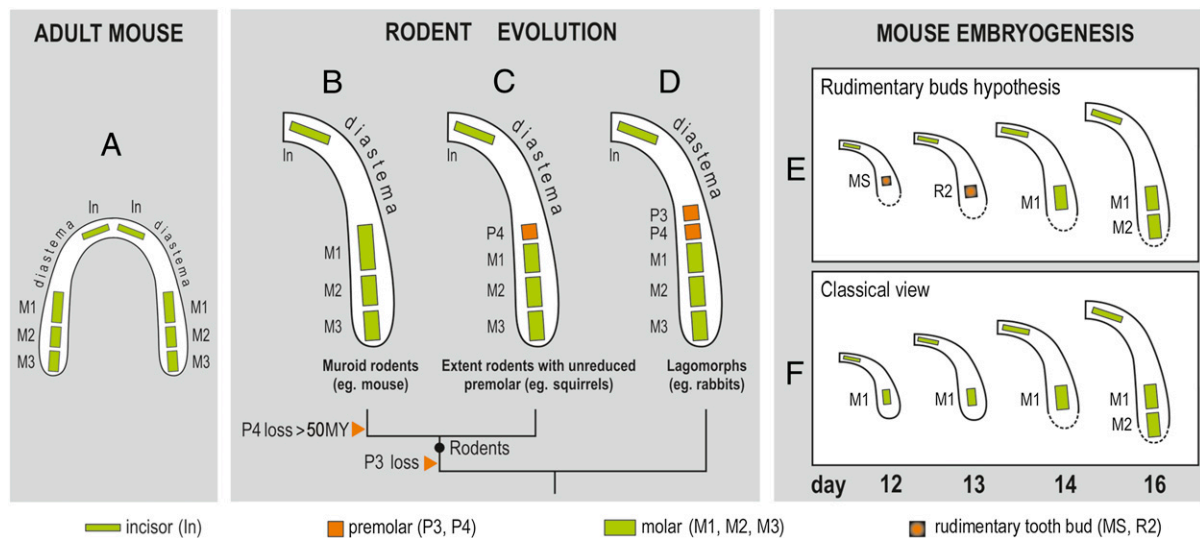


Fig. 1. Reduction of the lower cheek teeth during mouse evolution and their pattern during mouse ontogeny. (A) Dentition in the adult mouse is considerably reduced. Each jaw quadrant comprises only one incisor (In) and three molars (M1, M2, M3); a large toothless diastema occurs at the place of missing canine and premolar teeth. (B–D) Evolution of the mouse lower molars from a common ancestor of lagomorphs and rodents. (D) Two premolars (called P3 and P4) were lost in the mouse lineage (B). (E and F) The two current interpretations of mouse lower molar development. The “rudimentary buds hypothesis” of mouse lower molar row development (E) has a basis in descriptive morphological studies and evolutionary data: Two rudimentary premolar buds (MS and R2) are the first tooth primordia, which sequentially develop in the cheek region of mandible, before and in front of molars. These buds’ progression is stopped by apoptosis. (F) In the classic view, the first molar (M1) is the first tooth primordium that appears in the cheek region of the mandible. Afterward, the other molars (M2, M3) are sequentially added.

in the cheek region of embryonic mandible, we first assessed *Shh* expression, which is widely recognized as a marker of early tooth development in mammals (24), and also in fish (25), at closely spaced intervals using *Shh*-EGFP mice (26), in which EGFP is inserted at the *Shh* locus.

To avoid heterogeneity of data resulting from the intra- and interlitter variability in developmental progress of embryos harvested at a similar day of pregnancy, both age- and weight-staging criteria (27) were used: the age of embryos counted in number of ED postcoitum was further refined using wet body weight in milligrams (for details, see *Materials and Methods*). Body weight has been shown to be a reliable indicator of small stage differences, which allows for fine-ranking embryos of similar age, and enables a detailed series of progressive stages of tooth development (27).

Because of the detailed staging, three distinct periods of bright GFP expression were revealed in the cheek region of the developing mandible. These periods of bright signal alternated with periods of a weak or indistinct signal (Fig. 2A). Time-lapse microscopy of mandibles cultured in vitro (Fig. 2B, Fig. S1, and Movie S1) and *Shh* in situ hybridization of dissected mandibles (Fig. 2A and Fig. S2) confirmed this dynamic change in pattern of expression.

The distinct domains of strong *Shh* expression became progressively more posterior in the mandible over time (Fig. S1 and Movie S1). This pattern was consistent with the notion that these domains corresponded to sequentially developing MS, R2, and M1. We next analyzed sections through *Shh*-hybridized mandibles, followed by 3D reconstructions of dental epithelium. The *Shh* expression was indeed found at the tip of the morphological structures called MS, R2, or M1 bud, at ED 12.7, 13.3, or 14.3, respectively (Fig. 2A). Of note, two signals (a small anterior and a larger posterior *Shh* domain) occasionally coexisted in ED 13.3 embryos (Fig. S2). Such a double signal has already been reported in day 13 mouse embryos (19, 22): the anterior weak signal has been attributed to an extra (possibly vestigial) tooth and the posterior, larger signal to the developing M1. According to the dynamics of *Shh* expression reported here, we propose that both these *Shh* spots in fact mark rudimentary signaling centers: one disappearing in the MS rudiment (weak anterior signal) and an-

other newly formed in the R2 rudiment (strong posterior signal) (Fig. S2). In contrast, the M1 signaling center (primary enamel knot) appears 1 d later and even more posteriorly (Fig. 2).

The finding of a series of three *Shh*-signaling centers, which colocalized with three successive buds (MS, R2, and M1, respectively) (Figs. 1E and 2A), strongly contrasts with the classical interpretation of *Shh* expression in the cheek region of mouse mandible, which attributes the *Shh* expression at ED 12 to 14 to successive stages of M1 development (Fig. 1F).

Rudimentary Buds Have Their Own Signaling Center Resembling the M1 Signaling Center, Known as the “Primary Enamel Knot.” An important consequence of the colocalization of the *Shh* expression at ED 12 and 13 to MS and R2, respectively, was that *Shh* expression in M1 was first found at the late-bud stage of M1 epithelium at day 14 (more exactly at ED 14.3 in the present study). In M2, which contrary to M1 cannot be confused with a rudimentary structure, *Shh* expression is also not found before a late-bud stage, consistent with the present interpretation of M1 (Fig. S3). This *Shh* expression coincided with onset of formation of the molar primary enamel knot (pEK), a recognizable morphological structure (28) with signaling center properties (24, 29). The *Shh* expression in molars just preceded the transition to the cap stage of tooth development and was maintained during that stage. Two days and 1 d before, the respective MS and R2 buds also had their own *Shh* signaling center (Fig. 2 and Fig. S1), but failed to maintain it. This observation suggested that MS and R2 initiate a pEK but fail to maintain it. In agreement with this view, a rudimentary enamel knot was described in R2 [in terms of cell arrangement, presence of apoptosis, and *Shh* expression (8, 15)]. We therefore looked for other markers (Fig. 3) that are typical of the cap stage M1 pEK signaling center, such as activation of the Wnt pathway reported by TOPGAL transgene activity and expression of *Edar*, *p21*, *Bmp4*, and *Fgf4* (29–31). Most of these markers could indeed be detected in both MS and R2 bud, although at lower levels than in M1 bud (Fig. 3). Only *Fgf4* could not be detected in MS bud, which may reflect its growth arrest at an earlier developmental stage compared with R2.

may explain why the two rudimentary tooth buds have been maintained over approximately 50 million years. First, gene networks acting in the rudimentary buds could to some extent be preserved because they are fundamental for odontogenesis, being shared with developing molars that were maintained. Indeed, the present data showed that several genes are expressed in both rudimentary and M1 buds (Fig. 3). Second, the sequential development of the cheek tooth row is likely to be an integrated system, in which the development of molars and rudimentary buds is not independent. Recent articles have shown that during the first, second, and third molar sequential development, each developing molar exerts an inhibitory influence on the next developing molar (36, 37). The present study suggests that this model should be extended to include the rudimentary buds that presumably represent premolars, meaning that the premolar rudiments would have an influence on patterning of molars (Fig. 4C). Moreover, the rudiments may function as a barrier between the developing molars and inhibitory influences found in the diastema [such as *Gas1*, an antagonist of the *Shh* pathway (40)]. The third mechanism more specifically concerns the R2 bud. The present data demonstrated that R2 is incorporated into M1 during development, when M1 pEK elongates anteriorly to encompass R2. This phenomenon may be related to the formation of a prolonged anterior part (the anteroconid) in the mouse M1, especially as this part arose, evolutionarily speaking, following the loss of premolars (Fig. 4D) (7). This hypothesis can be tested in several manners. In mice, one can compare M1 with M2 development, because M2 looks like the M1 deprived of anteroconid in WT mice (Fig. S34), but can develop a small anteroconid in some “boosted” conditions (22). Furthermore, M1 in genetically altered mice with an extra tooth in the premolar position should be examined in more detail, as some of these mice have the extra tooth and a well-developed M1 anteroconid (12, 19, 22), but others have an extra tooth but reduced anteroconid (13, 16, 17). This difference has been proposed to result from differential participation of the rudiments in supernumerary tooth formation: MS or R2 could be involved where the anteroconid is maintained or reduced, respectively (16, 35). Finally, a comparison with other species (e.g., rodent species that retained a premolar) will be very helpful to better understand the specificities of mouse first molar development.

We propose a two-step model for mouse molar row evolution in which sharing of genetic networks and developmental integration might have slowed down rudiment regression, but still allows a certain degree of freedom, thus facilitating morphological innovation of the first molar. Work at the intersection of developmental biology and paleontology will help to test this model by further focusing on development and evolution of the anterior part of M1.

Materials and Methods

Mouse Breeding. The CD1 mice were purchased from the Charles River. C57BL/6 mouse strain carrying fusion protein *Shh*-EGFP and Cre recombinase from endogenous *Shh* locus (*B6.Cg-Shh^{tm1(EGFP)cre}Cj*), first introduced by Harfe (26), were purchased from The Jackson Laboratory. The transgenic mice were genotyped using Jackson's Lab Protocol for fluorescent proteins. TOPGAL mice [*Tg(Fos-lacZ)34Efu*] carry three LEF1/TCF1 binding sites fused to a minimal *c-fos* promoter driving *lacZ* expression (41). For experiments, CD1 males, *Shh*-EGFP males or TOPGAL males were crossed with WT CD1 females. All of the animals' treatment satisfied the requirements of the Institutional Review Board of the Institute of Experimental Medicine, Academy of Sciences of the Czech Republic, Prague, Czech Republic, and of the Institut de Génomique Fonctionnelle de Lyon, Université de Lyon, Lyon, France.

Embryo Harvesting and Staging. Mice were mated overnight and vaginal plugs were detected in the next morning, noon being indicated as ED 0.5. Pregnant females were killed by a cervical dislocation at 3:00 to 4:00 PM on ED 12 and 13 (stages ED 12.7 and 13.7, respectively), or at 7 to 8 AM on ED 13 and 14 (stages ED 13.3 or 14.3, respectively). These two harvesting terms allowed

getting a broader spectrum of developmental stages of the mouse embryos during the period under observation.

An important variability in stages of morphological development may exist not only among litters but even within litters harvested at a similar day of pregnancy (ED) (e.g., ref. 42). The wet body weight allows further sorting of the embryos of a specific chronological age, being a very good indicator of developmental progress of tooth development (27). Therefore, each embryo was weighed after a drop of a fluid on its surface was removed by gentle dabbing on a dry Petri dish. For example, in Fig. 2, the embryos harvested at 3:00 to 4:00 PM at ED 12 (when counted according to the day of detection of vaginal plug = day 0), were said to be ED 12.7 embryos (according to the present counting, when the midnight before morning detection = ED 0.0), and were further ranked according to their body weight from 65 to 110 mg.

Then, the *Shh*-EGFP embryos were sorted according to the presence/absence of a green fluorescence in their tails under inverted fluorescence microscope Leica AF6000. For further experiments, only the EGFP-positive embryos were used. The lower jaw arch was dissected and split at a midline. The left half was always used for *Shh* whole mount in situ hybridization, and the right one for detection of *Shh*-EGFP during in vitro culture (time-lapse microscopy, microinjection).

Mandible Epithelium Dissociations. Mandibles were dissected in Hank's medium and treated with Dispase II (Roche) 10 mg/mL at 37 °C for 1 to 2 h, depending on embryonic stage. Epithelium was carefully removed and fixed overnight in PFA 4%.

Whole-Mount in Situ Hybridization and X-Gal Staining. Embryonic mandibles or dissociated epithelia were fixed in 4% PFA solution overnight at 4 °C and in situ hybridization was done according to a standard protocol. DIG RNA probes were transcribed in vitro from plasmids described elsewhere: *Shh* (43), *Edar* (44), *Fgf4* (29), and *Bmp4* (45), except for *p21*, which was made from a PCR fragment amplified with primers GAGCAAAGTGTGCCGTGTCTCT and ACCAATCTGCGCTTTGGAGTGATA and cloned in Topo-pCRII (Invitrogen). TOPGAL embryonic mandibles or dissociated epithelia were fixed in 4% PFA for 15 min only and stained with X-gal according to a standard protocol. The samples were documented by a Leica MZ6 stereomicroscope with a Leica DC480 digital camera or on a Zeiss LUMAR stereomicroscope with a CCD CoolSNAP camera (PLATIM).

Cryosections and 3D Reconstruction. The hybridized jaw halves were embedded in a series of graded solutions of sucrose (Sigma) diluted in PBS (pH 7.4). Next, the specimens were embedded in OCT Tissue Tek (Sakura) diluted 1:1 with 20% sucrose and frozen in isopentane (Sigma) cooled on dry ice to -60 °C, and sectioned on a cryostat microtome Mikrom HM 560 (Mikrom) in 10- μ m sections. The sections were postfixed in 4% formaldehyde and counterstained by Nuclear fast red (Fluka), dehydrated, and mounted in Neomount (Merck).

Computer-Aided 3D Reconstruction. Contours of the dental and adjacent oral epithelium were drawn from consecutive sections using a Leica DMLB microscope equipped with a drawing chamber at a magnification of 320 \times . The digitalization of the serial drawings and the correlation of successive images have been previously described (46). The generation of 3D pictures was made using VG Studio Max 2.0 software (VG Studio Max).

In Vitro Culture. Dentition explants were dissected under sterile conditions from mandibles of ED 12.7 and 13.3 embryos, and cultured in an agarose semisolid medium for 60 h. The semisolid culture medium was prepared according to Hu et al. (47).

Time Lapse Microscopy. Mandibles from heterozygous *Shh*-EGFP embryos at ED 12.7 (80–90 mg) were cultured in vitro. The time lapse experiments were made on the inverted fluorescence microscope Leica AF6000 with transparent incubator associated with humidifier, and CO₂- (5%) and temperature- (37.5 °C) regulating units. Experiments were driven and evaluated by LeicaAF software with a well-plate acquisition software module (Leica). For the overlay of time-lapse pictures, three pictures taken respectively at 0, 31, and 60 h were first converted to artificial colors (respectively, blue, red, and green). They were put together by using original Leica software, and adjusted according to the shape of dental epithelium and the autofluorescence of necrotic zone.

Dil Labeling. Upon dissection (at ED 12.7 or 13.3) and accommodation of an explant in a semisolid medium, Dil microinjection was targeted into EGFP fluorescence area selected under green fluorescence cube. Dil was kept as a stock solution (solution of 0.25 $\mu\text{g}/\mu\text{L}$ Dil in 100% DMSO). Before use, the stock solution was dissolved 1:1 by 50% glycerol in aqua pro injectione. Micromanipulator (Narishige) and microinjector (Narishige) were connected with the Leica microscope working station described above. Microinjection itself was performed with a capillary needle (Narishige) with 5 μm in diameter.

ACKNOWLEDGMENTS. We thank B. Hu for sharing his skills with *in vitro* molar culture, D. Lyons (University of California, San Francisco, CA) for kindly providing the epithelium dissociation protocol, A. McMahon (Harvard University, Cambridge, MA), S. Vincent (Institut de Génomique Fonctionnelle de Lyon, University of Lyon, Lyon, France), I. Thesleff (Institute of Biotechnology, University of Helsinki, Helsinki, Finland), D. Duprez (Université Pierre et Marie Curie, Paris, France), and M. Vieux-Rochas (Evolution des Régulations Endocriniennes, Mu-

séum National d'Histoire Naturelle, Paris, France) for kindly providing probe plasmids, L. Krasny, H. Sanderová (Institute of Microbiology Academy of Sciences of the Czech Republic) and R. Sedláček with his colleagues (Institute of Molecular Genetics, Academy of Sciences of the Czech Republic) for providing technical support; the Plateau d'Imagerie (IFR128) staff and B. Rokytova for imaging assistance; the Plateau de Biologie Expérimentale de la Souris (IFR128) staff for animal care and breeding; and F. Spoutil for helpful discussion and critical reading of the manuscript. This work was supported by the Grant Agency of the Czech Republic (304/07/0223), Ministry of Education, Youth, and Sports of the Czech Republic (MSM0021620843), the Center National pour la Recherche Scientifique, the Ecole Normale Supérieure de Lyon, the Région Rhône-Alpes, the Fondation pour la Recherche Médicale, the "Fondation Singer-Polignac," the Agriculture and Natural Resources program "Quenottes," and a grant for supporting project for Strategic Research of Nihon University School of Dentistry at Matsudo from the Japanese Ministry of Education, Culture, Sports, Science, and Technology (MEXT), 2008–2012.

- Hall BK (2003) Descent with modification: the unity underlying homology and homoplasy as seen through an analysis of development and evolution. *Biol Rev Camb Philos Soc* 78:409–433.
- Müller GB (2002) Vestigial organs and structures. *Encyclopedia of Evolution*, ed Pagel M (Oxford University Press, New York), Vol 2, pp 1131–1132.
- Darwin C (1859) *On the Origin of Species. A Facsimile of the First Edition*. (Harvard University Press, Cambridge, Massachusetts) Sixteenth printing, 2000.
- Walker-Larsen J, Harder LD (2001) Vestigial organs as opportunities for functional innovation: The example of the Penstemon staminode. *Evolution* 55:477–487.
- Lockett W, Hartenberger J-L (1985) *The Order Rodentia: Major Questions on Their Evolutionary Origin, Relationships and Suprafamilial Systematics* (Plenum press, New York).
- Peterková R, Peterka M, Viriot L, Lesot H (2000) Dentition development and budding morphogenesis. *J Craniofac Genet Dev Biol* 20:158–172.
- Viriot L, Peterková R, Peterka M, Lesot H (2002) Evolutionary implications of the occurrence of two vestigial tooth germs during early odontogenesis in the mouse lower jaw. *Connect Tissue Res* 43:129–133.
- Peterková R, Peterka M, Viriot L, Lesot H (2002) Development of the vestigial tooth primordia as part of mouse odontogenesis. *Connect Tissue Res* 43:120–128.
- Viriot L, et al. (2000) The presence of rudimentary odontogenic structures in the mouse embryonic mandible requires reinterpretation of developmental control of first lower molar histomorphogenesis. *Int J Dev Biol* 44:233–240.
- Jernvall J, Thesleff I (2000) Iterative signaling and patterning during mammalian tooth morphogenesis. *Mech Dev* 92:19–29.
- Grüneberg H (1965) Genes and genotypes affecting the teeth of the mouse. *J Embryol Exp Morphol* 14:137–159.
- Klein OD, et al. (2006) Sprouty genes control diastema tooth development via bidirectional antagonism of epithelial-mesenchymal FGF signaling. *Dev Cell* 11:181–190.
- Ohazama A, et al. (2009) Primary cilia regulate Shh activity in the control of molar tooth number. *Development* 136:897–903.
- Ohazama A, et al. (2008) Lrp4 modulates extracellular integration of cell signaling pathways in development. *PLoS ONE* 3:e4092.
- Peterkova R, et al. (2009) Revitalization of a diastemal tooth primordium in *Spry2* null mice results from increased proliferation and decreased apoptosis. *J Exp Zool B Mol Dev Evol* 312B:292–308.
- Peterková R, Lesot H, Viriot L, Peterka M (2005) The supernumerary cheek tooth in tabby/EDA mice—a reminiscence of the premolar in mouse ancestors. *Arch Oral Biol* 50:219–225.
- Charles C, et al. (2009) Distinct impacts of Eda and Edar loss of function on the mouse dentition. *PLoS One* 4:e4985.
- Kristenová-Cermáková P, Peterka M, Lisi S, Lesot H, Peterková R (2002) Postnatal lower jaw dentition in different phenotypes of tabby mice. *Connect Tissue Res* 43:283–288.
- Mustonen T, et al. (2004) Ectodysplasin A1 promotes placodal cell fate during early morphogenesis of ectodermal appendages. *Development* 131:4907–4919.
- Pispa J, et al. (2004) Tooth patterning and enamel formation can be manipulated by misexpression of TNF receptor Edar. *Dev Dyn* 231:432–440.
- Tucker AS, Headon DJ, Courtney JM, Overbeek P, Sharpe PT (2004) The activation level of the TNF family receptor, Edar, determines cusp number and tooth number during tooth development. *Dev Biol* 268:185–194.
- Kangas AT, Evans AR, Thesleff I, Jernvall J (2004) Nonindependence of mammalian dental characters. *Nature* 432:211–214.
- Kasai Y, et al. (2005) Regulation of mammalian tooth cusp patterning by ectodin. *Science* 309:2067–2070.
- Thesleff I, Keränen S, Jernvall J (2001) Enamel knots as signaling centers linking tooth morphogenesis and odontoblast differentiation. *Adv Dent Res* 15:14–18.
- Fraser GJ, Graham A, Smith MM (2004) Conserved deployment of genes during odontogenesis across osteichthyans. *Proc Biol Sci* 271:2311–2317.
- Harfe BD, et al. (2004) Evidence for an expansion-based temporal Shh gradient in specifying vertebrate digit identities. *Cell* 118:517–528.
- Peterka M, Lesot H, Peterková R (2002) Body weight in mouse embryos specifies staging of tooth development. *Connect Tissue Res* 43:186–190.
- Butler PM (1956) The ontogeny of molar teeth. *Biol Rev Camb Philos Soc* 31:30–70.
- Jernvall J, Kettunen P, Karavanova I, Martin LB, Thesleff I (1994) Evidence for the role of the enamel knot as a control center in mammalian tooth cusp formation: Non-dividing cells express growth stimulating Fgf-4 gene. *Int J Dev Biol* 38:463–469.
- Liu F, et al. (2008) Wnt/beta-catenin signaling directs multiple stages of tooth morphogenesis. *Dev Biol* 313:210–224.
- Tucker AS, et al. (2000) Edar/Eda interactions regulate enamel knot formation in tooth morphogenesis. *Development* 127:4691–4700.
- Adloff P (1916) *Die Entwicklung des Zahnsystems der Säugetiere und des Menschen* (Berlin, Verlag von Hermann Meusser).
- Kükenthal W (1892) Über den Ursprung und die Entwicklung der Säugertierzähne (About the origin and evolution of mammalian teeth). *Jenaer Zeitsch Naturwiss* 26:469–489.
- Röse C (1892) Über die Entstehung und Formveränderungen des menschlichen Molaren (About the formation and shape changes of human molars). *Anatomischer Anzeiger* 7:393–421.
- Peterkova R, Lesot H, Peterka M (2006) Phylogenetic memory of developing mammalian dentition. *J Exp Zool B Mol Dev Evol* 306:234–250.
- Kavanagh KD, Evans AR, Jernvall J (2007) Predicting evolutionary patterns of mammalian teeth from development. *Nature* 449:427–432.
- Renois E, et al. (2009) Evolution of mammal tooth patterns: New insights from a developmental prediction model. *Evolution* 63:1327–1340.
- Huysseune A, Witten PE (2006) Developmental mechanisms underlying tooth patterning in continuously replacing osteichthyan dentitions. *J Exp Zool B Mol Dev Evol* 306:204–215.
- Dassule HR, McMahon AP (1998) Analysis of epithelial-mesenchymal interactions in the initial morphogenesis of the mammalian tooth. *Dev Biol* 202:215–227.
- Cobourne MT, Miletich I, Sharpe PT (2004) Restriction of sonic hedgehog signalling during early tooth development. *Development* 131:2875–2885.
- DasGupta R, Fuchs E (1999) Multiple roles for activated LEF/TCF transcription complexes during hair follicle development and differentiation. *Development* 126:4557–4568.
- Miyake T, Cameron AM, Hall BK (1996) Detailed staging of inbred C57BL/6 mice between Theiler's [1972] stages 18 and 21 (11–13 days of gestation) based on craniofacial development. *J Craniofac Genet Dev Biol* 16:1–31.
- Echelard Y, et al. (1993) Sonic hedgehog, a member of a family of putative signaling molecules, is implicated in the regulation of CNS polarity. *Cell* 75:1417–1430.
- Laurikkala J, et al. (2001) TNF signaling via the ligand-receptor pair ectodysplasin and edar controls the function of epithelial signaling centers and is regulated by Wnt and activin during tooth organogenesis. *Dev Biol* 229:443–455.
- Merlo GR, et al. (2002) The *Dlx5* homeobox gene is essential for vestibular morphogenesis in the mouse embryo through a BMP4-mediated pathway. *Dev Biol* 248:157–169.
- Lesot H, et al. (1996) Mouse molar morphogenesis revisited by three-dimensional reconstruction. II. Spatial distribution of mitoses and apoptosis in cap to bell staged first and second upper molar teeth. *Int J Dev Biol* 40:1017–1031.
- Hu B, Nadiri A, Bopp-Küchler S, Perrin-Schmitt F, Lesot H (2005) Dental epithelial histomorphogenesis *in vitro*. *J Dent Res* 84:521–525.

Revitalization of a Diastemal Tooth Primordium in *Spry2* Null Mice Results From Increased Proliferation and Decreased Apoptosis

RENATA PETERKOVA^{1*}, SVATAVA CHURAVA^{1,2}, HERVE LESOT^{3–5},
MICHAELA ROTHOVA^{1,6}, JAN PROCHAZKA^{1,6}, MIROSLAV PETERKA^{1,2},
AND OPHIR D. KLEIN^{7–9*}

¹Department of Teratology, Institute of Experimental Medicine, Academy of Sciences of the Czech Republic, Prague, Czech Republic

²Department of Anthropology, Faculty of Science, Charles University, Prague, Czech Republic

³INSERM U595, Faculté de Médecine, Université Louis Pasteur, Strasbourg, France

⁴Faculté de Chirurgie Dentaire, Université Louis Pasteur, Strasbourg, France

⁵International Collaborating Centre in Oro-Facial Genetics and Development, University of Liverpool, Liverpool, United Kingdom

⁶Department of Developmental Biology, Faculty of Science, Charles University, Prague, Czech Republic

⁷Department of Orofacial Sciences, University of California, San Francisco, California

⁸Department of Pediatrics, University of California, San Francisco, California

⁹Institutes of Human Genetics and Regeneration Medicine, University of California, San Francisco, California

ABSTRACT An understanding of the factors that promote or inhibit tooth development is essential for designing biological tooth replacements. The embryonic mouse dentition provides an ideal system for studying such factors because it consists of two types of tooth primordia. One type of primordium will go on to form a functional tooth, whereas the other initiates development but arrests at or before the bud stage. This developmental arrest contributes to the formation of the toothless mouse diastema. It is accompanied by the apoptosis of the rudimentary diastemal buds, which presumably results from the insufficient activity of anti-apoptotic signals such as fibroblast growth factors (FGFs). We have previously shown that the arrest of a rudimentary tooth bud can be rescued by inactivating *Spry2*, an antagonist of FGF signaling. Here, we studied the role of the epithelial cell death and proliferation in this process by comparing the development of a rudimentary diastemal tooth bud (R_2) and the first molar in the mandibles of *Spry2*^{-/-} and wild-type (WT) embryos using histological sections, image analysis and 3D reconstructions. In the WT R_2 at embryonic day 13.5, significantly increased apoptosis and decreased proliferation were found compared with the first molar. In contrast, increased levels of FGF signaling in *Spry2*^{-/-} embryos led to significantly decreased apoptosis and increased proliferation in the R_2 bud. Consequently, the R_2 was involved in the formation of a supernumerary tooth primordium. Studies of the revitalization of

Grant sponsor: Grant Agency of the Czech Republic; Grant numbers: 304/05/2665; and 304/07/0223; Grant sponsor: Ministry of Education, Youth and Sports of the Czech Republic; Grant numbers: MSM0021620843; and COST B23.002; Grant sponsor: U.C.S.F. Sandler Family Foundation; Grant sponsor: NIH; Grant number: K08-DE017654.

*Correspondence to: Renata Peterkova, Department of Teratology, Institute of Experimental Medicine, Academy of Sciences of the Czech Republic, v.v.i., Videnska 1083, 14220 Prague, Czech Republic. E-mail: repete@biomed.cas.cz; Ophir D. Klein, Departments of Orofacial Sciences and Pediatrics, University of California, San Francisco, CA 94143-0442 USA. E-mail: Ophir.Klein@ucsf.edu

Received 19 November 2008; Accepted 20 November 2008
Published online 6 January 2009 in Wiley InterScience (www.interscience.wiley.com). DOI: 10.1002/jez.b.21266

rudimentary tooth primordia in mutant mice can help to lay the foundation for tooth regeneration by enhancing our knowledge of mechanisms that regulate tooth formation. *J. Exp. Zool. (Mol. Dev. Evol.)* 312B:292–308, 2009. © 2009 Wiley-Liss, Inc.

How to cite this article: Peterkova R, Churava S, Lesot H, Rothova M, Prochazka J, Peterka M, Klein OD. 2009. Revitalization of a diastemal tooth primordium in *Spry2* null mice results from increased proliferation and decreased apoptosis. *J. Exp. Zool. (Mol. Dev. Evol.)* 312B:292–308.

The mouse embryonic dentition provides a natural model for studying the factors that support or inhibit tooth development, as it contains not only germs of functional teeth but also several types of rudimentary tooth primordia (Fig. 1). These rudiments undergo the initial stages of tooth morphogenesis but then are repressed, either through regression or by merging with primordia of functional dentition. These rudimentary primordia have been hypothesized to represent vestiges of ancestral teeth that were suppressed during evolution (Peterkova et al., 2000, 2002a). The coexistence of rudimentary primordia and primordia of prospective functional teeth in the jaw allows comparison of the molecular control of their development in the same animal as well as between wild-type (WT) and mutant mice. The observation that these rudiments can form functional teeth in mutant mice also raises the stimulating possibility that these structures can serve as models of controlled tooth regeneration (Peterkova et al., 2006; D'Souza and Klein, 2007).

Adult mice have a greatly reduced number of teeth compared with other mammals. In each jaw quadrant, they have only one incisor and three molars (Fig. 1A). The incisor and molars are separated by a toothless gap (diastema) where other mammals have incisors, canines and premolars. The embryonic mouse diastema transiently contains the above-mentioned rudimentary (vestigial) tooth primordia (Fig. 1B). The most prominent of these rudiments are two large buds that are present in the posterior part of the diastema, just anterior to the first molar, in each maxilla or mandible. These two rudiments are initially even larger than the first molar itself, and therefore can be mistaken for the first molar primordium at early stages. However, the development of these large diastemal buds ceases before the cap stage, and programmed cell death (apoptosis) occurs in their epithelium (Peterkova et al., '96, 2000; Viriot et al., 2000). These large rudimentary buds have been homologized to the premolars lost during mouse evolution (Peterkova et al., 2000; Viriot et al., 2002).

Mutations in both ectodysplasin (*Eda*) and sprouty (*Spry*) genes can stimulate the revival of the large diastemal buds leading to the development of a supernumerary cheek tooth in front of the first molar (Peterkova et al., 2005; Klein et al., 2006). Such a supernumerary tooth can be thought of as a tooth atavism because it is located in the position of a lost premolar (Peterkova et al., 2005, 2006).

Sprouty genes encode negative feedback antagonists of signaling by fibroblast growth factors (FGFs) and other receptor-tyrosine kinase ligands (Minowada et al., '99). The FGF signaling pathway is evolutionarily conserved and plays crucial roles in the development of many craniofacial structures, including teeth (Nie et al., 2006). The effect of decreased FGF signaling during tooth development has been studied in mouse embryos lacking the epithelium-specific b-isoform of FGF receptor 2. In such mice, tooth development is arrested at the bud stage (Celli et al., '98). In contrast to FGF receptor mutants, in sprouty null mice FGF signaling is increased which leads to several abnormalities in tooth development (Klein et al., 2006, 2008). In WT mice, *Spry2* and *Spry4* are expressed in different tissue compartments during early tooth development: *Spry2* in the epithelium and *Spry4* in the mesenchyme. In mice carrying mutations in either *Spry2* or *Spry4*, supernumerary teeth develop in front of the first lower molars as a result of the abnormal survival and development of diastemal tooth buds (Klein et al., 2006).

Apoptosis is involved in the repression of the development of the large rudimentary tooth buds in the posterior part of the diastema in WT mice at embryonic day (ED) 12.5–13.5 (Peterkova et al., '96; Viriot et al., 2000) (Fig. 1B). We have proposed that apoptosis in dental epithelium is stimulated by a relative predominance of growth inhibitors (Fig. 1C), and that a relative increase in growth activators (e.g. FGFs) can downregulate apoptosis and support further growth (Peterkova et al., 2003). Therefore, we set out to test the following hypothesis: the absence of an FGF antagonist leads to the abnormal survival of diastemal tooth

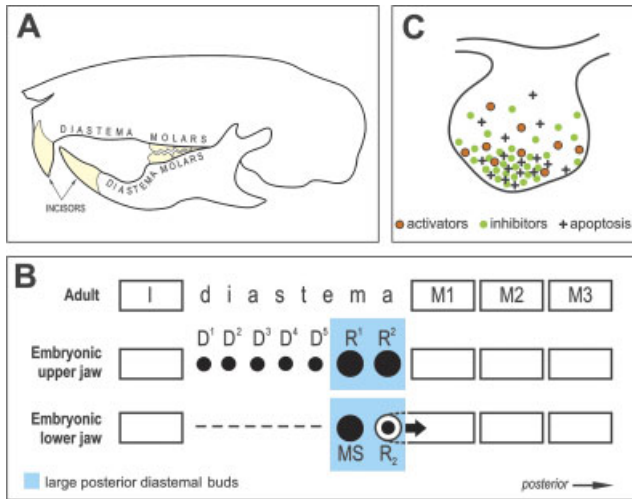


Fig. 1. Schematic of tooth pattern in the adult and embryonic mouse and a model of apoptosis regulation in tooth buds. (A) Each quadrant of the adult mouse dentition has one incisor and three molars separated by a toothless diastema. (B) Schematic of tooth pattern in one jaw quadrant in adult and embryonic mouse. In the anterior part of the embryonic diastema, either rudimentary small placodes/buds (D^1 – D^5) or an epithelial thickening (dashed line) develops in the maxilla or mandible, respectively, until ED 13.0, at which point they start to disappear (Peterkova et al., '95; Lesot et al., '99). In the posterior part of the diastema, two large rudimentary buds consecutively appear and become the most prominent tooth primordia in the cheek region at ED 12.5 and 13.5, respectively (R^1 and R^2 in the maxilla; MS and R_2 in the mandible), before their development ceases. After ED 13.0, R^1 , R^2 and MS regress, whereas the R_2 bud is incorporated (large arrow) into the anterior part of the first molar cap (Peterkova et al., '96; Viriot et al., 2000). The remnants of R^1 , R^2 and MS are thought to contribute during later morphogenesis to expansion of the first molar (Lesot et al., '96; Peterkova et al., 2005). Black spots indicate the primordia affected by programmed cell death (apoptosis), which occurs during elimination of D^1 – D^5 , regression of R^1 , R^2 and MS and growth retardation of R_2 (Tureckova et al., '96; Peterkova et al., '96; Viriot et al., 2000). The upper mouse incisor originates from five to six tooth placodes, whereas three placodes might occur in the lower incisor region at initial stages (Peterkova et al., 2002a) (not shown). I, incisor; M1, M2, M3, first, second and third molars, respectively. (C) A model for the regulation of apoptosis at the tip of a tooth bud by interaction between growth activators (e.g. FGFs) and inhibitors (e.g. BMPs). A local excess of inhibitors leads to the epithelial cells' failure to receive adequate growth-activating (apoptosis-suppressing) signals (e.g. FGF). This signaling imbalance (relative predominance of inhibitors) can stimulate apoptosis (modified from Peterkova et al., 2003). ED, embryonic day; FGF, fibroblast growth factor; BMP, bone morphogenetic protein.

buds in *Spry2* null embryos by causing decreased apoptosis and increased proliferation, thus preventing the growth arrest that normally occurs in these rudiments. We compared the development of the posterior diastemal bud (R_2) and the molar

epithelium in the mandible of *Spry2*^{-/-} and WT mice using histological sections, 3D reconstructions, morphometry and quantitative evaluation of proliferation and apoptosis.

MATERIALS AND METHODS

Mouse lines and staging of embryos

Mouse lines carrying mutant alleles of *Spry2* were maintained and genotyped as reported (Shim et al., 2005). The females were mated overnight and noon after the detection of the vaginal plug was considered as ED 0.5. The pregnant mice were killed by cervical dislocation and their offspring were harvested at ED 13.5, 14.0, 14.5 and 15.5. Immediately after taking the embryo out of the uterus, the drop of amniotic fluid on its surface was gently removed by dabbing on a filter paper and the wet body weight was determined (Peterka et al., 2002). Each embryo was individually put in a bottle with Bouin fluid and fixed at room temperature for 10 days. Age/body weight-matched WT embryos were used as controls.

Histology

We processed 14 WT and 14 mutant embryonic heads at ED 13.5–15.5 for histology. Heads were embedded in paraffin, cut in 7 μ m frontal serial sections and stained with a modified Mallory method (alcian blue–hematoxylin–eosin) (Fig. 2).

3D reconstructions of dental epithelium and apoptosis distribution

Computer-aided 3D reconstructions of the developing lower cheek dentition were made in age/weight-matched pairs of *Spry2*^{-/-} and WT mice at ED 13.5, 14.0, 14.5 and 15.5 (Fig. 3). Contours of the dental and adjacent oral epithelium were drawn from histological sections at 7 μ m intervals using a Leica DMLB microscope (Leica Microsystems GmbH, Wetzlar, Germany) equipped with a drawing chamber at a magnification of 320 \times . At ED 13.5, apoptotic cells and bodies (Fig. 2A) were identified in the dental epithelium on histological sections based on morphological criteria (Tureckova et al., '96). These were recorded into a drawing and distinguished according to their position in one of the following three regions of dental epithelium: the superficial zone (thickness similar to the adjacent oral epithelium), the internal

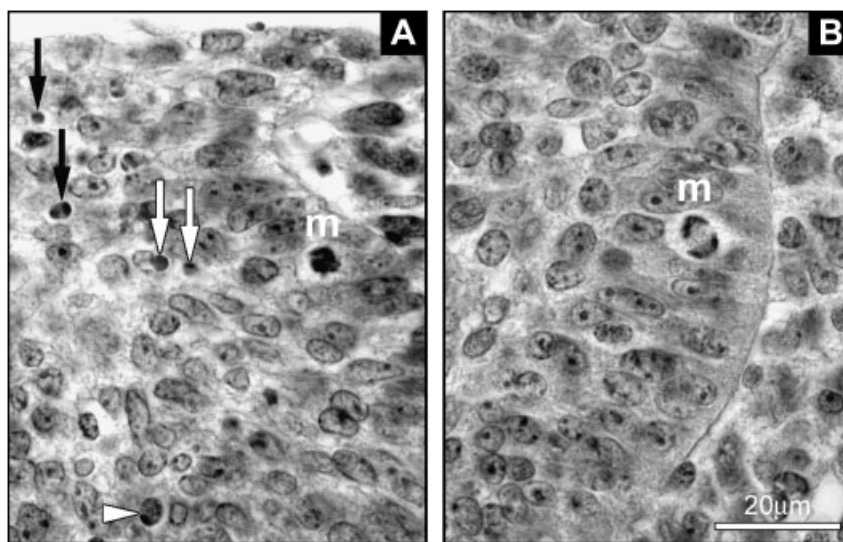


Fig. 2. Histological pictures of apoptosis and mitosis in the dental epithelium. (A) Examples of an apoptotic cell (arrowhead) and apoptotic bodies (white and black arrows) in the R_2 rudiment. m, mitosis. (B) A mitotic cell (m) in molar epithelium.

zone and the enamel knot zone (Fig. 4), corresponding to blue, white and red spots, respectively (see Fig. 6). The digitalization of the serial drawings, the correlation of successive images and the generation of 3D pictures have been previously described (Lesot et al., '96).

Morphometry of dental epithelium

The size of the dental epithelium was compared in age/weight-matched pairs of *Spry2*^{-/-} and WT embryos at ED 13.5, 14.0 and 14.5 (Fig. 5). We employed the same specimens that were used for 3D reconstructions. The area of the dental epithelium on frontal sections in the cheek region of the mandible was measured on every fifth section (i.e. at 35 µm intervals) along the antero-posterior jaw axes (Fig. 5). The first evaluated section was the one in which the lingual side of the infolding of the dental epithelium and the adjacent oral epithelium were at an angle close to or less than 90°. The last evaluated section was the one in which the dental epithelium still protruded into the mesenchyme.

We measured the frontal section area of the dental epithelium (at a magnification of 1,250 ×) on digitalized images made by Leica DMLB microscope (Leica Microsystems GmbH, Wetzlar, Germany) equipped with a camera Leica DC480 (Leica Microsystems GmbH, Wetzlar, Germany) using PC software ImageJ (<http://rsb.info.nih.gov/ij/>). The measured area was delimited by the basement membrane, the oral surface of the epithelium and by the places where the thickness of the dental epithelium decreased to the thickness of the

medially and laterally adjacent oral epithelium. The values were converted to µm² and plotted (Fig. 5).

Quantitative evaluation of apoptosis

We analyzed the number of apoptotic cells and bodies (Fig. 2A) in the posterior diastemal bud R_2 and the molar epithelium in *Spry2*^{-/-} and WT embryos at ED 13.5 (Fig. 7, Table 1). In order to compare WT and mutant tooth primordia at similar stage of odontogenesis, we selected from among ED 13.5 embryos one group of WT and one group of *Spry2*^{-/-} embryos of similar body weight. The embryonic body weight has been shown to correlate very well with the stage of mouse tooth development (Peterka et al., 2002). The control group was composed of ten right and left lower jaw quadrants of five WT embryos (weight range 154–178 mg), and the mutant group was composed of six right and left jaw quadrants of three mutant embryos (weight range 167–182 mg) (Table 1).

In each lower jaw quadrant, apoptosis was analyzed in two segments of the dental epithelium representing the R_2 diastemal bud and the molar epithelium (Fig. 7). Each segment comprised ten consecutive 7 µm thick histological sections. The segments were separated by a gap of 70 µm (ten sections). The boundaries of the segments were determined on the basis of the position of the middle of the R_2 segment. This corresponded to a section with the most pronounced enamel knot at the tip of the bud R_2 (compare with Fig. 4).

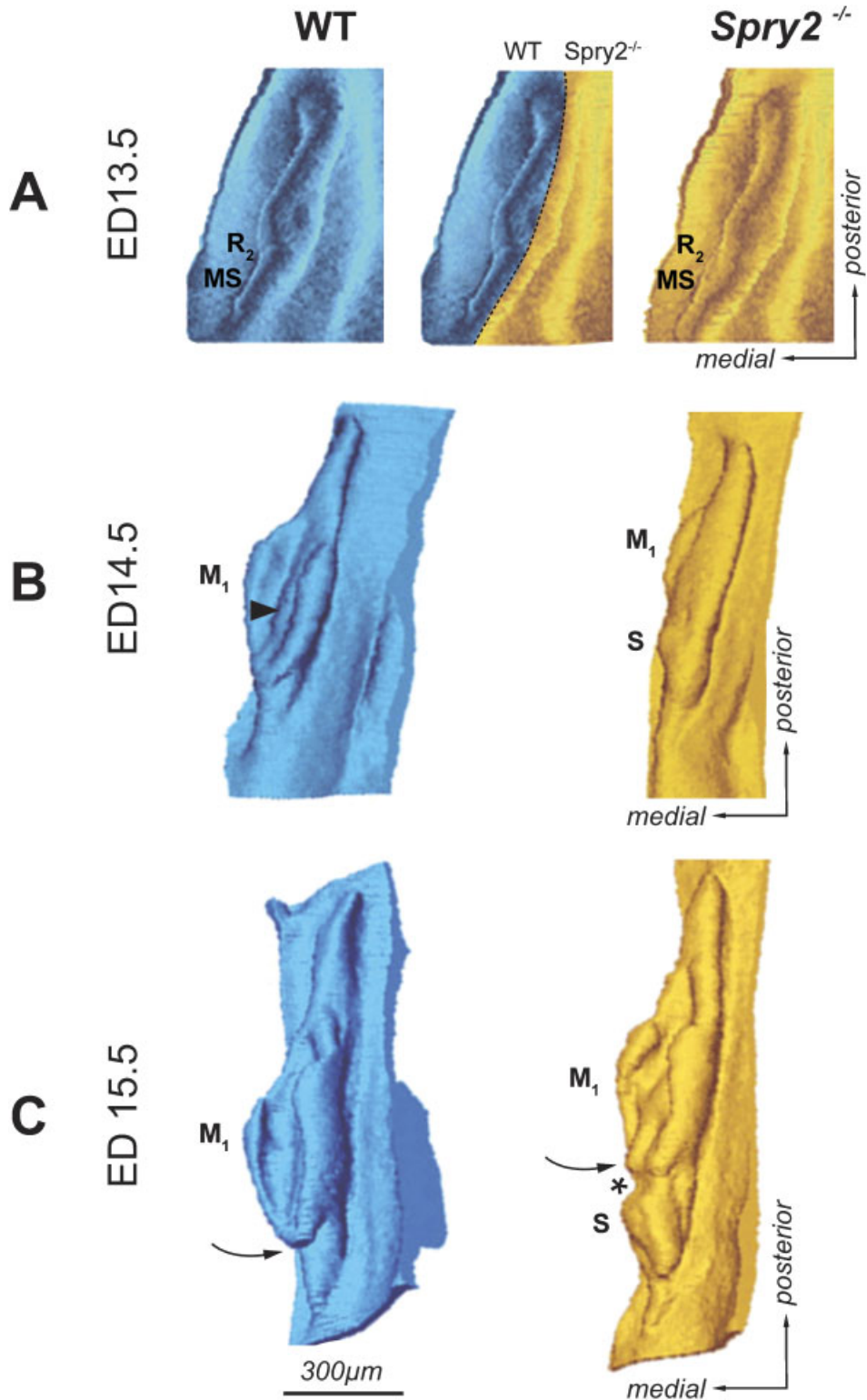


Fig. 3. Three-dimensional reconstructions of the dental epithelium. Mesenchymal view of the dental and adjacent oral epithelium in the cheek region of the mandible is presented in (A) aerial and (B, C) antero-lateral views at embryonic days (ED) 13.5, 14.5 and 15.5. Dark—wild-type (WT) embryos; light—*Spry2*^{-/-} embryos. An epithelial ridge (MS) represents the residuum of the anterior diastemal bud (Fig. 1B), which is most prominent at ED 12.5. R₂, posterior diastemal bud; S, supernumerary tooth primordium; M₁, enamel organ of the first lower molar. Curved arrow points to the anterior end of the M₁ enamel organ, which is closed in controls and open in mutants. Arrowhead indicates the enamel knot area bulging into the mesenchyme. Asterisk shows the position of the connection between S and M₁.

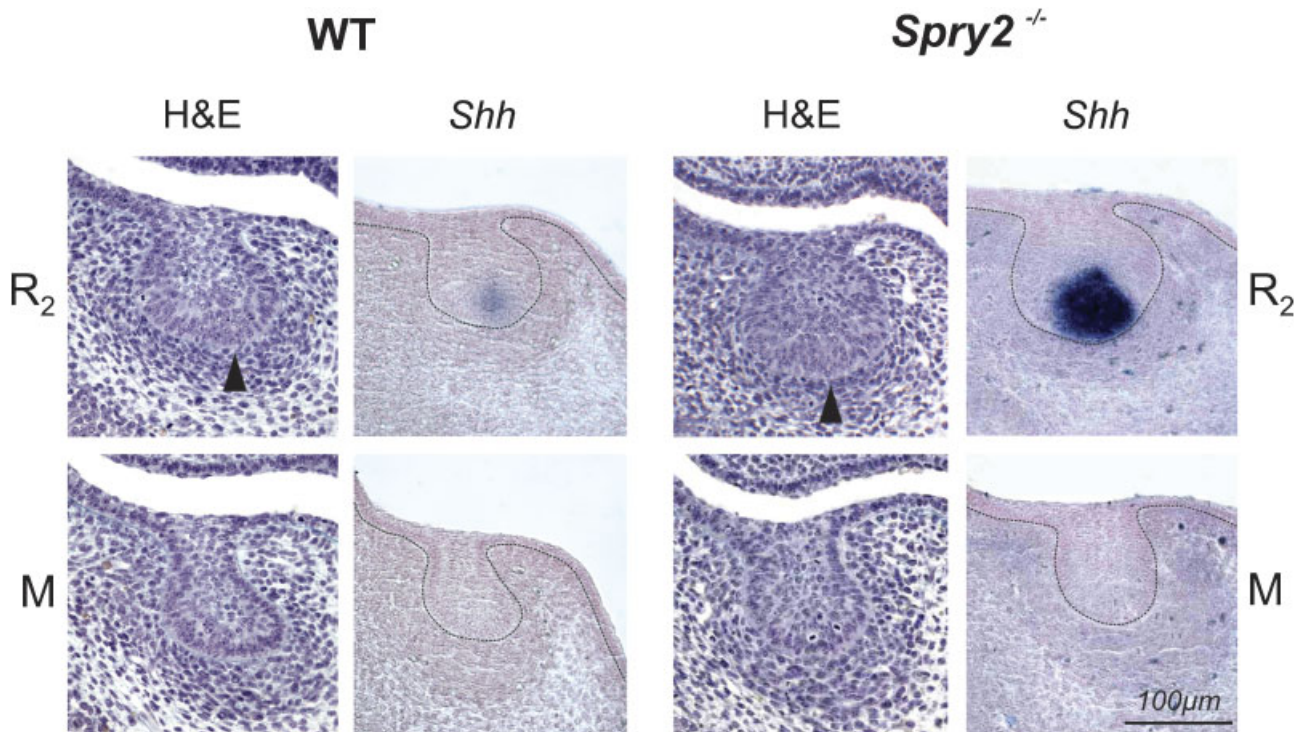


Fig. 4. Dental epithelium on frontal sections of mandible at embryonic day 13.5. In each wild-type (WT) and mutant (*Spry2*^{-/-}) embryo, the large posterior diastemal bud (R_2) and molar epithelium (M) is presented on histological sections stained with hematoxylin–eosin prestained with alcian blue (H&E) and after *Shh* whole mount in situ hybridization. At the enamel knot area at the tip of the R_2 bud (arrowhead) in WT and *Spry2*^{-/-} embryos, *Shh* is expressed, whereas it is absent in the molar epithelium. Note the increased *Shh* expression in the mutant R_2 bud.

The apoptotic rate was calculated as the number of apoptotic cells and bodies per square unit ($\times 10^3 \mu\text{m}^2$) of epithelium. This could be determined for individual sections, individual jaw segments or individual groups of jaws (Table 1). Apoptotic cells and bodies were recorded into the drawings of the dental epithelium made from sections (see above—“3D reconstructions”). The size of the dental epithelium on frontal sections was measured using computer software ImageJ (see above—“Morphometry of dental epithelium”). The apoptotic rate was evaluated either in the entire dental epithelium (see the blue+white+red dots in Fig. 6) or separately in the superficial cells (see the blue dots in Fig. 6) and interior cells (see the white and red dots in Fig. 6). Fischer’s exact test was used to determine the statistical significance between the total values (Table 1) in a group of WT and mutant tooth primordia.

Quantitative evaluation of mitoses

The proliferation was evaluated at ED 13.5 in the same segments of dental epithelium (Fig. 7) used for the quantitative evaluation of apoptosis

(see above). In each section, the total number of epithelial cells and the number of mitotic cells (from early metaphase to early telophase) were counted on digitalized images (at a magnification of $1,250\times$) made by Leica DMLB microscope (Leica Microsystems GmbH, Wetzlar, Germany) equipped with a camera Leica DC480 (Leica Microsystems GmbH, Wetzlar, Germany). The mitotic stage was then checked under a $100\times$ immersion objective (Fig. 2). Fischer’s exact test was used to determine the statistical significance between the total values (Table 2) in a group of WT and mutant tooth primordia.

Whole mount in situ hybridization

RNA in situ hybridization was performed according to standard protocols on ED 13.5 jaws that were fixed in 4% paraformaldehyde, hybridized in whole mount, embedded in paraffin, sectioned in $10\mu\text{m}$ thick frontal sections and counterstained by Nuclear Fast Red (Fluka/Sigma-Aldrich Chemie GmbH, Buchs SG, Switzerland). To generate digoxigenin-labeled probes, we used plasmids containing mouse *Shh* sequences

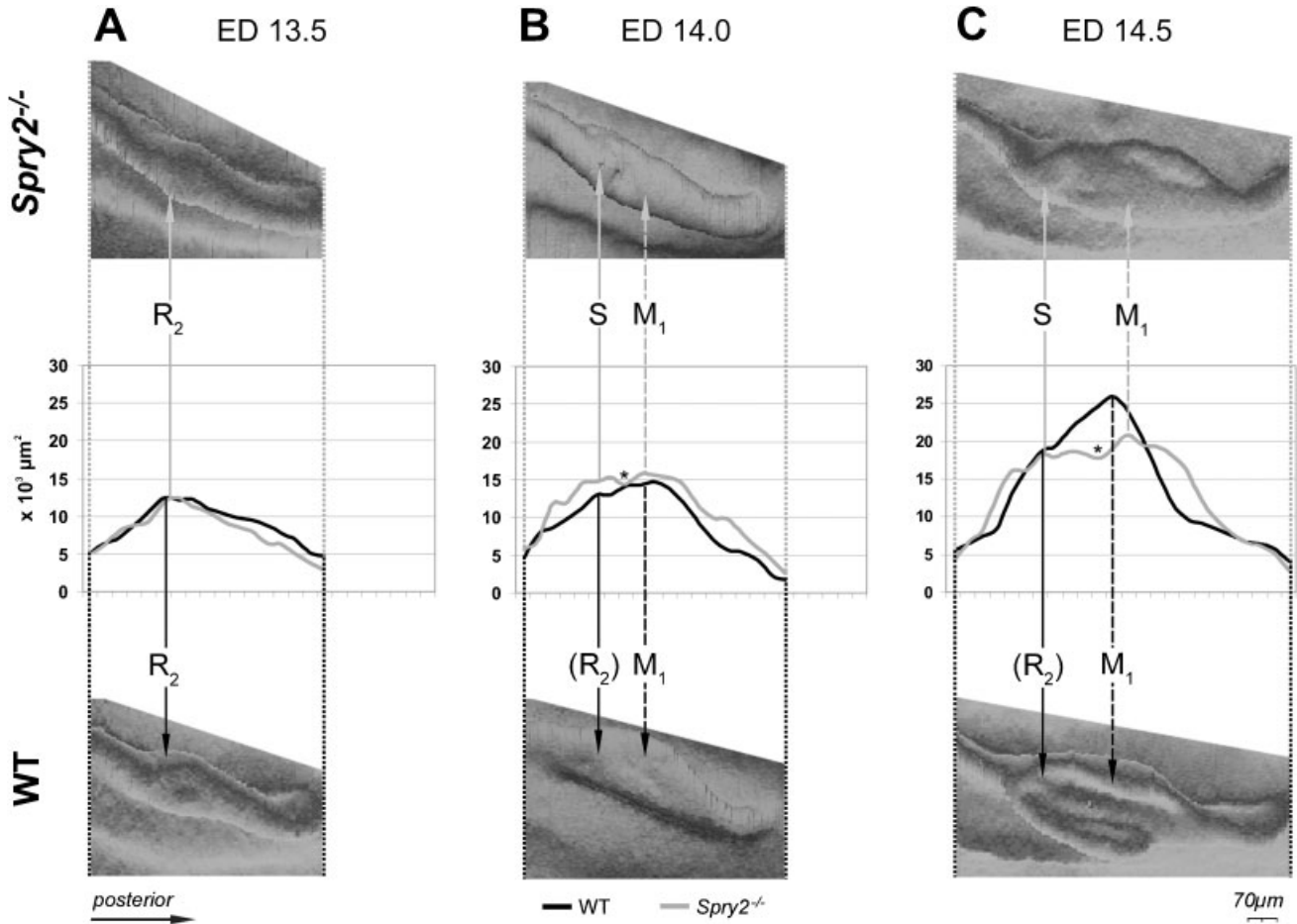


Fig. 5. Changes in size of the dental epithelium along the antero-posterior axis. Graphs depict changes in the area ($\times 10^3 \mu\text{m}^2$) of the dental epithelium measured on frontal sections along the antero-posterior axes in the cheek region of the mandible at embryonic day (ED) 13.5 (A), 14.0 (B) and 14.5 (C). Three-dimensional reconstructions of the measured wild-type and mutant dental epithelium are shown below and above the curves, respectively. Solid arrows point to the position of the posterior diastemal R_2 bud at ED 13.5, its estimated position (R_2) in WT mice at ED 14.0 and 14.5 or the position of a supernumerary tooth primordium S in mutants at ED 14.0 and 14.5. M_1 , the first lower molar. Dashed arrow points to the largest region of the M_1 . Asterisk indicates the area between S and M_1 . The residuum of the anterior diastemal rudiment (MS-Fig. 1B) is located in front of the R_2 bud, and its increased size in $Spry2^{-/-}$ embryos is reflected by the anterior part of the anterior elevation on the curve (B, C). WT, wild type.

for in vitro transcription as previously reported (Klein et al., 2006).

RESULTS

Morphogenesis of dental epithelium

In order to elucidate the relationship between the development of the supernumerary tooth and the morphogenesis of R_2 and M_1 , changes in the size and morphology of the dental epithelium were investigated in the mandibular cheek region from ED 13.5 to 15.5 (Figs. 3–5).

At ED 13.5, the dental epithelium had a bud shape on most frontal sections in WT and $Spry2^{-/-}$ embryos (Fig. 4). The bud-shaped dental

epithelium on sections corresponded to a “mound” shape on 3D reconstructions (Fig. 3A). The morphology and antero-posterior extent of this dental mound were similar in $Spry2^{-/-}$ and WT specimens. At the middle part of the epithelial mound, a swelling of the R_2 bud (Fig. 1B) was visualized on 3D pictures (Fig. 3A). The anterior part of the swelling included the enamel knot of the R_2 (compare with Figs. 4 and 6). The dental epithelium located anteriorly to the R_2 bud corresponded to the residuum of the MS rudiment (Fig. 1B), which undergoes regression at ED 13.5. The size (area) of the dental epithelium varied along the antero-posterior axis of the mandible. These changes were similar in WT and $Spry2^{-/-}$

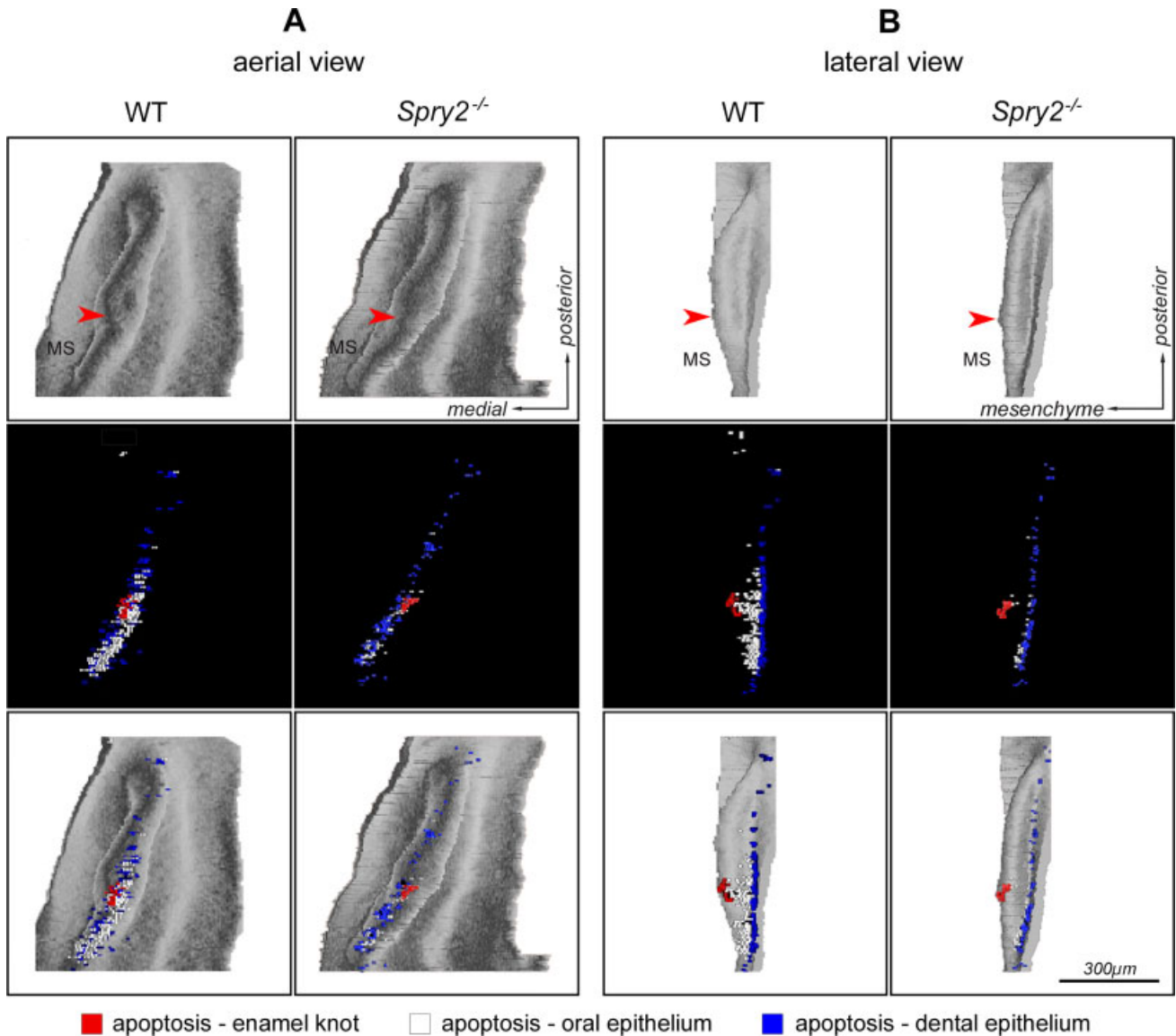


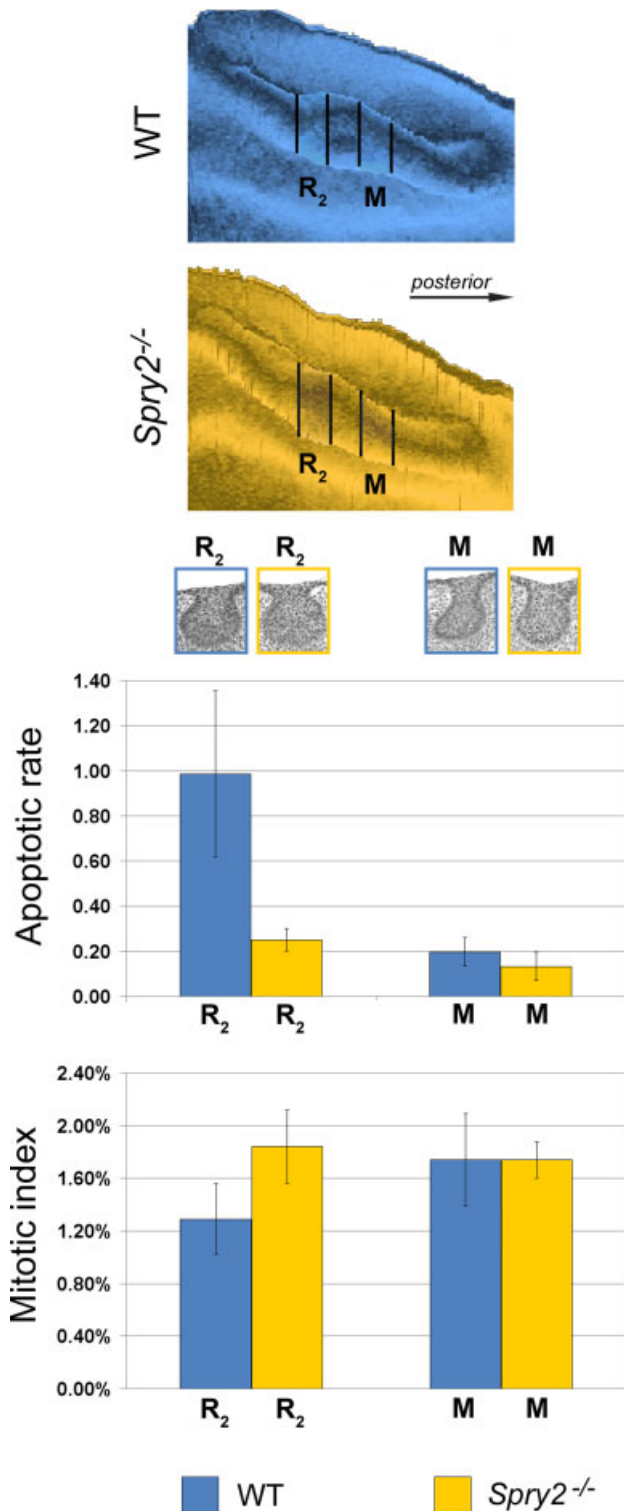
Fig. 6. Distribution of apoptosis in the dental epithelium on 3D reconstructions at embryonic day 13.5. The dental and adjacent oral epithelium in the cheek region of mandible of wild-type (WT) and *Spry2*^{-/-} embryos is presented in (A) aerial view or (B) lateral view. The first and second rows show the shape of the epithelium and apoptosis distribution, respectively. The third row images are overlays of the first and second rows. Blue and white dots indicate apoptosis in the superficial and internal areas of dental epithelium, respectively. The red dots indicate apoptosis in the enamel knot at the tip (arrowhead) of a wide diastemal bud R₂.

embryos (Fig. 5A). The area of the dental epithelium was small anteriorly, gradually increased in the posterior direction until reaching a maximum where the rudimentary bud R₂ was located and then decreased. The R₂ bud could be identified on frontal sections (Fig. 4) according to its large size, typical shape, increased number of apoptotic bodies and presence of an enamel knot structure at its tip. *Shh* expression was assessed to show that this marker of the enamel knot was indeed expressed at the tip of the R₂ bud. The

expression was more pronounced in mutants than in controls (Fig. 4).

At ED 14.0–15.5, the antero-posterior length of the dental epithelium increased (Figs. 3 and 5). In contrast to WT mice, where R₂ is incorporated into the anterior part of the rapidly growing M₁ cap (Viriot et al., 2000), the anterior part of the dental epithelium conspicuously increased in *Spry2*^{-/-} fetuses. It progressively separated from the developing M₁ cap, giving rise to the supernumerary tooth primordium (Fig. 3). In comparison with WT

mice, the M_1 in age/weight-matched mutants was developmentally retarded (early cap stage) at ED 14.5, and remained open at its anterior end at ED 15.5 (Fig. 3C). The morphometric analysis (Fig. 5)



clearly showed that the antero-posterior elongation of the dental epithelium mainly involved a region posterior to the area where the R_2 was incorporated into the M_1 in controls or where the supernumerary tooth developed in mutants. Although the length of the dental epithelium was similar in stage/weight-matched WT and *Spry2*^{-/-} mice, size differences of the dental epithelium became progressively more evident between control and mutant fetuses (Figs. 3 and 5). In WT mice, only one major elevation was present on the curve. However, its maximum values were higher and located more posteriorly than those at ED 13.5 (Fig. 5). The maximum values reflected the largest middle part of the M_1 cap. An accessory peak on the anterior slope on the curve marked the incorporated R_2 bud. In contrast, the curves in *Spry2*^{-/-} stage/weight-matched animals showed two elevations separated by a depression (Fig. 5B, C). The anterior elevation reflected the developing supernumerary tooth, whereas the posterior elevation corresponded to the forming M_1 cap in mutants (Fig. 3B, C). The maximum values of the anterior elevation were observed at the R_2 position (compare Fig. 5A, B). However, this anterior elevation also included the area in front of the R_2 (Fig. 5) where the anterior diastemal rudiment MS (Fig. 1B) occurred. Thus, not only the R_2 but also the MS was increased in mutants, suggesting that both of these rudiments contribute to the formation of the supernumerary tooth. The depression between the anterior and posterior elevations on the curves in mutants corresponded to the gap between the supernumerary tooth and the M_1 primordium (compare Figs. 3B, C and 5B, C). Interestingly, the position of this gap fit into the largest part of M_1 in controls (Fig. 5C).

A defect in the segmentation of the dental epithelium along the antero-posterior jaw axes (Peterkova et al., 2002b) was apparent in *Spry2*^{-/-} mandibles. Although the total antero-posterior length of the dental epithelium was similar in

Fig. 7. The apoptotic rate and mitotic index in the R_2 bud and molar epithelium at embryonic day 13.5. Two segments of dental epithelium (represented in the aerial view in 3D reconstructions at the top) of wild-type (WT) and *Spry2*^{-/-} embryos were evaluated; colors as in legend. R_2 and M refer to the segment of the rudimentary diastemal bud and molar epithelium, respectively. Representative dental epithelia are shown in the frontal sections below the reconstructions, and have been adjusted to the graphs. Compared with the molar region, note the higher level of apoptosis in the R_2 in controls, and its dramatic decrease in mutants. In contrast, the mitotic index was significantly lower in the R_2 than in the molar region in controls and significantly increased in mutants.

TABLE 1. Summary of data on the quantitative evaluation of apoptosis

	R ₂				M			
	Number of sections	Total area (μm ²)	Total number of apoptotic elements	Apoptotic rate	Number of sections	Total area (μm ²)	Total number of apoptotic elements	Apoptotic rate
<i>Spry2</i> ^{-/-}	60	800 × 10 ³	201	0.25 × 10 ⁻³	60	559 × 10 ³	74	0.13 × 10 ⁻³
WT	100	1,099 × 10 ³	1,084	0.99 × 10 ⁻³	100	944 × 10 ³	186	0.20 × 10 ⁻³

Apoptotic rate, number of apoptotic elements/μm²; R₂, the posterior diastema bud in the mandible; M, the molar epithelium in the mandible; WT, wild type.

WT and *Spry2*^{-/-} animals, the anterior boundary of the M₁ was located more posteriorly in mutants than in WT mice, because of the presence of a supernumerary tooth anlage (Fig. 5B, C). The distinct separation of the supernumerary tooth primordium from M₁ (Fig. 3C) was not observed in all mutant embryos; some specimens only had hyperplasia of the anterior part of the M₁ (data not shown).

Apoptosis

In order to test the hypothesis that apoptosis is decreased in the R₂ bud in *Spry2*^{-/-} embryos, the distribution of apoptotic bodies and cells (Fig. 2A) was evaluated on frontal sections and represented in 3D reconstructions (Fig. 6) and by quantitative measurements (Table 1, Fig. 7) at ED 13.5.

In WT embryos, apoptosis was mainly concentrated in the anterior part of the dental epithelium, where the diastemal rudiments (MS, R₂) were repressed. The apoptotic cells and bodies were abundant in both the internal and superficial cells (see the white and blue dots in Fig. 6), and they were typically located in the enamel knot at the tip of the wide bud R₂ (see the red dots in Fig. 6). Interestingly, apoptosis occurred only rarely in the internal cells of the posterior part of the dental epithelium, that is, posterior to the R₂ bud (Fig. 6).

In *Spry2* mutants, the apoptotic bodies and cells were also more concentrated in the anterior part of the dental epithelium. However, they were much less abundant in mutant than in WT specimens and were largely absent from the internal parts of the epithelium where both diastemal rudiments were located (see white dots in Fig. 6). In the posterior part of the dental epithelium, the apoptosis distribution did not exhibit a marked difference between WT and mutant specimens and was almost exclusively present in the superficial cells (Fig. 6).

Quantitative evaluation of the number of apoptotic cells and bodies was compared in the R₂ bud and the molar epithelium between WT and

Spry2^{-/-} embryos at ED 13.5 (Table 1, Fig. 7). In the R₂ of WT mice, the number of apoptotic cells and bodies was significantly higher ($P < 0.01$) than that in the molar region in both WT and *Spry2*^{-/-} embryos. However, compared with the R₂ in WT animals, the number of apoptotic elements (in the whole structure as well as in the internal or superficial parts) was significantly decreased ($P < 0.01$) in the R₂ in mutants (Fig. 7). The number of apoptotic elements was also significantly lower ($P < 0.01$) in the molar area of mutants than in WT embryos. The number of apoptotic elements in the mutant R₂ did not differ from the molar epithelium in WT embryos ($P > 0.05$).

Proliferation

To assess whether proliferation is increased in the R₂ bud of *Spry2* mutant embryos, the mitotic index was evaluated and compared in the R₂ bud and the molar epithelium in WT and *Spry2*^{-/-} mandibles at ED 13.5 (Table 2). In WT mandibles, the mitotic index was significantly lower ($P < 0.01$) in the R₂ bud than in the molar region. In contrast, the mitotic index in the R₂ was significantly higher in *Spry2*^{-/-} than in WT embryos and was similar to that in the molar region. The mitotic index in the molar region showed no significant difference ($P > 0.05$) between WT and mutant jaws (Fig. 7).

DISCUSSION

We have previously documented that the loss of *Spry2* function leads the diastemal buds to develop into supernumerary teeth (Klein et al., 2006). However, it was not known whether this process occurs as a result of increased proliferation, decreased cell death or both. Here, we show that both decreased apoptosis and increased proliferation were found in the diastemal rudimentary bud R₂ (the presumed premolar vestige) in *Spry2*^{-/-} embryos at ED 13.5. This was followed by

TABLE 2. Summary of data on the quantitative evaluation of proliferation

	R ₂				M			
	Number of sections	Total number of cells	Total number of mitoses	Mitotic index (%)	Number of sections	Total number of cells	Total number of mitoses	Mitotic index (%)
<i>Spry2</i> ^{-/-}	60	12,151	255	2.10	60	8,842	175	1.98
WT	100	17,131	242	1.41	100	13,988	279	1.99

Mitotic index, percentage of mitotic cells in 100 cells; R₂, the posterior diastema bud in the mandible; M, the molar epithelium in the mandible; WT, wild type.

hyperplasia of the anterior part of the dental epithelium, where the R₂ was located, and by separation of this region from M₁, leading to the formation of a supernumerary tooth primordium.

Morphogenesis of the dental epithelium

In WT mice, the initial development of the rudimentary R₂ bud, followed by growth retardation and epithelial apoptosis, and finally incorporation into the anterior part of M₁, occurred as we previously described (Viriot et al., 2000).

The R₂ rudiment has a specific wide-bud shape on frontal sections at ED 13.5 (Fig. 4). In the cheek region, the tooth primordia that have a bud shape on frontal sections appear as ill-defined swellings on a continuous mound of dental epithelium in three dimensions (Fig. 3A) in both mice (Peterkova et al., 2000) and humans (Hovorakova et al., 2005). This dental mound has the appearance of a long cylinder extending along the jaw arch. However, both the epithelial mound and the tooth swellings exhibit a bud shape on frontal sections, and differ primarily in terms of area. This can make it difficult to distinguish tooth primordia from surrounding dental epithelium and explains why the anterior and posterior tooth boundaries are not yet distinct at the bud stage (Hovorakova et al., 2005).

Here, as in previous reports, we observed a swelling on the dental mound in 3D reconstructions at ED 13.5 (Figs. 3A and 5A), which indicated the presence of a distinct bud-stage tooth primordium. Anteriorly, in this swelling, the tip of the R₂ bud was marked by the presence of apoptosis (Fig. 6) and had morphological characteristics that are typically present in the enamel knot of the first molar cap (Lesot et al., '96). We suggest that the existence of the R₂ primordium as a discrete, active structure can be inferred by the apparent presence of a signaling

center, as marked by expression of *Shh* (Fig. 4). *Shh* expression at this location has generally been thought to correspond to the enamel knot of M₁ at day 13.

In WT mice, the anterior boundary of the lower M₁ becomes apparent at ED 14.5–15.5, when the M₁ cap differentiates (Viriot et al., '97) (Fig. 3B, C). However, the well-differentiated enamel organ of the lower M₁ at ED 15.5 only corresponds to the anterior two-thirds of the prospective tooth crown (Lesot et al., '99), i.e. to the prospective cusps B1, B2, L1, L2 (terminology by Gaunt, '55). The posterior part of M₁ has not yet formed and the enamel organ remains open posteriorly such that the posterior boundary is not yet apparent at ED 15.5 (compare with Fig. 3C). The posterior part of M₁ (cusps B3, L3, 4) develops at later stages, long after the primary enamel knot structure of M₁ has disappeared (Lesot et al., '99; Obara and Lesot, 2007).

The rudimentary diastemal primordia can advance as far as the bud stage before their arrest (Fig. 1B). Interestingly, the arrest of molar or incisor development in many mouse mutants that lack teeth also occurs at the bud stage (e.g. Peters and Balling, '99). It is not yet known why this is the case, and the identification of factors that regulate physiological tooth arrest in mouse diastemal buds can help to address this question. We have recently shown that the expression of *Spry2* and *Spry4* in the epithelium and mesenchyme, respectively, prevents diastemal tooth formation by making diastemal buds refractory to the FGF signaling that normally sustains tooth development (Klein et al., 2006). The data presented here document the cellular effects of the loss of *Spry2* on morphogenesis. In comparison with the molar region, decreased cell proliferation and increased apoptosis occurred during the physiological growth arrest of the R₂ bud in WT embryos. In contrast, both cell proliferation and apoptosis in

the R₂ bud remained similar to the molar area in *Spry2* mutants (Fig. 7) and allowed for further growth of the diastemal rudiment.

Supernumerary cheek teeth in mice with genetic alterations

In several mutant or transgenic mice, a supernumerary tooth is found anterior to the first molar. A classical example is the supernumerary cheek tooth in tabby, downless or sleek mutant mice (Gruneberg, '66; Sofaer, '69), which exhibit defects in the EDA signaling pathway (e.g. Elomaa et al., 2001). A supernumerary tooth in front of the first molar has also been reported in Tg737^{orp^k} mice (Zhang et al., 2003), in transgenic mice overexpressing the EDA receptor EDAR (Tucker et al., 2004) or the EDA protein itself (Kangas et al., 2004), in ectodin/WISE-deficient mice (Kassai et al., 2005) and in mice homozygous for a null allele of *Spry2* or *Spry4* (Klein et al., 2006).

The supernumerary tooth appears to originate from a rudimentary diastemal bud, whose development is not suppressed as it is in normal mice (Peterkova et al., 2005; Klein et al., 2006). In the case of sprouty null mice, the lack of an FGF antagonist leads to the upregulation of an epithelial-mesenchymal signaling loop that culminates in the formation of a supernumerary tooth in the diastema (Klein et al., 2006).

The incorporation of a rudimentary diastemal bud (Viriot et al., 2000) appears to render the anterior part of the mouse M₁ more susceptible to developmental alterations than the rest of the cheek dentition (Boran et al., 2005). The large rudimentary buds in the mouse diastema (Fig. 1B) have been hypothesized to represent vestiges of ancestral premolars suppressed during evolution (Peterkova et al., 2000; Viriot et al., 2002). We have proposed that the incorporation of the rudimentary diastemal bud (premolar vestige) into the M₁ fails in some mouse mutants and that the rudiment takes part in the formation of a supernumerary tooth. Such a tooth in front of the first molar in mutant mice might be, at least in part, homologous to a premolar lost during the evolution of muroids, and can be thought of as an evolutionary throwback (atavism) (Peterkova et al., 2005, 2006). This hypothesis is supported by (1) the development and incorporation of the R₂ bud into the lower M₁ in WT mice (Viriot et al., 2000), (2) the concentration of apoptotic cells and bodies in the anterior part of the dental

epithelium in WT mice at early and later prenatal stages (Viriot et al., 2000; Boran et al., 2005), (3) the origin of a supernumerary tooth primordium in the location of R₂ in tabby homo/hemizygous embryos (Peterkova et al., 2002b, 2005) and (4) paleontological data, as follows. During the evolution of muroid rodents (about 50 million years ago), the disappearance of the last premolar correlated with the extension of the anterior part of the first lower molar (Viriot et al., 2002). Thus, mutant mice with a supernumerary tooth in front of M₁ are more similar in terms of dentition to nonmuroid rodents with maintained premolars than are WT mice (Peterkova et al., 2005, 2006).

If a rudimentary bud participates in the development of the anterior part of M₁ in WT mice, then the anterior domain of M₁ should be reduced when the rudimentary bud is involved in the formation of a supernumerary tooth in mutants. Indeed, a number of studies document such a reduction in the anterior part of M₁ adjacent to a supernumerary tooth in mice with different genetic alterations (e.g. Gruneberg, '66; Kangas et al., 2004; Tucker et al., 2004; Kassai et al., 2005). This reduction has been proposed to result from the inhibitory influence of the developing supernumerary tooth (e.g. Sofaer, '75). However, our previous study (Peterkova et al., 2002b, 2005) has clearly shown that the supernumerary tooth in tabby homo/hemizygous mice forms where the diastemal bud is incorporated into the anterior part of the M₁ cap in WT mice. This is followed by a defect in the segmentation of the dental epithelium: the total antero-posterior length of the dental epithelium is similar in WT and mutant embryos. However, this epithelium is differently distributed to give rise to tooth primordia. The larger the most anterior (supernumerary) tooth primordium, the shorter, more posteriorly located and developmentally less advanced are the successive cheek teeth. Consequently, the positions of tooth boundaries do not match those of the WT molars (Peterkova et al., 2002b, 2005). This reciprocal correlation between the length of the first cheek tooth and the second or third tooth, together with a stable total length of the dental row, has also been reported in adult tabby homo/hemizygous mice (Kristenova et al., 2002). The existence of size interactions between molar teeth in mice has been proposed and led to the conclusion that the first molar controls the ultimate form of the whole molar row, which tends to maintain a stable length (Gruneberg, '65; Sofaer, '69; Kavanagh et al., 2007).

A defect in the segmentation of the dental epithelium was also found in the *Spry2*^{-/-} embryos reported here. In a similar antero-posterior length of the dental epithelium, M₁ only developed in controls, whereas both supernumerary tooth and M₁ primordia developed in mutants at early stages (Figs. 3 and 5). The supernumerary tooth originated in the location that corresponded to the anterior part of the control M₁. The mutant M₁ was located more posteriorly and exhibited a reduction in its anterior part, where the enclosure by the cervical loop was missing (Fig. 3C). Despite these marked prenatal differences, the adult lower M₁ adjacent to the supernumerary tooth is surprisingly almost completely normal in *Spry2*^{-/-} mice (Klein et al., 2006). In these cases, the supernumerary tooth does not develop at the expense of M₁, but has to include some additional material at the anterior end of M₁, which is not normally present there. A large supernumerary tooth in front of an almost normal M₁ occurs in some tabby heterozygous mice, and the anterior diastemal rudiment MS (Fig. 1B) is thought to take a part in its origin (Peterkova et al., 2005). It is possible that the MS rudiment, in addition to the R₂, participates in the morphogenesis of the supernumerary tooth in *Spry2*^{-/-} embryos. This is indicated by the increased size of the epithelium (Fig. 5A) and decreased amount of apoptosis (Fig. 6) in both R₂ and MS in these mutants. The specific roles of each of these diastemal rudiments in the origin of supernumerary teeth in sprouty mutants will be the focus of future studies.

Apoptosis

In WT embryonic mouse mandibles apoptosis concentrates in the anterior part of the dental epithelium in the cheek region, where the large diastemal buds have arrested (Viriot et al., 2000). At ED 13.5, apoptosis is also specifically located in the enamel knot (see below), which is transiently present at the tip of the R₂ (Peterkova et al., 2002a). The concentration of apoptosis in the anterior part of the M₁ epithelium is present during cap formation, which points to the incorporation of the R₂ bud there (Viriot et al., 2000).

As the development continues, apoptosis remains concentrated at the base of the anterior part of the M₁ at late cap and early bell stages (Viriot et al., '97; Boran et al., 2005). This suggests that, although incorporated into the M₁, the R₂ epithelium (the presumptive premolar vestige) is somehow distinct from the rest of the molar in WT

mice and represents a "locus minoris resistentiae," a region that is prone to developmental anomalies in genetically altered mice (Boran et al., 2005).

During further tooth development, apoptosis is specifically concentrated in the primary enamel knot of M₁, which is a cluster of epithelial cells located in the middle of the molar cap and adjacent to the papilla mesenchyme (Fig. 3B) (Butler, '56; Lesot et al., '96). The enamel knot is thought to play an important role during tooth morphogenesis (Bolk, '22; Butler, '56; MacKenzie et al., '92; Jernvall et al., '94, '98; Lesot et al., '96, '99; Vaahtokari et al., '96a; Coin et al., '99, 2000a). Interestingly, although caspase-3, caspase-9 and APAF-1 are all thought to be involved in the regulation of apoptosis in the molar enamel knot, these do not seem to be required for molar tooth formation (Matalova et al., 2006; Setkova et al., 2007). Similarly, inhibition of apoptosis in the primary enamel knot using a caspase inhibitor (Z-VAD-fmk) in vitro does not affect mouse tooth crown morphogenesis (Coin et al., 2000b). These studies focused exclusively on apoptosis in the enamel knot in the middle part of the M₁ cap. No experimental data are available regarding the regulation or effect of inhibition of apoptosis during development of the large diastemal buds (Peterkova et al., 2003).

We demonstrated that the absence of *Spry2*, by changing the equilibrium between growth activators and inhibitors (Fig. 1C), leads to a revival of a diastemal bud owing to the downregulation of apoptosis and increased proliferation (Fig. 7). As a consequence, the anterior part of the dental epithelium in the cheek region of the mandible was more abundant. Instead of growth arrest of the diastemal buds and incorporation of R₂ into M₁, as is found in WT mice, the rudimentary dental epithelium was revitalized and tended to separate from M₁, forming an independent, supernumerary tooth (Figs. 3 and 5).

Molecular considerations

We have proposed a hypothesis to explain the regulation of epithelial apoptosis during tooth formation by integrating two concepts (Peterkova et al., 2003): (1) The reaction/diffusion model of budding morphogenesis controlled by the relative balance of growth-activating and -inhibiting signals (for a review, see Peterkova et al., 2000, 2002a), and (2) a model of apoptosis regulation by

the relative balance between death-suppressing and death-stimulating signals (Raff, '92) (Fig. 1C).

It appears that FGF signaling from dental mesenchyme to epithelium is increased in *Spry2*^{-/-} mice because of the absence of Spry2 in the epithelium. This is probably owing to increased sensitivity to FGF10, which is only weakly expressed in diastemal mesenchyme in WT mice, and to FGF3 from the adjacent first molar. In contrast, *Fgf10* and *Fgf3* are strongly expressed in

the M₁ mesenchyme in WT mice (e.g. Klein et al., 2006). As a consequence of inactivation of *Spry2*, there is more intense *Shh* expression in the signaling center of the diastemal bud in mutant than in WT embryos (Fig. 4). It is also striking that *Fgf4* expression is seen in the diastemal bud in mutants, as this has never been seen in controls (Klein et al., 2006). Thus, it is possible that FGF4 is a direct or indirect target of SHH signaling.

The epithelial *Fgf4* expression is under the control of the transcription factor LEF1, which is an effector of canonical Wnt signaling. It has previously been shown that FGF4 added exogenously to cultured isolated WT dental mesenchyme prevents apoptosis (Vaah Tokari et al., '96b) in the dental epithelium of *Lef1*^{-/-} mice (Sasaki et al., 2005). In *Lef1*^{-/-} embryos, tooth development is arrested at the bud stage (Kratochwil et al., 2002). EDA, which promotes tooth development, is also under the control of LEF1 (Laurikkala et al., 2001), and EDA can upregulate *Shh* expression in ectodermal derivatives (Pummila et al., 2007). These data suggest that the level of EDA signaling could be a key parameter that controls *Shh* expression. We hypothesize that the upregulation of FGF signaling stabilizes tooth bud development by stimulating the canonical Wnt signaling pathway, which reinforces *Fgf4*, *Shh* and *Eda* expression. These latter molecules then act as growth activators in the epithelium.

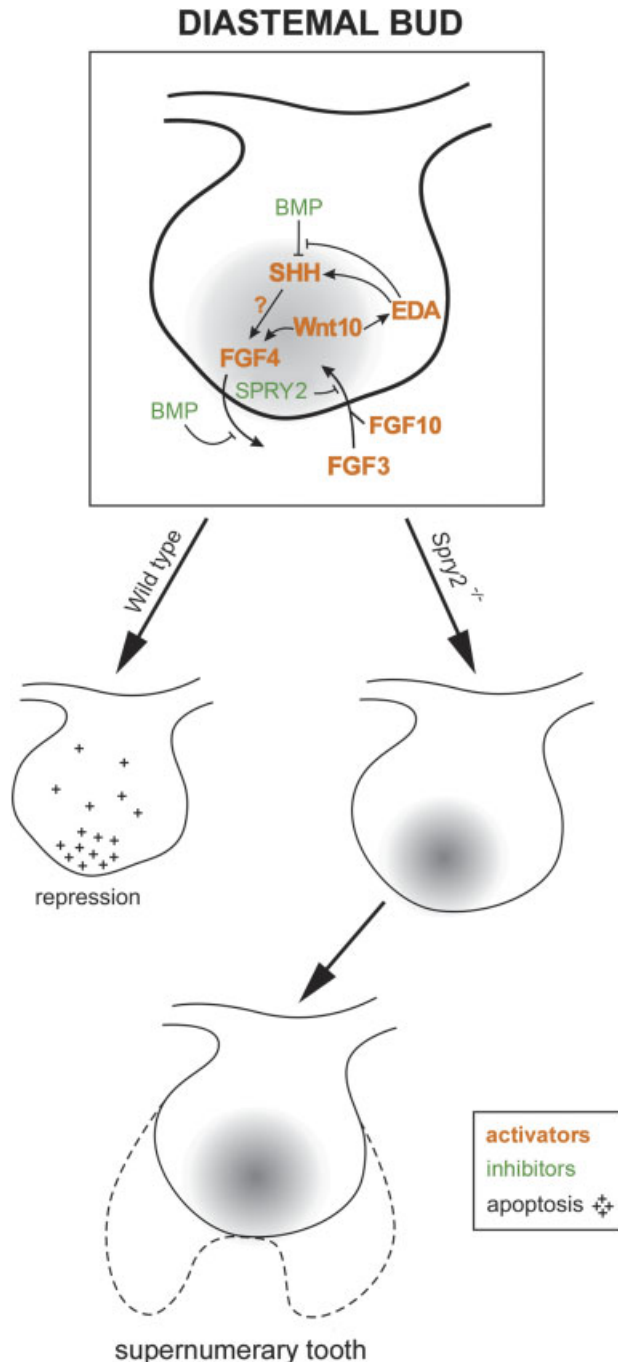


Fig. 8. Model of revitalization of a diastemal bud. A drawing of a posterior diastemal bud (R₂) at ED 13.5 with a signaling center (gray) at its tip (compare with Fig. 3). Growth inhibitors (e.g. BMP) and growth activators (e.g. SHH, Wnt10, FGF3, FGF4, FGF10, EDA) are distinguished by colors, as in legend (compare with Fig. 1C). We propose that FGF signaling from the mesenchyme can induce expression of FGF4, SHH and EDA, perhaps by the stimulation of the Wnt/LEF1 pathway, and SPRY2 can antagonize this cascade. In wild-type diastemal buds, *Spry2* is expressed, the growth-activation pathway is blocked and bud growth is stopped by a relative prevalence of growth inhibitors. The mitotic index is decreased and apoptosis occurs in the epithelium (crosses). In *Spry2* mutants, development of the rudimentary bud is not arrested. In contrast to WT embryos, apoptosis is decreased in the rudimentary bud, whereas its mitotic index is as high as in the molar region. Determination of the extent of the contribution of the R₂ rudiment to the supernumerary tooth will require future studies. This model is based on findings reported in this study and on previously reported studies (Hogan, '99; Peterkova et al., 2000, 2003; Zhang et al., 2000; Laurikkala et al., 2001; Kratochwil et al., 2002; Nadiri et al., 2004; Klein et al., 2006; Pummila et al., 2007). ED, embryonic day; BMP, bone morphogenetic protein; FGF, fibroblast growth factor; SHH, Sonic hedgehog; EDA, ectodysplasin; SPRY, sprouty; LEF, lymphoid enhancer binding factor.

Bone morphogenetic proteins (BMPs) can act as growth inhibitors during epithelial budding in feathers, hair and lungs (Hogan, '99), during tooth cusp formation (Weiss et al., '98; Jernvall and Thesleff, 2000) and during budding of rudimentary tooth primordia (Peterkova et al., 2000). BMPs have been detected in the epithelium and mesenchyme at the bud stage of tooth development (Tureckova et al., '95; Vaahtokari et al., '96a; Nadiri et al., 2004) and stimulate apoptosis and inhibit growth in the dental epithelium (Tureckova et al., '96; Vaahtokari et al., '96b; Jernvall et al., '98; Peterkova et al., 2003). In addition, BMP4 is able to inhibit *Shh* expression in tooth primordia culture (Zhang et al., 2000). The BMPs appear to inhibit growth in two ways: by affecting the SHH and/or FGF signaling pathways and by promoting cell cycle arrest (Fig. 8). BMP4 activity can be blocked by the EDA pathway, as this pathway can increase the expression of BMP inhibitors such as CCN2 and follistatin (Pummila et al., 2007). Thus, EDA can exert its growth-activation effect either by the stimulation of *Shh* expression or by the inhibition of BMPs (Fig. 8).

CONCLUDING STATEMENT

In summary, our data have documented for the first time that *Shh* is expressed in the rudimental diastemal R₂ bud at ED 13.5. We demonstrated using quantitative techniques that the R₂ structure, which is often thought to be M₁ at ED 13.5, is arrested in WT mice owing to significantly increased apoptosis and decreased proliferation compared with the molar region. In contrast, the growth arrest of the R₂ was prevented in *Spry2* null mice by the upregulated FGF signaling. There the epithelial proliferation and apoptosis in the R₂ rudiment remained similar to the molar area. Instead of undergoing arrest and incorporation into the M₁ cap at ED 14–15, as it is in WT mice, the R₂ was revitalized and involved in the formation of the supernumerary tooth in mutants. These changes show that the evolutionary suppression of the premolar anlage can be rescued by a relative predominance of growth activators (such as FGF, EDA or SHH) over growth inhibitors.

Our studies may represent an alternative to tooth tissue engineering (Duailibi et al., 2006; Hu et al., 2006; Yen and Sharpe, 2006) by raising the stimulating possibility that the rudimental tooth structures can serve as models of controlled tooth regeneration (Peterkova et al., 2006; D'Souza and Klein, 2007). It is indeed possible that the

reactivation of the dental lamina to form teeth, as shown here with an embryonic diastemal element, can be extended to other regions of the jaw and to other timepoints in development or adult life.

ACKNOWLEDGMENTS

We thank Iva Koppova, Zdenka Lisa, J. Fluck and David Lyons for their excellent technical assistance, and Dr. Gail Martin for the support and encouragement during these studies. O. K. was supported by a grant from the NIH (K08-DE017654).

LITERATURE CITED

- Bolk L. 1922. Odontological essays. On the relation between reptilian and mammalian teeth. *J Anat* 56:107–136.
- Boran T, Lesot H, Peterka M, Peterkova R. 2005. Increased apoptosis during morphogenesis of the lower cheek teeth in tabby/EDA mice. *J Dent Res* 84:228–233.
- Butler PM. 1956. The ontogeny of molar teeth. *Biol Rev* 31:30–70.
- Celli G, Larochelle WJ, Mackem S, Sharp R, Merlino G. 1998. Soluble dominant-negative receptor uncovers essential roles for fibroblast growth factors in multi-organ induction and patterning. *EMBO J* 17:1642–1655.
- Coin R, Lesot H, Vonesch JL, Haikel Y, Ruch JV. 1999. Aspects of cell proliferation kinetics of the dental epithelium during mouse molar and incisor morphogenesis: a reappraisal of the role of the enamel knot area. *Int J Dev Biol* 43:261–267.
- Coin R, Schmitt R, Lesot H, Vonesch JL, Ruch JV. 2000a. Regeneration of halved embryonic lower first mouse molars: correlation with the distribution pattern of non dividing IDE cells, the putative organizers of morphogenetic units, the cusps. *Int J Dev Biol* 44:289–295.
- Coin R, Kieffer S, Lesot H, Vonesch JL, Ruch JV. 2000b. Inhibition of apoptosis in the primary enamel knot does not affect specific tooth crown morphogenesis in the mouse. *Int J Dev Biol* 44:389–396.
- D'Souza RN, Klein OD. 2007. Unraveling the molecular mechanisms that lead to supernumerary teeth in mice and men: current concepts and novel approaches. *Cells Tissues Organs* 186:60–69.
- Duailibi SE, Duailibi MT, Vacanti JP, Yelick PC. 2006. Prospects for tooth regeneration. *Periodontol* 2000 41: 177–187.
- Elomaa O, Pulkkinen K, Hannelius U, Mikkola M, Saarialho-Kere U, Kere J. 2001. Ectodysplasin is released by proteolytic shedding and binds to the EDAR protein. *Hum Mol Genet* 10:953–962.
- Gaunt WA. 1955. The development of the molar pattern of the mouse (*Mus musculus*). *Acta Anat (Basel)* 24:249–268.
- Gruneberg H. 1965. Genes and genotypes affecting the teeth of the mouse. *J Embryol Exp Morphol* 14:137–159.
- Gruneberg H. 1966. The molars of the tabby mouse, and a test for the 'single-active X-chromosome' hypothesis. *J Embryol Exp Morphol* 15:223–244.
- Hogan BLM. 1999. Morphogenesis. *Cell* 96:225–233.

- Hovorakova M, Lesot H, Peterka M, Peterkova R. 2005. The developmental relationship between the deciduous dentition and the oral vestibule in human embryos. *Anat Embryol* 209:303–313.
- Hu B, Nadiri A, Kuchler-Bopp S, Perrin-Schmitt F, Peters H, Lesot H. 2006. Tissue engineering of tooth crown, root, and periodontium. *Tissue Eng* 12:2069–2075.
- Jernvall J, Thesleff I. 2000. Reiterative signaling and patterning during mammalian tooth morphogenesis. *Mech Dev* 92:19–29.
- Jernvall J, Kettunen P, Karavanova I, Martin LB, Thesleff I. 1994. Evidence for the role of the enamel knot as a control center in mammalian tooth cusp formation: non-dividing cells express growth stimulating Fgf-4 gene. *Int J Dev Biol* 38:463–469.
- Jernvall J, Åberg T, Ketunen P, Keranen S, Thesleff I. 1998. The life history of an embryonic signaling center: BMP-4 induces p21 and is associated with apoptosis in the mouse tooth enamel knot. *Development* 125:161–169.
- Kangas AT, Evans AR, Thesleff I, Jernvall J. 2004. Non-independence of mammalian dental characters. *Dev Biol* 268:185–194.
- Kassai Y, Munne P, Hotta Y, Penttila E, Kavanagh K, Ohbayashi N, Takada S, Thesleff I, Jernvall J, Itoh N. 2005. Regulation of mammalian tooth cusp patterning by ectodin. *Science* 309:2067–2070.
- Kavanagh KD, Evans AR, Jernvall J. 2007. Predicting evolutionary patterns of mammalian teeth from development. *449:427–432*.
- Klein OD, Minowada G, Peterkova R, Kangas A, Yu BD, Lesot H, Peterka M, Jernvall J, Martin GR. 2006. Sprouty genes control diastema tooth development via bidirectional antagonism of epithelial–mesenchymal FGF signaling. *Dev Cell* 11:181–190.
- Klein OD, Lyons DB, Balloch G, Marshall GW, Basson MA, Peterka M, Boran T, Peterkova R, Martin GR. 2008. An FGF signaling loop sustains the generation of differentiated progeny from stem cells in mouse incisors. *Development* 135:377–385.
- Kratochwil K, Galceran J, Thontsch S, Roth W, Grosschedl R. 2002. FGF4, a direct target of LEF1 and Wnt signaling, can rescue the arrest of tooth organogenesis in *Lef1*($-/-$) mice. *Genes Dev* 16:3173–3185.
- Kristenova P, Peterka M, Lisi S, Gendrault JL, Lesot H, Peterkova R. 2002. Different morphotypes of functional dentition in the lower molar region of tabby (EDA) mice. *Orthod Craniofac Res* 5:205–214.
- Laurikkala J, Mikkola M, Mustonen T, Åberg T, Koppinen P, Pispä J, Nieminen P, Galceran J, Grosschedl R, Thesleff I. 2001. TNF signaling via the ligand–receptor pair ectodysplasin and edar controls the function of epithelial signaling centers and is regulated by Wnt and activin during tooth organogenesis. *Dev Biol* 229:443–455.
- Lesot H, Vonesch JL, Peterka M, Tureckova J, Peterkova R, Ruch JV. 1996. Mouse molar morphogenesis revisited by three dimensional reconstruction: II) spatial distribution of mitoses and apoptosis in cap to bell stages first and second molar teeth. *Int J Dev Biol* 40:1017–1031.
- Lesot H, Peterkova R, Schmitt R, Meyer JM, Viriot L, Vonesch JL, Senger B, Peterka M, Ruch JV. 1999. Initial features of the inner dental epithelium histomorphogenesis in the first lower molar in mouse. *Int J Dev Biol* 43:245–254.
- MacKenzie A, Ferguson MW, Sharpe PT. 1992. Expression patterns of the homeobox gene, *Hox-8*, in the mouse embryo suggest a role in specifying tooth initiation and shape. *Development* 115:403–420.
- Matalova E, Sharpe PT, Lakhani SA, Roth KA, Flavell RA, Setkova J, Misek I, Tucker AS. 2006. Molar tooth development in caspase-3 deficient mice. *Int J Dev Biol* 50:491–497.
- Minowada G, Jarvis LA, Chi CL, Neubuser A, Sun X, Hacoen N, Krasnow MA, Martin GR. 1999. Vertebrate Sprouty genes are induced by FGF signaling and can cause chondrodysplasia when overexpressed. *Development* 126:4465–4475.
- Nadiri A, Kuchler-Bopp S, Haikel Y, Lesot H. 2004. Immunolocalization of BMP-2/-4, FGF-4, and WNT10b in the developing mouse first lower molar. *J Histochem Cytochem* 52:103–112.
- Nie X, Luukko K, Kettunen P. 2006. FGF signalling in craniofacial development and developmental disorders. *Oral Dis* 12:102–111.
- Obara N, Lesot H. 2007. Asymmetrical growth, differential cell proliferation, and dynamic cell rearrangement underlie epithelial morphogenesis in mouse molar development. *Cell Tissue Res* 330:461–473.
- Peterka M, Lesot H, Peterkova R. 2002. Body weight in mouse embryos specifies staging of tooth development. *Connect Tissue Res* 43:186–190.
- Peterkova R, Peterka M, Vonesch JL, Ruch JV. 1995. Contribution of 3-D computer assisted reconstructions to the study of the initial steps of mouse odontogenesis. *Int J Dev Biol* 39:239–247.
- Peterkova R, Lesot H, Vonesch JL, Peterka M, Ruch JV. 1996. Mouse molar morphogenesis revisited by three dimensional reconstruction: I) analysis of initial stages of the first upper molar development revealed two transient buds. *Int J Dev Biol* 40:1009–1016.
- Peterkova R, Peterka M, Viriot L, Lesot H. 2000. Dentition development and budding morphogenesis. *J Craniofac Genet Dev Biol* 20:158–172.
- Peterkova R, Peterka M, Viriot L, Lesot H. 2002a. Development of the vestigial tooth primordia as part of mouse odontogenesis. *Connect Tissue Res* 43:120–128.
- Peterkova R, Kristenova P, Lesot H, Lisi S, Vonesch JL, Gendrault JL, Peterka M. 2002b. Different morphotypes of the tabby (EDA) dentition in the mouse mandible result from a defect in the mesio-distal segmentation of dental epithelium. *Orthod Craniofac Res* 5:215–226.
- Peterkova R, Peterka M, Lesot H. 2003. The developing mouse dentition: a new tool for apoptosis study. *Ann N Y Acad Sci* 1010:453–466.
- Peterkova R, Lesot H, Viriot L, Peterka M. 2005. The supernumerary cheek tooth in tabby/EDA mice—a reminiscence of the premolar in mouse ancestors. *Arch Oral Biol* 50:219–225.
- Peterkova R, Lesot H, Peterka M. 2006. Phylogenetic memory of developing mammalian dentition. *J Exp Zool B Mol Dev Evol* 306:234–250.
- Peters H, Balling R. 1999. Teeth. Where and how to make them. *Trends Genet* 15:59–65.
- Pummila AM, Fliniaux I, Jaatinen R, James MJ, Laurikkala J, Schneider P, Thesleff I, Mikkola ML. 2007. Ectodysplasin has a dual role in ectodermal organogenesis: inhibition of Bmp activity and induction of Shh expression. *Development* 134:117–125.
- Raff MC. 1992. Social controls on cell survival and cell death. *Nature* 356:397–400.

- Sasaki T, Ito Y, Xu X, Han J, Bringas Jr P, Maeda T, Slavkin HC, Groschedl R, Chai Y. 2005. LEF1 is a critical epithelial survival factor during tooth morphogenesis. *Dev Biol* 278:130–143.
- Setkova J, Matalova E, Sharpe PT, Misek I, Tucker AS. 2007. Primary enamel knot cell death in Apaf-1 and caspase-9 deficient mice. *Arch Oral Biol* 52:15–19.
- Shim K, Minowada G, Coling DE, Martin GR. 2005. Sprouty2, a mouse deafness gene, regulates cell fate decisions in the auditory sensory epithelium by antagonizing FGF signaling. *Dev Cell* 8:553–564.
- Sofaer JA. 1969. Aspects of the tabby-crinkled-downless syndrome. I. The development of tabby teeth. *J Embryol Exp Morphol* 22:181–205.
- Sofaer JA. 1975. Interaction between tooth germs and the adjacent dental lamina in the mouse. *Arch Oral Biol* 20:57–61.
- Tucker AS, Headon DJ, Courtney JM, Overbeek P, Sharpe PT. 2004. The activation level of the TNF family receptor, Edar, determines cusp number and tooth number during tooth development. *Dev Biol* 268:185–194.
- Tureckova J, Sahlberg C, Aberg T, Ruch JV, Thesleff I, Peterkova R. 1995. Comparison of expression of the *msx-1*, *msx-2*, *BMP-2* and *BMP-4* genes in the mouse upper diastemal and molar tooth primordia. *Int J Dev Biol* 39:459–468.
- Tureckova J, Lesot H, Vonesch JL, Peterka M, Peterkova R, Ruch JV. 1996. Apoptosis is involved in the disappearance of the diastemal dental primordia in mouse embryo. *Int J Dev Biol* 40:483–489.
- Vaahokari A, Aberg T, Jernvall J, Keränen S, Thesleff I. 1996a. The enamel knot as a signaling center in the developing mouse tooth. *Mech Dev* 54:39–43.
- Vaahokari A, Aberg T, Thesleff I. 1996b. Apoptosis in the developing tooth: association with an embryonic signaling center and suppression by EGF and FGF-4. *Development* 122:121–129.
- Viriort L, Peterkova R, Vonesch JL, Peterka M, Ruch JV, Lesot H. 1997. Mouse molar morphogenesis revisited by three dimensional reconstruction: III) spatial distribution of mitoses and apoptoses up to bell-staged first lower molar teeth. *Int J Dev Biol* 41:679–690.
- Viriort L, Lesot H, Vonesch JL, Ruch JV, Peterka M, Peterkova R. 2000. The presence of rudimentary odontogenic structures in the mouse embryonic mandible requires reinterpretation of developmental control of first lower molar histomorphogenesis. *Int J Dev Biol* 44:233–240.
- Viriort L, Peterkova R, Peterka M, Lesot H. 2002. Evolutionary implications of the occurrence of two vestigial tooth germs during early odontogenesis in the mouse lower jaw. *Connect Tissue Res* 43:129–133.
- Weiss KM, Stock DW, Zhao Z. 1998. Dynamic interactions and the evolutionary genetics of dental patterning. *Crit Rev Oral Biol Med* 9:369–398.
- Yen AH, Sharpe PT. 2006. Regeneration of teeth using stem cell-based tissue engineering. *Expert Opin Biol Ther* 6:9–16.
- Zhang Y, Zhang Z, Zhao X, Yu X, Hu Y, Geronimo B, Fromm SH, Chen YP. 2000. A new function of BMP4: dual role for BMP4 in regulation of Sonic hedgehog expression in the mouse tooth germ. *Development* 127:1431–1443.
- Zhang Q, Murcia NS, Chittenden LR, Richards WG, Michaud EJ, Woychik RP, Yoder BK. 2003. Loss of the Tg737 protein results in skeletal patterning defects. *Dev Dyn* 27:78–90.

Research article

Open Access

Patterning of palatal rugae through sequential addition reveals an anterior/posterior boundary in palatal development

Sophie Pantalacci*¹, Jan Prochazka^{†2}, Arnaud Martin^{†1}, Michaela Rothova², Anne Lambert¹, Laure Bernard¹, Cyril Charles³, Laurent Viriot⁴, Renata Peterkova² and Vincent Laudet¹

Address: ¹"Molecular Zoology", Institut de Génomique Fonctionnelle de Lyon ; Université de Lyon ; Université Lyon 1 ; CNRS ; INRA ; Ecole Normale Supérieure de Lyon, 46 allée d'Italie, 69364 Lyon Cedex 07, France, ²Department of Teratology, Institute of Experimental Medicine – Academy of Sciences CR, vvi, Videnska 1083, 14220 Prague 4, Czech Republic, ³IPHEP – CNRS UMR 604, UFR SFA, Université de Poitiers, 40 avenue du recteur Pineau, 86022 Poitiers Cedex, France and ⁴"Evo-Devo of Vertebrate Dentition", Institut de Génomique Fonctionnelle de Lyon ; Université de Lyon ; Université Lyon 1 ; CNRS ; INRA ; Ecole Normale Supérieure de Lyon, 46 allée d'Italie, 69364 Lyon Cedex 07, France

Email: Sophie Pantalacci* - sophie.pantalacci@ens-lyon.fr; Jan Prochazka - janproch@biomed.cas.cz; Arnaud Martin - arnaudm@uci.edu; Michaela Rothova - rothovam@biomed.cas.cz; Anne Lambert - anne.lambert@ens-lyon.fr; Laure Bernard - laure.bernard@ens-lyon.fr; Cyril Charles - cyril.charles@etu.univ-poitiers.fr; Laurent Viriot - Laurent.Viriot@ens-lyon.fr; Renata Peterkova - repete@biomed.cas.cz; Vincent Laudet - vincent.laudet@ens-lyon.fr

* Corresponding author †Equal contributors

Published: 16 December 2008

Received: 4 July 2008

BMC Developmental Biology 2008, 8:116 doi:10.1186/1471-213X-8-116

Accepted: 16 December 2008

This article is available from: <http://www.biomedcentral.com/1471-213X/8/116>

© 2008 Pantalacci et al; licensee BioMed Central Ltd.

This is an Open Access article distributed under the terms of the Creative Commons Attribution License (<http://creativecommons.org/licenses/by/2.0>), which permits unrestricted use, distribution, and reproduction in any medium, provided the original work is properly cited.

Abstract

Background: The development of the secondary palate has been a main topic in craniofacial research, as its failure results in cleft palate, one of the most common birth defects in human. Nevertheless, palatal rugae (or *rugae palatinae*), which are transversal ridges developing on the secondary palate, received little attention. However, rugae could be useful as landmarks to monitor anterior/posterior (A/P) palatal growth, and they provide a simple model of mesenchymal-epithelial structures arranged in a serial pattern.

Results: We first determined in which order the nine mouse rugae appear during development. Our results revealed a reiterative process, which is coupled with A/P growth of palatal shelves, and by which rugae 3 to 7b are sequentially interposed, in the increasing distance between the second most anterior ruga, ruga 2, and the two most posterior rugae, rugae 8 and 9. We characterized the steps of ruga interposition in detail, showing that a new ruga forms from an active zone of high proliferation rate, next to the last formed ruga. Then, by analyzing the polymorphism of wild type and *Eda*^{Ta} mutant mice, we suggest that activation-inhibition mechanisms may be involved in positioning new rugae, like for other skin appendages. Finally, we show that the ruga in front of which new rugae form, i.e. ruga 8 in mouse, coincides with an A/P gene expression boundary in the palatal shelves (*Shox2/Meox2-Tbx22*). This coincidence is significant, since we also found it in hamster, despite differences in the adult ruga pattern of these two species.

Conclusion: We showed that palatal rugae are sequentially added to the growing palate, in an interposition process that appears to be dependent on activation-inhibition mechanisms and reveals a new developmental boundary in the growing palate. Further studies on rugae may help to shed light on both the development and evolution of structures arranged in regular patterns. Moreover, rugae will undoubtedly be powerful tools to further study the anteroposterior regionalization of the growing palate.

Background

The development of the mammalian secondary palate is a critical process whereby two bilateral outgrowths of the embryonic maxilla (the palatal shelves) come to fuse at the midline to separate the nasal from the oral cavities. Failure of this process is responsible for cleft palate, one of the most common birth defects in human. That is why the development of the mammalian secondary palate has been extensively studied in the last past thirty years (reviewed in [1]). Secondary palate can be divided in two parts, depending on the nature of the underlying structure: the hard palate, which is ossified (with contribution from two bones: maxilla and palatine), and the posterior soft palate, which is muscular. Both hard and soft palates are covered with a squamous pluristratified epithelium on their oral side. Palatal ridges or *rugae palatinae* are transversal ridges found on the hard palate of most mammalian species, but their number and arrangement are species specific [2]. Laboratory mouse strains have at least nine rugae, a tenth ruga (ruga 7b, Fig. 1) being more or less frequently present, depending on the strain [3,4]. Together with the teeth and the tongue, rugae take part in mastication by helping to sense, hold and mash the food (for review see [4]). Indeed, rugae harbor various types of intraepithelial sensory structures (such as Merckel cells, corpuscular endings and free nerve endings, [5]) and play a sensory role when the food is pressed by the tongue against the hard palate [6]. Moreover, in animals where they are very prominent (e.g. ruminants), rugae also have a mechanical function by helping in mastication and preventing slicing of a mouthful [7].

Compared with secondary palate development, which has been extensively studied, rugae development received little attention. Using electron microscopy scanning and histological sections, Peterkova et al. [4] followed rugae development in mouse soon after palatal shelves begin to form (Embryonic Day = 12.5) to the end of prenatal development and defined 5 stages: I – thickened epithelium burrowed into mesenchyme; II – protruding epithelium with condensed mesenchyme; III – epithelial and condensed mesenchymal cells specifically arranged in a manner resembling magnetic lines of power; IV – transition from primitive to definitive ruga: the fibrous stroma has formed and vaults in the oral direction the epithelium that becomes thinner; V – specific orientation of cells remains visible, the epithelium has started to keratinize and shows similar thickness to the adjacent oral epithelium. Ruga morphogenesis may be less spectacular than that of classically studied skin appendages (such as tooth, hair and feather). However, it shares obvious similarities in very early development with all skin appendages, and as development proceeds further, with a subset of them. Namely, the earliest steps of ruga development (thickening of the epithelium and condensation of the underlying

mesenchyme) are similar in all skin appendages. However, the ruga primordium, a protruding epithelium associated with a condensed mesenchyme, more closely resembles a feather or scale primordium, than a hair or tooth primordium (because in this case the epithelium is invaginated). Later on, the epithelium is vaulted and, on sagittal section, rugae are then similar to scales. Since hair, tooth but also feather and scale early development involves some common pathways [8,9], one can expect that rugae will be no exception. Indeed, there are some indications that key players of skin appendage development may be involved in rugae development: rugae pattern is disrupted in *EctodysplasinA (Eda)* mutant mice [3] and rugae are lost in *Fgf10* mutant mice [10].

Peterkova et al. [4] have shown that mouse anterior rugae develop first, but could not establish the precise ranking of rugae appearance by using only morphological criteria. Knowing this ranking would however allow the use of rugae as anterior/posterior (A/P) landmarks in the growing palate. While A/P regionalization and growth of the palate had been neglected in former studies, these aspects have recently received more attention, as underlined in recently published reviews [1,11]. The best described example is the anterior *Shox2* gene and the posterior *Meox2* gene, which are mutually exclusive [12-14]. Nevertheless data are still scarce, notably due to the difficulties in comparing gene expression borders from one study to another, or even within the same study, since mouse embryos of similar age can show significant differences in developmental stage (for review see [15]). The study of rugae development could help to rationalize these data and contribute to giving palate development a third (A/P) dimension. In the same way, this may also be beneficial to developmental studies devoted to teeth that are close neighbors of rugae.

Apart from their interest as morphological landmarks, rugae are also interesting for three additional reasons. First, study of their development may bring new insights into palatogenesis. Indeed, embryonic rugae have long been suspected to help palatal shelf elevation, the process whereby palatal shelves, which had been growing down the sides of the tongue, suddenly elevate to a horizontal position above the dorsum of the tongue in order to subsequently fuse along the midline. Several authors proposed that embryonic rugae could stiffen palatal shelves and even that cell reorganization in rugae might provide part of the forces needed to horizontalize palatal shelves [16-18]. Second, rugae provide a new and simple model for studying skin appendage formation, as compared with tooth, hair and feather that have long been studied but undergo a much more complex morphogenesis. From an evo-devo perspective, adding a new model to this list would further illuminate how similar, yet differ-

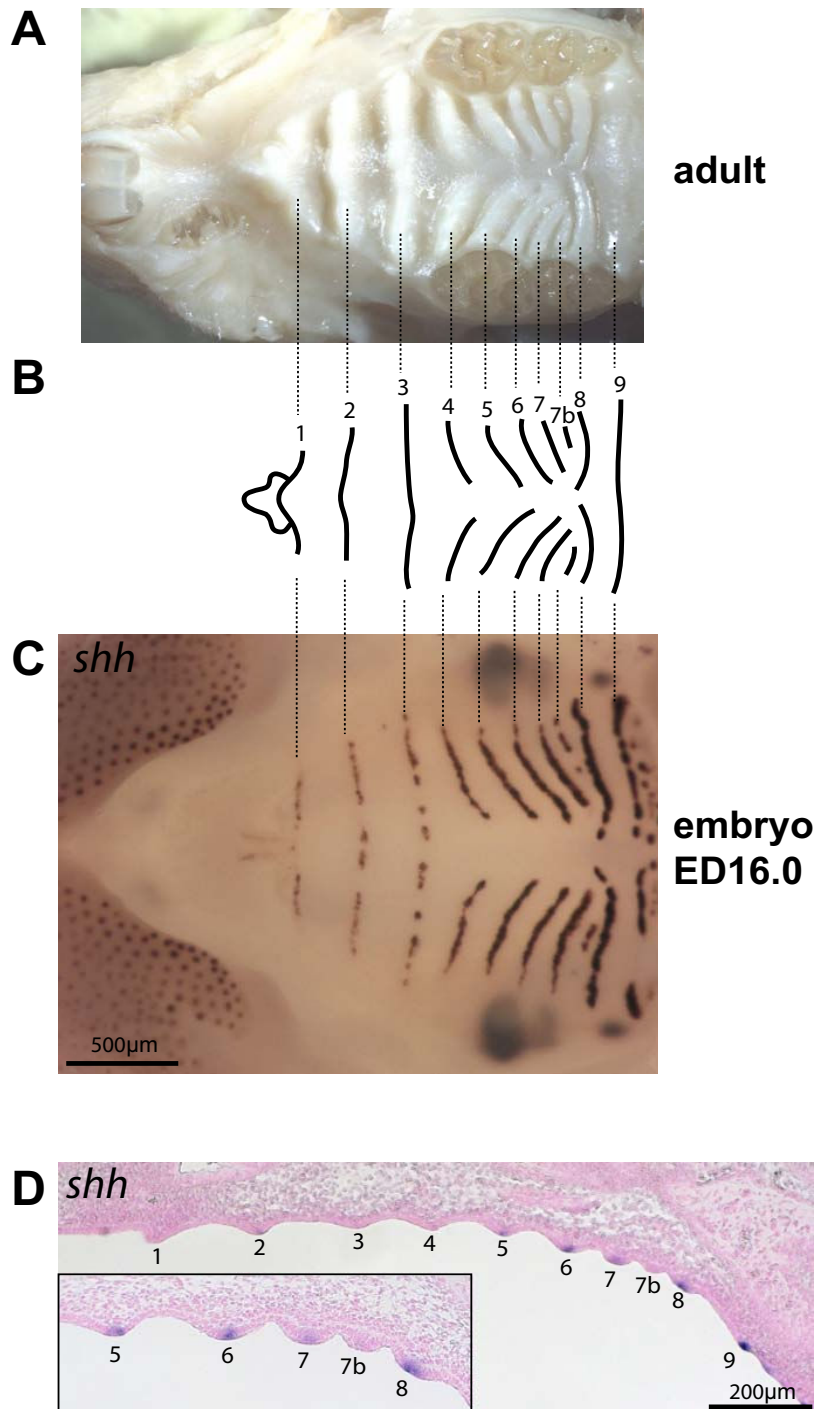


Figure 1
Mouse adult ruga pattern and its visualization in the fetus by *in situ* hybridization against *Shh* gene. (A) The roof of the oral cavity of an adult mouse showing the palatal ridges (*rugae palatinae*) on the hard palate. (B) Mouse rugae pattern with numbering used in this study. Note that ruga 7b was called 8b in other studies (Peterkova et al. 1987; Charles et al. 2007). (C) In ED16.0 fetus, *Shh* gene expression pattern (as seen by whole-mount *in situ* hybridization) prefigures the adult ruga pattern. (D) Sagittal section through the same embryo as in C, showing *Shh* expression in the epithelium at the tip of rugae (see magnification in the low left corner). The absence of *Shh* signal in the rugae 1–4 can be explained by its discontinuity in the anterior rugae at this stage (see C).

ent, genetic networks are used in skin appendage development to result in different shapes [8,19]. Finally, when considering their regular pattern, rugae provide a new model to study how regular arrangement of serial organs is achieved during development.

For all these reasons, we decided to investigate rugae development in more depth. First, we used *Shh* as a molecular marker to establish a precise temporal sequence for rugae appearance in mouse. Our results revealed a reiterative process, by which new rugae are sequentially interposed between the last formed ruga and the second last posterior ruga in the adult mouse, ruga 8. We characterized this interposition process in detail and we provide data suggesting that activation-inhibition mechanisms are involved. Finally, using both mouse and hamster, we show that this process reveals a conserved A/P boundary for palatal development.

Results

***Shh* expression reveals a sequential order for ruga appearance**

In late embryos (ED16.0), the *Shh* gene was expressed in rugae and its expression pattern closely mimicked the adult rugae pattern (compare panel C with panel A in Fig. 1). By looking at earlier stages, we found that the striped expression pattern of *Shh* appeared from very early during development (Fig. 2). As seen on sections, the stripes always corresponded to epithelial cells at the tip of rugae, that at least had reached stage I, i.e. thickened epithelium (for examples, see sections later in figure 5). We reasoned that we should be able to determine the order of appearance of *Shh* stripes by simply looking at a series of staged embryos. For this purpose we needed a reliable series of closely consecutive developmental stages, and to achieve this, we used the staging method proposed by Peterka et al. [15], in which embryo weight (in mg) allows a more precise specification of the developmental stage of embryos exhibiting the same chronological age (in ED = Embryonic Day). Then, starting with ED16.0 and looking back in developmental time to the first rugae initiation, we could identify *Shh* stripes according to numbering of rugae in adults. This method allowed us to trace the developmental fate for each ruga. For clarity however, we present here the results according to progressing developmental time (Fig. 2).

From very early stages and then on (ED12.0–16.0), the sharpest stripe of *Shh* expression corresponded to ruga 8 (shown in red, Fig. 2). Ruga 8 seemed to be the first ruga to appear, but it was very rapidly followed by two stripes corresponding to ruga 2 (in green, Fig. 2A) and ruga 9. From then on, new *Shh* stripes emerged between the last formed ruga and ruga 8. For example, ruga 3 emerged between rugae 2 and 8 (Compare Fig. 2B and 2C), ruga 4

between rugae 3 and 8 (Fig. 2D to 2F, note *Shh* expression was just beginning in Fig. 2E), ruga 5 between ruga 4 and 8 (Fig. 2F to 2H, note *Shh* expression was just beginning in Fig. 2G), and so on, until the last ruga was formed, i.e. ruga 7b (Fig. 2K to 2L; please note that we called this ruga "7b", instead of "8b" as in previous studies, as it was more consistent with order of appearance [3,4]). The only exception was the stripe corresponding to ruga 1 which emerged anteriorly to ruga 2 and almost contemporary with ruga 3 (Fig. 2C to 2E).

In conclusion, this analysis of *Shh* expression allowed us to define a temporal sequence for ruga appearance that is 8-(2,9)-(1,3)-4-5-6-7-7b. Thus, rugae 3 to 7b are consecutively interposed between the last formed ruga and ruga 8. This process, that we call "interposition process", is accompanied by a clear anteroposterior extension of the region between ruga 2 and 8, by comparison to the region between ruga 8 and 9 (compare Fig. 2A and 2L). Moreover, it closely follows the anteroposterior elongation of the whole jaw (see drawings of embryo heads on Fig. 2). During the rest of our study, we chose to focus on the "interposition process" of rugae 3–7b in front of ruga 8, because of the very interesting reiterative aspect of this process and because of its implications for palatal A/P growth.

During the interposition process, new rugae are added in the region immediately posterior to the last formed ruga

As the increasing rugae number results from reiterated steps of ruga interposition, we thought that a detailed description of one of these steps should give us a general understanding of the process. We decided to focus on ruga 5 interposition at ED13.5. This allowed investigation of rugae at different stages (ruga 5 being the youngest) and avoiding potential interference with the horizontalization process (which starts at ED14.0).

We first chose three embryos at three close developmental stages, which corresponded to ruga 5 interposition (ED13.5; embryos I, II, III in Fig. 3A). By counting mitotic and non-mitotic epithelial cells and measuring epithelium thickness on every two second frontal sections of the palatal shelf, we could determine the mitotic index (i.e. a number of mitotic cells per 100 cells) along the A/P axis of the palatal shelf, that is, in gap areas (white in Fig. 3A), in rugae areas (dark grey) and in the region of interest, anterior to ruga 8 (light grey). We found a higher mitotic index in the gap than in the rugae areas (see the gap between ruga 2 and ruga 3 or between ruga 3 and ruga 4, Fig. 3A). Moreover, the mitotic index of ruga 4 progressively decreased from embryo I, where ruga 4 was only poorly developed, to embryo III, where it was fully developed, suggesting that proliferation is progressively decreasing as ruga outgrowth is completed.

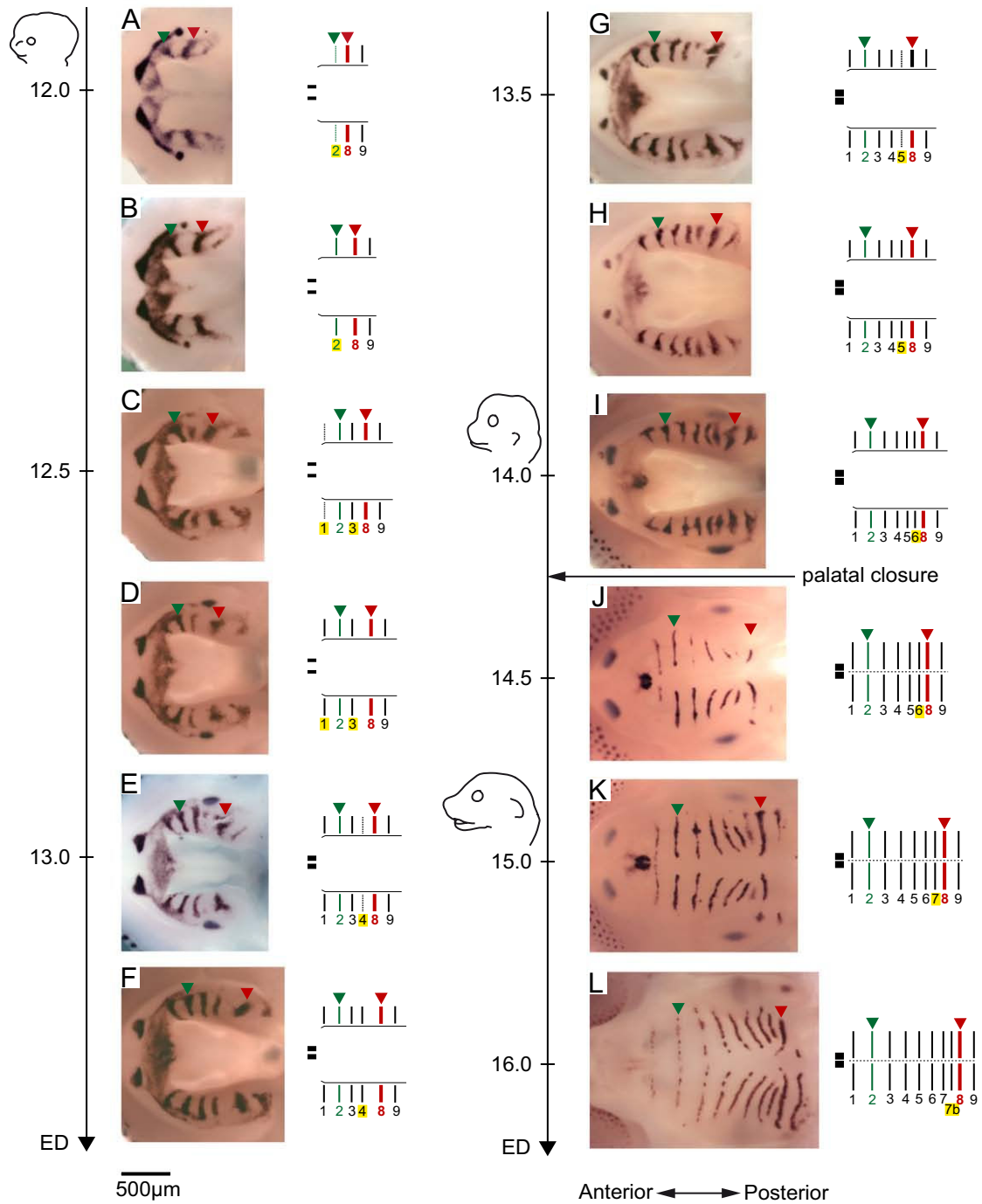


Figure 2
Sequence of mouse ruga appearance as determined by *Shh* expression pattern. Embryos were ranked according to their weight (A: 80–90 mg; B: 95 mg; C: 120–130 mg; D: 120–130 mg; E: 130–140 mg; F: 160–170 mg; G: 160–170 mg; H: 190–200 mg; I: 270–280 mg; J: 300–310 mg; K: 370–380 mg; L: 590–600 mg). Age of embryos (ED = embryonic day) is shown along the time scale. Dissected upper jaws hybridized with a mouse *Shh* probe are shown (left), together with a corresponding scheme showing ruga numbering (right). In this scheme, starting *Shh* expression is represented with dotted lines and the new forming (latest) ruga is underlined in yellow. Drawings of mouse heads are shown at ED 12.0, 14.0 and 15.0 to underline that the A/P elongation of the region delimited by ruga 2 (in green) and ruga 8 (in red) parallels the elongation of the snout. Note that in some cases ruga 9 has been removed during separation of the upper from the lower jaw.

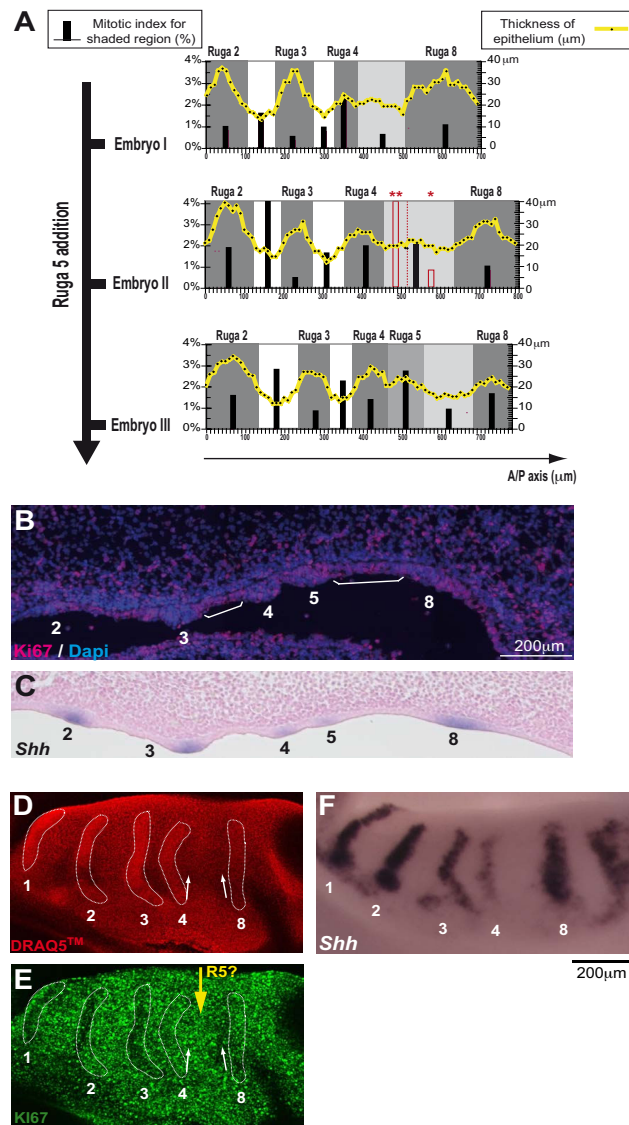


Figure 3

Proliferation in the palatal shelf epithelium. (A) For three embryos at three consecutive stages during ruga 5 addition (ED13.5), a graph is given correlating epithelium thickness and mitotic index along the anterior/posterior (A/P) axis of the palatal shelf. The individual measures of epithelium thickness correspond to black points, joined with a thick yellow line. The mitotic index of the epithelium was calculated for different regions as figured in grey (ruga region), white (gap region) or light grey (region of interest where ruga 5 appears). It is indicated with black bars. For embryo II, an extra mitotic index was also calculated for the anterior third (two red stars) and the posterior two-thirds (red star) of the region of interest and is indicated with red bars. (B) Proliferation along the A/P axis of the palatal shelf as visualized on sagittal cryosections with the Ki67 antibody at ED13.5 (ruga 5 formed) for an embryo of similar weight as embryo III in A. Ki67 positive cells (pink) are proliferating cells, while Ki67 negative cells (blue, dapi nuclear staining) are quiescent cells. White brackets point the ruga3-ruga4 gap and the region between the last formed ruga (5) and ruga 8. (C) For an equivalent embryonic stage and sectioning plane as in B, sagittal section of an embryo after whole mount *in situ* hybridization with the *Shh* probe. (D) A dissected palatal shelf at ED13.5 (ruga 5 in formation) was stained with the nuclear marker Draq5TM. The cells are more densely packed in well-formed rugae, allowing their visualization. (E) The same palatal shelf was immunolabeled with Ki67 to show proliferation in the epithelium. Note that Ki67 negative cells are found mainly in rugae (especially in more mature rugae 1–3) and in the region immediately anterior to ruga 8 (compare labeling in the regions pointed by the two white arrows). (F) A littermate embryo of similar weight was hybridized with the *Shh* probe to help staging. The large space between ruga 4 and 8 confirmed that ruga 5 is already developing, as for embryo II in A.

In the region anterior to ruga 8 (light gray), the epithelium was only a little bit thicker than in gap areas, and curiously, the mitotic index was low, except for embryo II. In this case however, we noticed that the repartition of mitosis was strongly biased in favor of the anterior third of the region (see the mitotic index in red). This might correspond to the formation of ruga 5, since in the older embryo III, ruga 5 thickening was now discernable just next to ruga 4. In conclusion, ruga 5 seems to form from a burst of proliferation in the region immediately posterior to ruga 4, while the region immediately anterior to ruga 8 tends to proliferate at lower level. A true gap between ruga 4 and ruga 5 is only formed later on (see later at ED14.0 on figure 5).

In order to confirm these results, we used the Ki67 antibody to label head sagittal cryosections of embryos showing similar weight to the embryo III (Fig. 3B–C). This antibody is known to label cells engaged in the cell cycle, but not quiescent cells. Moreover it discriminates interphasic cells (discrete nucleolar signal) from mitotic cells (very sharp signal), and can thus be used as an indicator of proliferation activity. Results were consistent with the quantitative evaluation of mitotic index. Quiescent cells (non labeled cells) were found mostly in rugae, thus explaining their overall low mitotic index (Fig. 3B). The forming ruga 5 had more mitotic cells as compared with other rugae, in agreement with its higher mitotic index. Finally, it seems that the gap region just in front of ruga 8 had more quiescent cells than other gap regions (compare with the gap between ruga 3 and 4, white brackets), in agreement with a low mitotic index.

To complete these results obtained on sagittal sections, we used a complementary, whole mount approach. We performed whole-mount immunohistochemistry with Ki67 antibody and visualized the surface epithelium with confocal microscopy (Fig. 3D–F). Post-staining with DRAQ5TM allowed visualization of cell nuclei. Therefore the rugae could be well detected, possibly because cells are more densely packed there (Fig. 3D). This pattern closely resembled that seen through *Shh* expression in a littermate embryo of similar weight (Fig. 3F). As judged from the distance between ruga 4 and ruga 8, the stage seemed equivalent to that of "embryo II" in Fig. 3A. Results were again fully consistent with counting of mitotic index: unlabeled, quiescent, cells were mostly found in rugae and in the region next to ruga 8; on the other hand labeled, proliferating, cells were mostly found in gaps and in the region next to ruga 4, where ruga 5 will form (compare the two white arrows in Fig. 3E). We concluded that epithelial proliferation is high in all gaps, except in a quiescent zone just anterior to ruga 8. In contrast, proliferation is low in rugae, except in the new ruga, which seems

to form from an active zone just posterior to lastly formed ruga.

Observations on wild type and *Eda^{Ta}* mutant strains suggest that formation of a new ruga is only allowed at a distance from flanking rugae

In a previous study, we studied variations of the ruga pattern in *Eda^{Ta}* mice and in their wild type counterpart [3]. These variations had drawn our attention because they revealed morphological correlations between consecutive rugae.

First, in the wild-type sample we studied, ruga7b was highly polymorphic, as reported for other wild type backgrounds [4,20]. It was either absent, short or fully formed (respectively in 9%, 56% and 35% of palatal halves Fig. 4A). As shown above, ruga 7b forms last, between ruga 7 and ruga 8 (Fig. 2). We found that its presence was associated with a higher distance between ruga 7 and 8 (Fig. 4A). A clear threshold in distance was systematically exceeded in half palates with ruga 7b and never reached in half palates without 7b (Fig. 4A). Moreover, whether ruga 7b was fully formed was also clearly correlated with higher distance between ruga 7 and 8 (Fig. 4A). Finally, variations in medio-lateral position and shape of ruga 7b also correlated with variations of the distance between ruga 7 and 8 (arrows in Fig. 4A). In summary, presence of ruga material correlated with exceeding a threshold distance between ruga 7 and 8.

These observations suggest a model where formation of a new ruga "n+1" somehow depends on the distance to its neighboring rugae at the time it forms, i.e. rugae "n" and 8. If true, then we expect that any mis-positioning of ruga "n" should be propagated to ruga "n+1" (Fig. 4B). We had seen this kind of correlations in the *Eda^{Ta}* mice, in which patterning anomalies are frequently found in adults [3]. These anomalies occur non symmetrically and include ectopic rugae, short rugae and mispositioning disrupting symmetry. From then on, our purpose was not to decipher how these anomalies occur, but whether and in which way an anomaly on ruga "n" is linked with an anomaly of ruga "n+1". According to our putative model, several predictions can be made depending on the type of anomaly in ruga "n" (Fig. 4B), which can be tested in *Eda^{Ta}* mice. In order to detect even subtle patterning anomalies, we chose to look at the *Shh* pattern in late embryos (ED14.5–15.0) rather than at the adult ruga pattern.

In a model where ruga formation is only allowed at a distance from preexisting rugae (i.e. out of grayed regions in Fig. 4B), an abnormal bending (towards posterior or anterior) of ruga "n" should be propagated to ruga "n+1". For example, ruga "n" bending towards posterior should repel ruga "n+1" formation (both in space and time: until ruga

n to ruga 8 distance is wide enough); on the contrary, ruga "n" bending towards anterior should precipitate ruga "n+1" formation. Both cases were found in tabby mice (Fig. 4D–E; yellow and green arrows, compare with the normal pattern in 4C). Then, the model predicts that a shortening of ruga "n" should result in bending of corresponding extremity of ruga "n+1" towards the free place anterior (Fig. 4B). In *Eda^{Ta}* mice, shortening of ruga 5 was indeed followed by a bending of ruga 6 towards the anterior (Fig. 4F–G; blue arrows). Finally, a small patch of ectopic ruga posterior to ruga "n" should repel ruga "n+1" formation and result in ruga "n+1" posterior bending. Alternatively, such an ectopic patch may form after its flanking rugae, because at this site, the two of them are abnormally distant and consequently fail to prevent ruga formation. Whatever the case, ectopic patches should be found associated with ruga bending (Fig. 4B). In *Eda^{Ta}* mice, small ectopic patches were eventually found between ruga 2 and 3 (Fig. 4D, 4E, 4H; pink arrows) and ruga 4 and 5 (Fig. 4D, 4H, 4I; pink arrows). In each case, the lateral extremity of ruga 3 and ruga 5 were abnormally bent towards the posterior (compare with Fig. 4C which represents the normal pattern). In conclusion, all these observations are consistent with a model where ruga interposition is only allowed at a certain distance from the flanking rugae.

Ruga 8 marks a boundary of gene expression in the developing palate

As shown by the previous observations, ruga 8 has a very special position in the palatal shelf and we wondered if it may delimit different territories in the developing palate. We thus looked at expression of three genes, *Shox2*, *Meox2* and *Tbx22*, that are known to be differentially expressed along the anterior/posterior axis [12,14,21,22]. Interestingly, whatever the embryonic stage we looked at (ED12.5, ED13.5, ED14.0), *Shox2* was found expressed in the mesenchyme anterior to ruga 8 (including the mesenchyme directly adjacent to ruga 8), while *Meox2* and *Tbx22* were always found expressed in the mesenchyme just posterior to ruga 8 (Fig. 5). Thus, the limit of expression of *Shox2*, *Meox2* and *Tbx22* genes in the underlying mesenchyme coincides with ruga 8 at consecutive embryonic stages, at least before palatal shelves elevation. Taken together, these data suggested that ruga 8 marks a developmental boundary delimiting two distinct parts of the palatal shelves.

The golden hamster ruga 7 is equivalent to mouse ruga 8 and marks the same boundary of gene expression

In order to further explore the possibility that mouse ruga 8 indeed represents an important developmental boundary, we looked at rugae development in a distant murid, the golden hamster (*Mesocricetus auratus*). Its posterior palate morphology is quite different from the mouse (Fig.

6A). This species harbors only 7 obvious rugae and a smooth eighth one bordering the soft palate. As for the mouse, we used a probe against the *Shh* gene (ma *Shh*) to determine the order of rugae appearance. Due to difficulties in detecting pregnant females at young embryonic stages, we could not determine the order of appearance for the earliest rugae, and our series started with embryos having already 5 *Shh*-stripes corresponding to rugae 1,2,3,7,8. From then on, rugae were progressively added by interposition between the latter formed ruga and ruga 7 (Fig. 6B), resulting in the partial sequence (1,2,3,7)-4-5-6. Ruga 7 in hamster is thus functionally equivalent to ruga 8 in mouse, and we called these very special rugae the "boundary rugae".

As compared with the mouse, the boundary ruga is found relatively more anteriorly than in the mouse (Fig. 6C). Nevertheless, in hamster as in mouse, the boundary ruga corresponded to the boundary between *Shox2/Meox2* expression in embryos of weight class 190–200 mg (Fig. 6D, and see sections in Fig. 6E). We concluded that, since it is found in two species with different ruga number and pattern, the overlap between the boundary ruga and the *Shox2/Meox2* boundary is unlikely to be fortuitous. Rather, it strongly suggests that the boundary ruga marks a conserved developmental boundary in the murid palate.

Discussion

Murid rugae appear through posterior interposition

As many other mesenchymal-epithelial organs, palatal rugae show *Shh* expression at an early stage of their development [23]. However, in rugae, this expression also persists during most stages of their development (Fig. 2). In the present paper, we used this early and persistent marker to decipher the sequence of mouse palatal rugae formation from an early stage where only ruga 2, 8 and 9 are clearly discernable. We showed that mouse palatal rugae 3 to 7b form in a sequential manner, whereby they are interposed between the last formed ruga and ruga 8: first ruga 3 between ruga 2 and 8, then ruga 4 between ruga 3 and 8, and so on (Fig. 2). We called this process "posterior interposition", and we called ruga 8 the "boundary ruga". We further showed that the same process is found during the development of another murid rodent, the golden hamster *Mesocricetus auratus*, but in that case less rugae are present and ruga number 7 is the boundary ruga. Variations in number of rugae are common between close rodent species (see the monograph by Eisentraut [2] or variations in species of the *Praomys* complex [24]). They are even common among members of the same species, as exemplified here with ruga 7b of the laboratory mouse, or as also for wild rodent species [2]. These variations could be explained in the light of the interposition process: adding or removing one ruga may be easy to achieve, since it

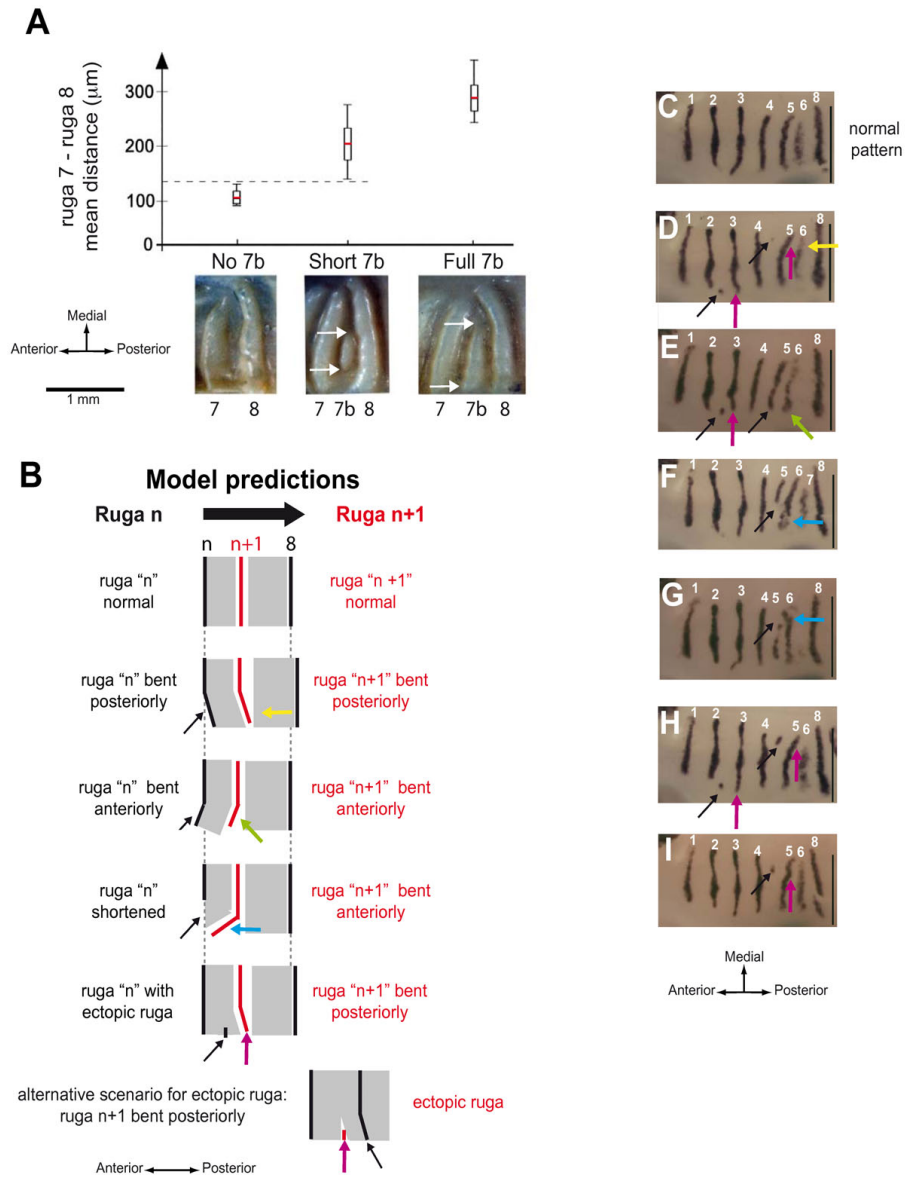


Figure 4

Interposition of a new ruga depends on the distance between previously formed rugae. (A) In wild type mouse adult palates, presence of ruga 7b, and in case of presence, full extension of ruga 7b, are correlated with higher distances between its neighbors, rugae 7 and 8. Pictures show the 3 possible states of ruga 7b: absent (no 7b), short (short 7b) or fully developed (full 7b). Adult half palates of wild type mice were distributed into three classes according to ruga 7b state and the inter-rugae distance between rugae 7 and 8 was measured (see material and methods for details). For each class, the graphics shows the mean inter-rugae distance value (red line), the standard deviation (white rectangle) and the range of variation (vertical black line). (B) In a model where a new ruga can only form at a threshold distance from pre-existing rugae, the shape of "ruga n" allows prediction of that of ruga "n+1". A simplified scheme of ruga "n+1" interposition is shown with ruga n, ruga 8 (in black) and the new ruga "n+1" (in red). In the model, formation of ruga is only allowed at a threshold distance from pre-existing rugae, i.e. out of grayed fields. An abnormal shape of ruga "n" (black arrow) will change the shape of the grayed field, and consequently the shape of ruga "n+1" (color arrow). (C – I) In *Eda^{Ta}* embryos, propagation of ruga shape anomalies from ruga "n" to ruga "n+1" fit with the previous model. The pictures show half palates of ED14.5–15.0 embryos heterozygous (C, E – I) or homozygous (D) for the *Eda^{Ta}* mutation and hybridized with *Shh* probe. As in B, paired arrows point the abnormal shape of ruga "n" (black arrow) and the associated abnormal shape of ruga "n+1" (color arrow, color according to B). For each picture, scale bar is 500 μm.

just involves one step more or one step less in the reiterative process of ruga interposition.

Ruga addition proceeds from an active zone at the posterior end of the last formed ruga

In order to better understand the mechanism of ruga interposition, we focused on close developmental stages around ED 13.5, from morphological appearance of ruga 4 to that of the next ruga, ruga 5.

First, we showed that the proliferation rate progressively decreased in the epithelium of ruga 4 as it became thicker, and finally reached the low level seen in older rugae 2 and 3. By opposition and, as shown previously [25,26], gaps between rugae showed a higher proliferation rate, consistent with the progressive moving away of rugae. The well formed embryonic ruga or "primitive ruga" (as defined by Peterkova in [4]) thus appears as a protruding thickened epithelium comprising cells with a low proliferation level. Of note, *Shh* expression is turned on only lately during formation of this primitive ruga, since it was always found associated with clear thickened epithelium. Interestingly, during tooth development, an epithelial signaling center known as the "enamel knot" is also formed by low (non-)proliferating and densely packed cells expressing *Shh* [27]. Moreover, another characteristic of the enamel knot, namely the presence of apoptotic cells, was also noted (in ruga 2 and 3 at ED13.5, M.R. data not shown – see also [28]). The enamel knot signals to the underlying mesenchyme and to the adjacent growing epithelium [27]. On a sagittal section, the primary ruga with the growing gap epithelium on both sides may thus be compared to the middle ridge of a tooth cap comprising the enamel knot and the adjacent growing epithelium.

Then, we showed that ruga 5 morphologically appears just next to ruga 4, from a region of intermediate epithelium thickness, which underwent a burst of proliferation. In contrast, the region situated immediately anterior to ruga 8 seemed silent: it showed a constant low proliferation rate. Importantly, what we showed here for ruga 5 probably holds true for other interposed rugae, since new rugae are always found closer to their predecessor than to ruga 8 (see with *Shh* stripes on Fig. 2, or on sections Fig. S2). Ruga formation seems thus to proceed by a burst of cell proliferation induced next to the last completed primitive ruga. But what exactly is this burst of proliferation responsible for? Indeed, ruga formation involves two merged events: i) A/P extension of the region between the last formed ruga and ruga 8 (in light grey in Fig. 3A) and ii) the formation of a new ruga (i.e. local thickening of the epithelium) in the free space. In principle, the burst of proliferation should participate at least in thickening since it just precedes it in time (Fig. 3A). It is less clear whether it also participates in A/P extension, since at the

time when we observed the mitotic burst, the A/P extension was already obvious (see Fig. 3A embryo 2 or Fig. 3C). However, since cell growth precedes cell mitosis, the A/P extension could in principle be seen before the mitotic burst itself. Alternatively, other mechanisms may also have been involved in this A/P extension, among which for example changes in cell shape or cell rearrangements. Further studies will be necessary to understand the precise dynamics of this region, and how the mechanism of ruga interposition is linked to A/P growth of the palate and of the whole jaw.

Positioning of a new ruga likely involves activation-inhibition mechanisms

We showed that normal patterning of rugae, and response of the patterning system to anomalies in one ruga, are fully consistent with a model according to which ruga formation is only allowed at a threshold distance from other rugae. Generation of such threshold distances for organ induction often relies on the antagonist activity of activators and inhibitors, in mechanisms known as "activation-inhibition". Of note, such mechanisms have been classically involved in spacing of other ectodermal organs, such as hair and feather [29-31], and they are followed by *Shh* expression in the newly formed placode [8]. Based on our data and by analogy with hair and feathers, we propose that activation-inhibition mechanisms are involved in positioning new rugae during the interposition process, which finally express *Shh*. From then on, we can use our knowledge of these mechanisms in hair and feathers to point candidate pathways to explore in future studies.

Activation of the Wnt/ β -catenin pathway is a key early event for early formation and spacing of hair and feathers [9,31,32]. During ruga interposition however, we could not detect any activation of the Wnt/ β -catenin pathway as revealed by the TOP-GAL reporter transgene (AM and SP, data not shown), whereas we found activation in hair and tooth, as previously reported [33,34]. Even if we cannot rule out that the TOP-GAL reporter failed to report Wnt/ β -cat pathway activation in rugae while it did correctly in neighboring teeth, this preliminary finding suggests that the canonical Wnt/ β -cat pathway is not involved in ruga interposition.

Two other pathways have been directly involved in correct spacing and early formation of both hair and feathers: the EDA/EDAR pathway favors placode formation [35,36] while proteins of the BMP superfamily are responsible for establishing an inhibitory field around forming placodes [30,37]. *Eda* (encoding the EDA ligand) is expressed in the epithelium of the palate (SP, data not shown and [38]), and we previously have shown increased variability and occurrence of anomalies in the ruga pattern of *Eda*^{Tabby} (*Eda*^{Ta}) null mutant mice [3]. However, we found no

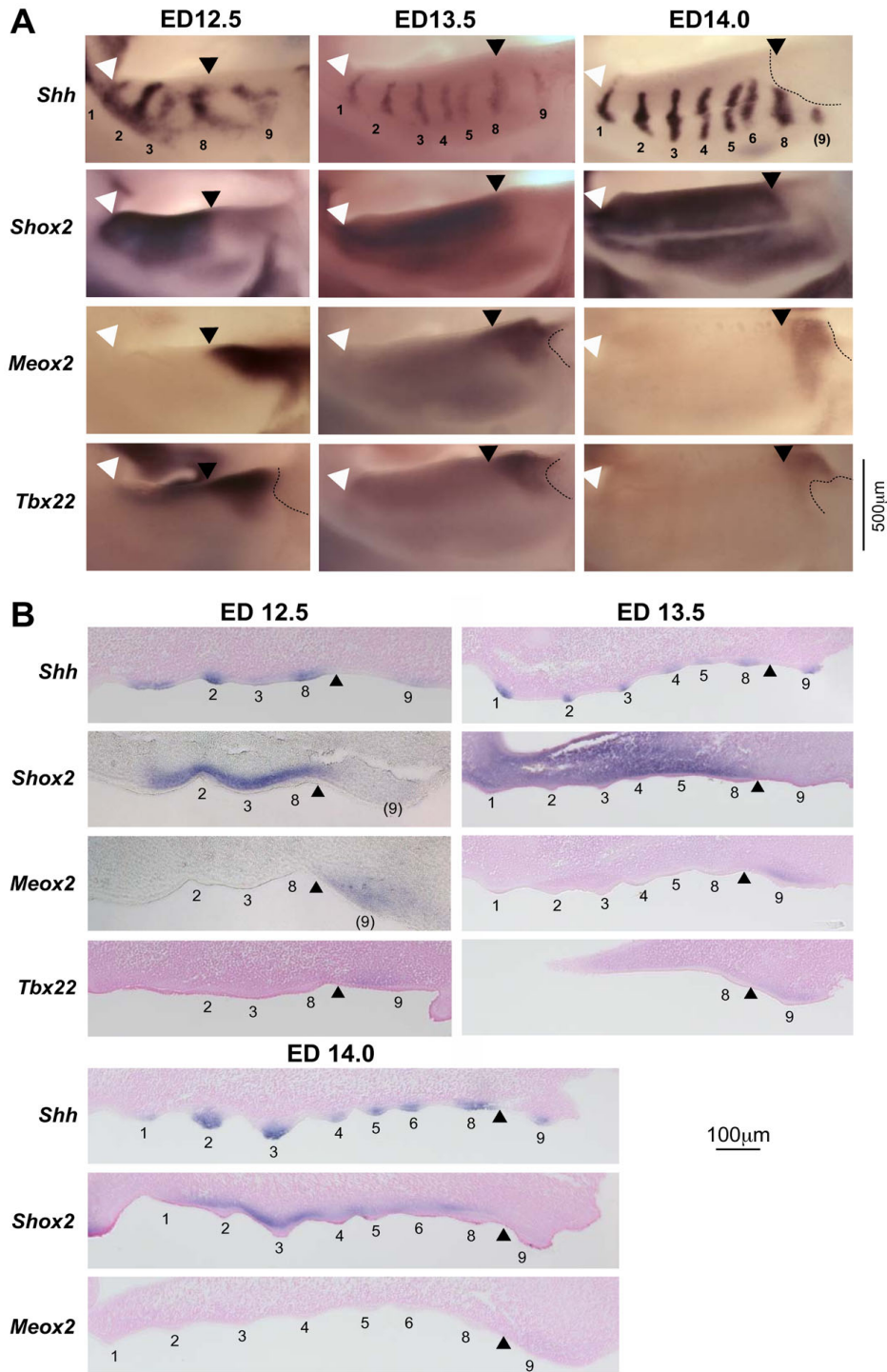


Figure 5

Anteroposterior limits of expression of *Shox2*, *Meox2* and *Tbx22* genes coincide with ruga 8 in the mouse.

Whole mount in situ hybridization for *Shh*, *Shox2*, *Meox2* and *Tbx22* were performed on dissected mouse upper jaws at three embryonic stages (ED12.5, ED13.5 and ED14.0, embryos of similar weight classes) (A), and were followed by sectioning, and counterstaining with nuclear red (except for *Shox2* and *Meox2* at ED12.5) (B). Rugae are numbered (with brackets when damaged by dissection). The white arrowhead points the anterior limit of the palatal shelf and the black arrowhead points ruga 8. The dashed line indicates where the very posterior part of the shelf was damaged by dissection.

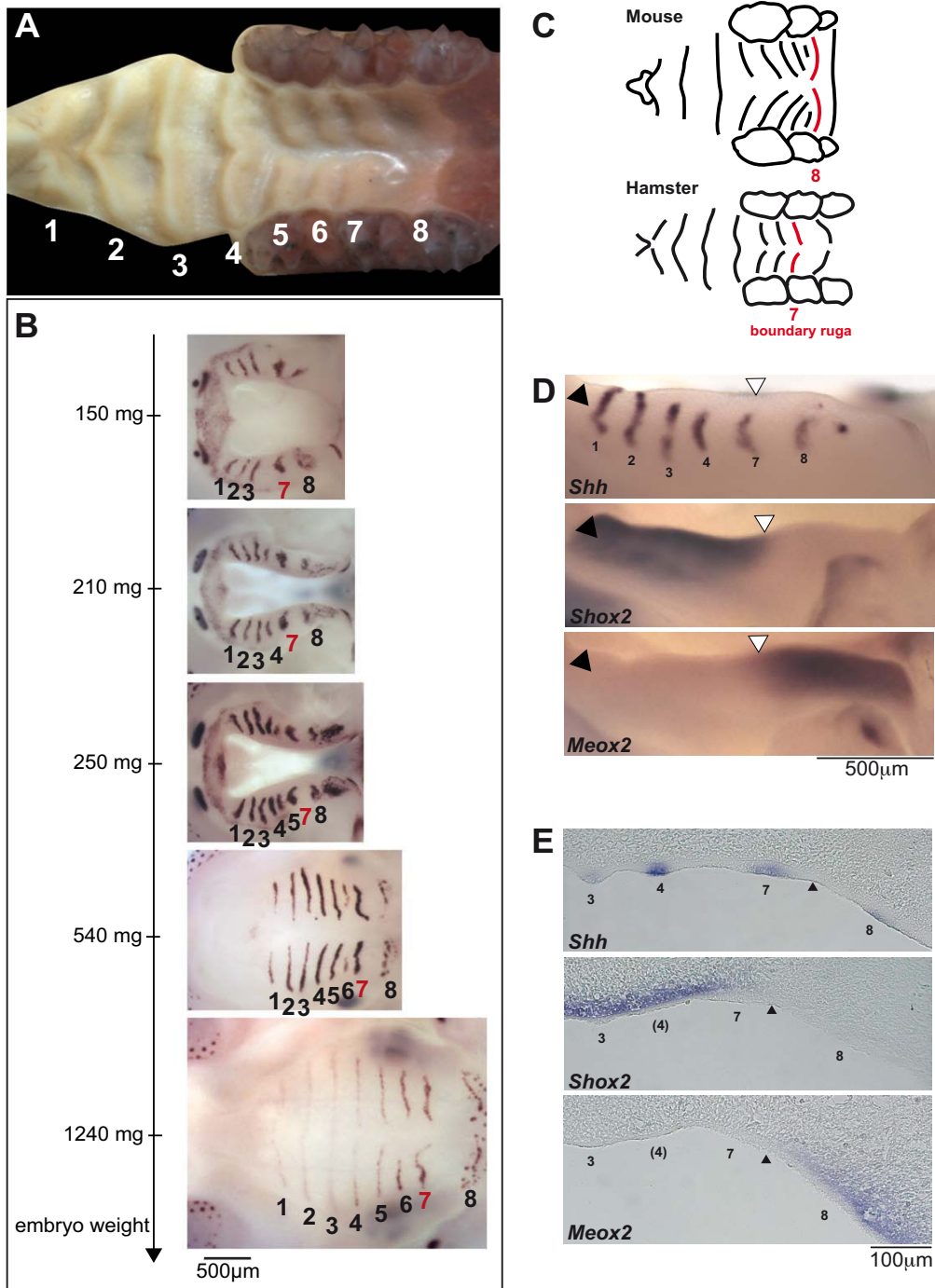


Figure 6
Ruga 7 in hamster is equivalent to ruga 8 in mouse and also coincides with A/P *Shox2/Meox2* expression boundary. (A) Ruga pattern and numbering in the hamster *Mesocricetus auratus*. (B) Sequence of hamster ruga appearance as followed with *Ma-Shh* probe. Embryos were ranked according to their weight. (C) Drawings of mouse and hamster palate showing that the boundary ruga is found more anteriorly in the hamster by comparison to the mouse. Drawings were made from pictures shown in Fig. 1A and 6A. Scale was adapted for comparison. (D) Whole mount *in situ* hybridization of hamster embryonic upper jaws (weight class: 170–180 mg) with *Ma-Shh*, *Shox2* and *Ma-Meox2* probes. (E) Sections of hamster embryonic upper jaws following whole mount hybridization with *Ma-Shh* (weight class: 170–180 mg), *Shox2* and *Ma-Meox2* (weight class: 160–170 mg) probes.

detectable expression of *Edar* in the developing palate, nor of I κ B (SP, data not shown), which is a feedback transcriptional target of EDAR signaling in both hair and tooth [35,39,40]. These results thus do not favor a direct role of the EDA/EDAR pathway in rugae interposition. In contrast, we found that *Bmp7* is expressed at the tip of the primitive rugae, in a pattern very similar to *Shh*. BMP7 is thus a good candidate for establishing an inhibitory field around rugae (Fig. 7).

FGF signaling is also involved in placode formation, although it has been formally demonstrated only for feathers but not yet for hair [41,42]. Here data from the literature suggest that it is actually another interesting pathway for ruga interposition. Indeed, epithelial FGFR2b is supposed to be activated by mesenchymal FGF10 and is necessary for *Shh* expression in rugae [10]. Moreover FGF10 beads can induce ectopic *Shh* expression, and *Fgf10* knock-out mice lack rugae [10]. Finally, Welsh et al. [10,43] demonstrated that an inhibitor of FGF signaling, SPRY2, is necessary to restrict the proliferation rate in the palate and to achieve the normal pattern of rugae. FGF signaling might thus be one component of the activation-inhibition mechanism that we propose (Fig. 7). Alternatively, it could also play a more indirect role, by favoring palatal growth, which in turn can change the activation-inhibition equilibrium.

In conclusion, this preliminary survey of candidate pathways suggests that ruga interposition only involves a limited number of the pathways that have been implicated in hair and feather initiation. While the Wnt and EDA-EDAR pathways do not seem to be involved, the FGF and BMP pathways should be investigated in the future. But what are the reasons for these differences? At least three aspects shown in this article may be relevant. First, new rugae form from a region of already intermediate epithelium thickness (by comparison to the oral epithelium). Second, an obvious difference between rugae and hair or feather is the extent of the growth following the early steps of development. In this respect also, rugae more closely resemble scales. Here it is interesting to note that the growth difference between scales and feathers has been suggested to rely on different levels of activation of the Wnt/ β -catenin pathway [9,31,32]. Third, new rugae do not form in a naïve field, like mouse primary hair (which arise periodically and simultaneously from a field with no apparent patterning information), nor in a field with an open side, like dorsal chicken feathers (for which a central row of feather buds is established and then rows are progressively added laterally), but they are interposed in a field between two already formed rugae. Similarly, it should be noted that formation of the very first rugae (i.e. formation of rugae 2 and 8, that was not addressed here) might require other pathways than ruga interposition.

Rugae reveal the allometry of palatal growth and a new developmental boundary for palate development

We propose that ruga 8 in mouse and ruga 7 in the golden hamster, which are the rugae in front of which new rugae are added, can be called "boundary rugae". Indeed, the palatal shelf can be divided in two parts (Fig. 7): one, anterior to the boundary ruga, which A/P elongation seems rapid and where new rugae are added, and a second, posterior to the boundary ruga, which A/P elongation seems slower. We show that in both species, the boundary ruga marks the posterior end of *Shox2* expression domain in the mesenchyme of the palatal shelf. In contrast, *Meox2* and *Tbx22* mesenchymal domains are found posteriorly to the boundary ruga. As a consequence of the different rate in A/P elongation between the anterior and the posterior part, this *Shox2/Meox2* boundary seems to move posteriorly during development (Fig. 5), as it was initially noted by Li et al. (2007, [13]). In their proliferation assay, these authors found no obvious difference that could explain the different rate of expansion of the two domains. As a consequence, they proposed that mesenchymal *Meox2* expressing cells could be recruited into the *Shox2* domain to allow its expansion (these cells would then turn off *Meox2* expression and turn on *Shox2* expression). Importantly, such a recruitment model is less conceivable for explaining the different rate of expansion of the upper epithelial domains, where the boundary ruga seems to represent a stable morphological boundary. This leaves two possibilities: either only the epithelial boundary is stable, and would be able to reprogram the underlying mesenchyme while new cells are recruited, or there is a stable mesenchymal-epithelial boundary, and the *Shox2* domain and *Meox2/Tbx22* domains are separated compartments. Only lineage studies will help to discriminate between these two possibilities. In any case, our results clearly demonstrate that the boundary ruga marks a developmental boundary in the A/P organization of the palate. Of note, this organization may be shared with human since *Shox2* expression is found in the anterior but not posterior palate of human embryos [14].

Finally, does this developmental boundary coincide with a known morphological boundary of the mouse head? In the adult head, the boundary ruga clearly does not coincide with the hard/soft palate limit, since both ruga 8 and 9 in the adult mouse (or ruga 7 and 8 in the hamster) are supported by the hard palate. However, we cannot exclude that, during the embryogenesis, the embryonic boundary ruga could actually correspond to the prospective hard/soft palate limit, but that this early relationship would be scrambled during later ontogenesis. In agreement with this view, *Shox2* has been related to hard tissue morphogenesis (limb chondrogenesis [44]) while *Meox2* has been related to soft tissue morphogenesis (limb muscle differentiation [45]). Alternatively, since in the adult

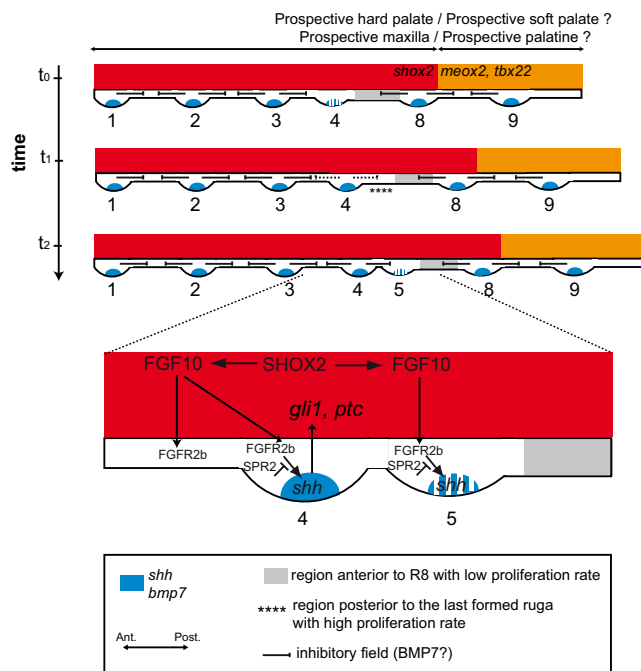


Figure 7
A tentative model for ruga interposition and palate organization. This model synthesizes data as shown in this paper together with data from the literature (see text for details).

mouse and hamster, the boundary ruga grossly sits on the top of the suture between the maxilla and the palatine bone, the identified developmental boundary might represent the prospective limit between the maxilla and the palatine. Again, lineage studies will be necessary to highlight the exact nature of this new developmental boundary.

A working model for coordinated ruga interposition and A-P growth of the palate

We propose a working model, where ruga interposition is coordinated with A/P growth of the palate (Fig. 7). In this model, the palate is organized in two domains: an anterior domain, including the rugae between ruga 1 and the boundary ruga 8, where the mesenchyme is *Shox2* positive, and a posterior domain, corresponding to the region posterior to ruga 8, and including both ruga 9 and the "soft palate", as generally defined, which is *Meox2* and *Tbx22* positive (but *Shox2* negative). The anterior domain grows rapidly (for example under the influence of FGF signaling), which progressively increases the distance between already formed rugae. These rugae maintain an inhibitory field around them and, for example, the BMP7 protein, by diffusing from the tip of rugae, and this could help to maintain cells in a "non rugal" fate (Fig. 7, t_0). We noticed that *Bmp7* expression was turned on late during

formation of one ruga (just as *Shh*). As a consequence, the inhibitory influence may be locally low just next to the last formed ruga, because A/P extension has moved more mature rugae away, and the last formed ruga still does not exert its inhibitory influence (see Fig. 7, t_0). The cells there may then be able to adopt rugal fate and undergo proliferation to form the ruga thickening (Fig. 7, t_1). Later on, *Shh* and *Bmp7* become expressed at the tip of the newly formed ruga, and a true gap is formed. As previously mentioned, FGF signaling (from mesenchyme) probably participates in the induction and/or maintenance of *Shh* expression [10]. In turn, epithelial *Shh* signals to the underneath mesenchyme where target genes like *Gli1* and *Ptc* are induced [23].

In summary, we propose that the continuous growth of the palate, coupled with a simple activation-inhibition mechanism, and a local disequilibrium (local low inhibition next to the last formed ruga), could generate oscillations that would be responsible for periodic and asymmetric ruga interposition. This working model could be tested in the future by combining mathematical modeling with functional test of candidate signaling molecules.

Conclusion

In this article, we showed that rugae are sequentially added to the growing palate, in an interposition process that seems to be dependent on activation-inhibition mechanisms and reveals a new developmental boundary in the growing palate. These findings open two main directions. First, they define rugae as a new and simple model for studying not only origins of differences in development of skin appendages but also the patterning of serial structures. The latter aspect may benefit from already extensively studied systems such as somites and, in turn, could help to understand the patterning of molars, which are neighboring but much more complex serial structures also belonging to skin appendages. Of note, the complex question of molar segmentation was first addressed only very recently and could involve the two pathways pointed out for rugae in our discussion: the FGF and BMP pathways [46]. Second, these findings reveal that the secondary palate can be divided in two parts regarding the boundary ruga (ruga 8 in mouse), the growth of the anterior part being stronger. In the future, rugae will undoubtedly be helpful markers to further shed light on the A/P organization and allometric growth of the secondary palate.

Methods

Harvesting and staging of embryos

CD1 (ICR) adult mice were purchased from Charles River. Tabby mice were bred at the PBES (Lyon). The colony was established by inbreeding from a mating pair (B6CBACa

Aw-J/A-Eda^{Ta}/J-XO female and B6CBACa Aw-J/A male) obtained by the Jackson Laboratory (Bar Harbor, Maine).

Mouse females were mated overnight and the noon after morning detection of a vaginal plug was indicated as embryonic day (ED) 0.5. Pregnant mice were killed by cervical dislocation and embryos were harvested and weighted as described earlier [15]. Mouse heterozygous and homozygous Eda^{Ta} embryos (ED14.5–15.0) used in this study (Fig. 4) were obtained from Eda^{Ta}/Eda^{Ta} females crossed with either Eda^{Ta}/Y or +/Y males, and, when necessary, phenotyped based on the absence of primary hair follicle in homozygous *versus* heterozygous mutant embryos.

Pregnant hamster females (*Mesocricetus auratus*, Hsd-Han:AURA) were purchased from Harlan. They were killed by cervical dislocation following anesthesia and embryos were harvested and weighted as described for mouse embryos [15].

Whole mount *in situ* hybridization

Heads of mouse embryos were fixed overnight in paraformaldehyde 4% at 4°C, dehydrated in a methanol series and kept for several weeks in 100% methanol. Heads were rehydrated and upper and lower jaw were separated before proceeding to whole mount *in situ* hybridization, which was done using standard methods [47]. Samples were imaged on a LUMAR stereomicroscope (Zeiss, PLATIM, Lyon). Following whole mount *in situ* hybridization, samples were embedded in paraffin and sectioned (5 µm). Sections were stained with nuclear fast red and imaged on a Zeiss microscope.

Several probes were as originally described: *Shh* [48]; *Shox2* [49]; *Bmp7* [50]. Other were made from RT-PCR products amplified from mouse or hamster embryonic total RNA and cloned in TOPO-PCR II (Invitrogen): *Meox2* (5' GGTCCTGTGTTCCAACATC and 3' GAAGCGTTCCTTTTTCACA); *Tbx22* (5' ACAAAGTGGAAGCAGTGGCTCA and 3' GGCTGGATACCAATGGGAATGA), *ma-Shh* (5' CAAAAAGCTGACCCCTTTCAGCCT and 3' AGGAAGGTGAGGAAGTTCGCTGTA), *ma-Meox2* (5' ATGGAACACCCSCTCTTTGG and 3' CCACACTTTCACCTGTCTTTCAGT).

Assessment of epithelium thickness and proliferation rate along the A/P axis of the palatal shelves

In order to trace the rapid dynamic of rugae development at ED13.5, we used CD1 (ICR) mouse embryos exhibiting a gradient series of weights: 179 mg, 192 mg, 208 mg. Heads were fixed individually in Bouin-Holland fluid and routinely embedded in paraffin. Series of 5 µm thick frontal sections were prepared and stained with alcian blue-hematoxylin-eosin.

For every two sections, we took into consideration the epithelium covering the oral surface of embryonic maxilla in a region of fixed area representing the central part of a palatal shelf. This fixed area was centered on a point situated at mid distance between the palatal shelf margin and either the lip furrow (in lip region) or the centre of a base of a tooth germ (in a cheek region) using Leica DMLB microscope.

In this fixed area of epithelium, we measured 3 parameters on each second section: (1) Thickness of the epithelium was measured using an objective 100× and a drawing chamber. After the projection of a section on a white surface (resultant magnification 800×), the epithelium thickness was measured by a straight edge. If the epithelium exhibited thickness and morphology of a common epithelium lining the oral cavity (i.e. a single layer of basal cells and a single layer of flat superficial cells, total thickness less than 18 µm), then the section was classified as part of a gap between rugae (white in Fig. 3). Otherwise, the section was considered as part of a ruga (dark grey in Fig. 3). The very special region anterior to ruga 8, where new rugae form, was treated separately (light grey in Fig. 3); (2) A number of epithelial cells in mitosis was counted on pictures captured using an objective 100×/1.25 and a Leica DC480 camera. The cells in mitosis and the mitosis phase were then verified directly in the microscope. Only the cells from early metaphase to early telophase were considered. (3) A total number of epithelial cells. All present epithelial cells were counted on identical images that were used for the counting of mitotic cells (see above). Finally, for gaps, rugae and the region of new ruga formation (determined on the basis of epithelium thickness – see above), we calculated a "mitotic index" as the percentage of the total number of mitotic cells in the total number of cells for the concerned sections.

Ki67 immunostaining on cryosections

The heads were dissected from CD1 (ICR) mouse embryos at ED 13.5 (weight range 204–210 mg) and frozen immediately in O.C.T. Tissue Tek (Sakura) diluted 1:1 with Hank's balanced solution. Frozen sections were post-fixed in 4% PFA for 10 minutes and processed by a Citrate buffer epitope retrieval method: 10 minutes boiling in 10 mM sodium citrate buffer pH 6, 0.05% Tween 20. The sections were then incubated at RT overnight with primary antibody Ki67 (Rabbit polyclonal IgG to Ki67, Abcam, #Ab15580) diluted 1:1000 in 1% BSA. The secondary antibody (Alexa Fluor® 568 goat anti-rabbit IgG, Invitrogen, #A11036) was diluted 1:800 in 1% BSA and incubated at RT for 45 min. Nuclei were stained with Prolong® Gold antifade reagent with DAPI (Invitrogen). The images were made using a microscope Leica DMI 6000B and camera DFC 490.

Ki67 whole mount immunostaining

Palatal halves were dissected in PBS from CD1 (ICR) embryos at 13.5 ED and fixed overnight in 4% PFA in PBS. Whole mount immunostaining was performed as described in Nagy et al., 2003. Anti-Ki67 (clone SP6) (1:200 dilution) was obtained from Lab Vision (#RM-9106) and detected with anti-rabbit-Alexa88 (Molecular Probes). Following, nuclei were labeled with Draq5™ as recommended by the manufacturer (Biostatus). Palatal shelves were imaged on a confocal microscope (Zeiss LSM510, PLATIM, Lyon).

Measurements in wild type adult palates

The sample, composed of 82 adult wild type mice of B6CBCa genetic background, was already described in our previous paper [3]. Palates were imaged using a Leica MZ 16 stereomicroscope (Leica, Wetzlar, Germany) and a LEICA DFC 320 CCD-camera. As left and right rugae originate independently, palatal halves were treated separately (hence n = 164). The distance between rugae 7 and 8 was the mean value of three measures taken at three different positions between the basements of the two rugae (1-lateral extremity of ruga 7 straight to ruga 8; 2-center of ruga 7 straight to ruga 8; 3-medial extremity of ruga 7 straight to ruga 8), using the Optimas software.

Abbreviations

ED: Embryonic Day; A/P: Anterior/Posterior; WISH: whole mount *in situ* hybridization

Authors' contributions

SP carried out *Shh* whole mount *in situ* hybridization on wild type and tabby mice and Ki67 whole mount immunolabeling, participated to the work on A/P regionalization, and generally conceived of the study, designed and coordinated it, and drafted the manuscript. JP characterized *Shh* expression on sections and worked setting up tissue culture experiments that were not conclusive enough to be included. AM did the work with hamster embryos, with TOP-GAL mice and the initial work on A/P regionalization. MR carried out mitotic countings and Ki67 labeling on sections. AL carried out the whole mount *in situ* hybridization and sections concerning the A/P regionalization of the palate. LB carried out *Shh* whole mount *in situ* hybridization on *Eda^{Ta}* mice. CC and LV carried out the analysis of ruga 7 – ruga 8 distance in adults. RP and VL both participated to the study conception and design, and helped to revise the manuscript.

All authors read and approved the final manuscript.

Acknowledgements

We thank Denis Duboule, John Cobb, Marion Wassef and Irma Thesleff for providing *in situ* hybridization probes, Karine Monier for providing antibodies, and Michaela Platerotti for providing the TOP-GAL mice. We thank Stéphane Vincent, Nicolas Fossat and Thomas Lamonerie for their help in

setting up techniques, for providing the Ki67 antibody and for helpful discussions. We thank Claire Lionnet for her assistance with confocal microscopy at the PLATIM, and the PBES staff for animal care and breeding. We thank Michael Schubert, Ingrid Masse, Frédéric Flamant and Maria Theodosiou for helpful reading of the manuscript.

This work was supported by the "programme Emergence" of the Région Rhône-Alpes, the "Agence Nationale pour la Recherche" ("Quenottes" program), the Centre National pour la Recherche Scientifique (CNRS) and the Ecole Normale Supérieure de Lyon, the Grant Agency of the Czech Republic (grant 304/07/0223), by MSMT CR (MSM0021620843), and the Région Charentes-Poitou. SP benefited from a grant of CNRS. A « short scientific mission » of SP in Prague was supported by the COST B-23 action (Brussels, EU).

References

- Gritli-Linde A: **Molecular control of secondary palate development.** *Dev Biol* 2007, **301**:309-26.
- Eisentraut: **Das Gaumenfaltenmuster der Säugetiere und seine Bedeutung für Stammesgeschichtliche und taxonomische Untersuchungen.** *Bonn* 1976.
- Charles C, Pantalacci S, Peterkova R, Peterka M, Laudet V, Viriot L: **Disruption of the palatal rugae pattern in Tabby (*eda*) mutant mice.** *Eur J Oral Sci* 2007, **115**:441-8.
- Peterkova R, Klepacek I, Peterka M: **Prenatal development of rugae palatinae in mice: scanning electron microscopic and histologic studies.** *J Craniofac Genet Dev Biol* 1987, **7**:169-89.
- Nunzi MG, Pisarek A, Mugnaini E: **Merkel cells, corpuscular nerve endings and free nerve endings in the mouse palatine mucosa express three subtypes of vesicular glutamate transporters.** *J Neurocytol* 2004, **33**:359-76.
- Ishizaki K, Sakurai K, Tazaki M, Inoue T: **Response of Merkel cells in the palatal rugae to the continuous mechanical stimulation by palatal plate.** *Somatosens Mot Res* 2006, **23**:63-72.
- Halata Z, Cooper BY, Baumann KI, Schwegmann C, Friedman RM: **Sensory nerve endings in the hard palate and papilla incisiva of the goat.** *Exp Brain Res* 1999, **129**:218-28.
- Mikkola ML: **Genetic basis of skin appendage development.** *Semin Cell Dev Biol* 2007, **18**:225-36.
- Widelitz RB, Jiang TX, Lu J, Chuong CM: **beta-catenin in epithelial morphogenesis: conversion of part of avian foot scales into feather buds with a mutated beta-catenin.** *Dev Biol* 2000, **219**:98-114.
- Rice R, Spencer-Dene B, Connor EC, Gritli-Linde A, McMahon AP, Dickson C, Thesleff I, Rice DP: **Disruption of *Fgf10/Fgfr2b*-coordinated epithelial-mesenchymal interactions causes cleft palate.** *J Clin Invest* 2004, **113**:1692-700.
- Hilliard SA, Yu L, Gu S, Zhang Z, Chen YP: **Regional regulation of palatal growth and patterning along the anterior-posterior axis in mice.** *J Anat* 2005, **207**:655-67.
- Jin JZ, Ding J: **Analysis of *Meox-2* mutant mice reveals a novel postfusion-based cleft palate.** *Dev Dyn* 2006, **235**:539-46.
- Li Q, Ding J: **Gene expression analysis reveals that formation of the mouse anterior secondary palate involves recruitment of cells from the posterior side.** *Int J Dev Biol* 2007, **51**:167-72.
- Yu L, Gu S, Alappat S, Song Y, Yan M, Zhang X, Zhang G, Jiang Y, Zhang Z, Zhang Y, et al.: ***Shox2*-deficient mice exhibit a rare type of incomplete clefting of the secondary palate.** *Development* 2005, **132**:4397-406.
- Peterka M, Lesot H, Peterkova R: **Body weight in mouse embryos specifies staging of tooth development.** *Connect Tissue Res* 2002, **43**:186-90.
- Bulleit RF, Zimmerman EF: **The influence of the epithelium on palate shelf reorientation.** *J Embryol Exp Morphol* 1985, **88**:265-79.
- Luke DA: **Epithelial proliferation and development of rugae in relation to palatal shelf elevation in the mouse.** *J Anat* 1984, **138**(Pt 2):251-8.
- Sakamoto MK, Nakamura K, Handa J, Kihara T, Tanimura T: **Morphogenesis of the secondary palate in mouse embryos with special reference to the development of rugae.** *Anat Rec* 1989, **223**:299-310.

19. Wu P, Hou L, Pliikus M, Hughes M, Scephnet J, Suksaweang S, Widelitz R, Jiang TX, Chuong CM: **Evo-Devo of amniote integuments and appendages.** *Int J Dev Biol* 2004, **48**:249-70.
20. Harris MJ, Juriloff DM, Peters CE: **Disruption of pattern formation in palatal rugae in fetal mice heterozygous for First arch (Far).** *J Craniofac Genet Dev Biol* 1990, **10**:363-71.
21. Bush JO, Lan Y, Maltby KM, Jiang R: **Isolation and developmental expression analysis of Tbx22, the mouse homolog of the human X-linked cleft palate gene.** *Dev Dyn* 2002, **225**:322-6.
22. Herr A, Meunier D, Muller I, Rump A, Fundele R, Ropers HH, Nuber UA: **Expression of mouse Tbx22 supports its role in palatogenesis and glossogenesis.** *Dev Dyn* 2003, **226**:579-86.
23. Rice R, Connor E, Rice DP: **Expression patterns of Hedgehog signalling pathway members during mouse palate development.** *Gene Expr Patterns* 2006, **6**:206-12.
24. Lecompte E, Granjon L, Denys C: **The phylogeny of the Praomys complex (Rodentia: Muridae) and its phylogeographic implications.** *Journal of Zoological Systematics and Evolutionary Research* 2002, **40**:8-25.
25. Amasaki H, Ogawa M, Nagasao J, Mutoh K, Ichihara N, Asari M, Shiota K: **Distributional changes of BrdU, PCNA, E2F1 and PAL31 molecules in developing murine palatal rugae.** *Ann Anat* 2003, **185**:517-23.
26. Takanosu M, Amasaki H, Iwama Y, Ogawa M, Hibi S, Suzuki K: **Epithelial cell proliferation and apoptosis in the developing murine palatal rugae.** *Anat Histol Embryol* 2002, **31**:9-14.
27. Thesleff I, Keranen S, Jernvall J: **Enamel knots as signaling centers linking tooth morphogenesis and odontoblast differentiation.** *Adv Dent Res* 2001, **15**:14-8.
28. Tureckova J, Lesot H, Vonesch JL, Peterka M, Peterkova R, Ruch JV: **Apoptosis is involved in the disappearance of the diastemal dental primordia in mouse embryo.** *Int J Dev Biol* 1996, **40**:483-9.
29. Meinhardt H, Gierer A: **Pattern formation by local self-activation and lateral inhibition.** *Bioessays* 2000, **22**:753-60.
30. Mou C, Jackson B, Schneider P, Overbeek PA, Headon DJ: **Generation of the primary hair follicle pattern.** *Proc Natl Acad Sci USA* 2006, **103**:9075-80.
31. Sick S, Reinker S, Timmer J, Schlake T: **WNT and DKK determine hair follicle spacing through a reaction-diffusion mechanism.** *Science* 2006, **314**:1447-50.
32. Noramly S, Freeman A, Morgan BA: **beta-catenin signaling can initiate feather bud development.** *Development* 1999, **126**:3509-21.
33. DasGupta R, Fuchs E: **Multiple roles for activated LEF/TCF transcription complexes during hair follicle development and differentiation.** *Development* 1999, **126**:4557-68.
34. Liu F, Chu EY, Watt B, Zhang Y, Gallant NM, Andl T, Yang SH, Lu MM, Piccolo S, Schmidt-Ullrich R, et al.: **Wnt/beta-catenin signaling directs multiple stages of tooth morphogenesis.** *Dev Biol* 2008, **313**:210-24.
35. Pummila M, Fliniaux I, Jaatinen R, James MJ, Laurikkala J, Schneider P, Thesleff I, Mikkola ML: **Ectodysplasin has a dual role in ectodermal organogenesis: inhibition of Bmp activity and induction of Shh expression.** *Development* 2007, **134**:117-25.
36. Drew CF, Lin CM, Jiang TX, Blunt G, Mou C, Chuong CM, Headon DJ: **The Edar subfamily in feather placode formation.** *Dev Biol* 2007, **305**:232-45.
37. Noramly S, Morgan BA: **BMPs mediate lateral inhibition at successive stages in feather tract development.** *Development* 1998, **125**:3775-87.
38. Pispá J, Mikkola ML, Mustonen T, Thesleff I: **Ectodysplasin, Edar and TNFRSF19 are expressed in complementary and overlapping patterns during mouse embryogenesis.** *Gene Expr Patterns* 2003, **3**:675-9.
39. Laurikkala J, Mikkola M, Mustonen T, Aberg T, Koppinen P, Pispá J, Nieminen P, Galceran J, Grosschedl R, Thesleff I: **TNF signaling via the ligand-receptor pair ectodysplasin and edar controls the function of epithelial signaling centers and is regulated by Wnt and activin during tooth organogenesis.** *Dev Biol* 2001, **229**:443-55.
40. Ohazama A, Hu Y, Schmidt-Ullrich R, Cao Y, Scheiderei C, Karin M, Sharpe PT: **A dual role for Ikk alpha in tooth development.** *Dev Cell* 2004, **6**:219-27.
41. Jung HS, Francis-West PH, Widelitz RB, Jiang TX, Ting-Berretth S, Tickle C, Wolpert L, Chuong CM: **Local inhibitory action of BMPs and their relationships with activators in feather formation: implications for periodic patterning.** *Dev Biol* 1998, **196**:11-23.
42. Mandler M, Neubuser A: **FGF signaling is required for initiation of feather placode development.** *Development* 2004, **131**:3333-43.
43. Welsh IC, Hagge-Greenberg A, O'Brien TP: **A dosage-dependent role for Spry2 in growth and patterning during palate development.** *Mech Dev* 2007, **124**:746-61.
44. Yu L, Liu H, Yan M, Yang J, Long F, Muneoka K, Chen Y: **Shox2 is required for chondrocyte proliferation and maturation in proximal limb skeleton.** *Dev Biol* 2007, **306**:549-59.
45. Mankoo BS, Collins NS, Ashby P, Grigorieva E, Pevny LH, Candia A, Wright CV, Rigby PV, Pachnis V: **Mox2 is a component of the genetic hierarchy controlling limb muscle development.** *Nature* 1999, **400**:69-73.
46. Kavanagh KD, Evans AR, Jernvall J: **Predicting evolutionary patterns of mammalian teeth from development.** *Nature* 2007, **449**:427-32.
47. BR Hogan BL, Costantini F, Lacy E: **Manipulating the mouse embryo, a laboratory manual.** 1994.
48. Echelard Y, Epstein DJ, St-Jacques B, Shen L, Mohler J, McMahon JA, McMahon AP: **Sonic hedgehog, a member of a family of putative signaling molecules, is implicated in the regulation of CNS polarity.** *Cell* 1993, **75**:1417-30.
49. Cobb J, Dierich A, Huss-Garcia Y, Duboule D: **A mouse model for human short-stature syndromes identifies Shox2 as an upstream regulator of Runx2 during long-bone development.** *Proc Natl Acad Sci USA* 2006, **103**:4511-5.
50. Furuta Y, Piston DW, Hogan BL: **Bone morphogenetic proteins (BMPs) as regulators of dorsal forebrain development.** *Development* 1997, **124**:2203-12.

Publish with **BioMed Central** and every scientist can read your work free of charge

"BioMed Central will be the most significant development for disseminating the results of biomedical research in our lifetime."

Sir Paul Nurse, Cancer Research UK

Your research papers will be:

- available free of charge to the entire biomedical community
- peer reviewed and published immediately upon acceptance
- cited in PubMed and archived on PubMed Central
- yours — you keep the copyright

Submit your manuscript here:
http://www.biomedcentral.com/info/publishing_adv.asp



Elsevier Editorial System(tm) for Developmental Biology
Manuscript Draft

Manuscript Number:

Title: NEW INSIGHT INTO THE ORIGIN OF THE DENTAL PAPILLA

Article Type: Regular Article

Section/Category: Developmental Biology - Main

Keywords: Tooth, papilla, follicle, development, fate map

Corresponding Author: Dr. Abigail S Tucker,

Corresponding Author's Institution: Kings College London

First Author: Michaela Rothova

Order of Authors: Michaela Rothova; Renata Peterkova; Abigail S Tucker

Abstract: Tooth development has been extensively studied over the last few decades with the majority of studies concentrating on the molecular mechanisms important in embryonic odontogenesis. Our work has focused on dynamic nature of tooth morphogenesis and development of the first molar, specifically on the origin of its dental papilla, which is assumed to correspond to the portion of the condensed dental mesenchyme enfolded by rapidly growing dental epithelium. By using in vitro culture combined with vital cell labelling and tissue grafting, we reveal that the dental papilla originates only from a restricted population of the cells within the condensed dental mesenchyme that are adjacent to the inner dental epithelium at the cap stage. We also show that the dental papilla cells contribute to the formation of the dental follicle already from cap stage of odontogenesis. Based on our data, we propose a new model of dental papilla origin, where the restricted dental papilla mesenchyme grows in parallel with the in-growing cervical loops, while the dental mesenchyme surrounding both the dental papilla epithelium and papilla gives rise to the dental follicle. This knowledge is essential for targeting the progenitors of odontoblasts and dental papilla cells during early stages of odontogenesis.

Suggested Reviewers: Mina Mina

Department of Craniofacial Sciences, School of Dental Medicine, University of Connecticut Health Center, Farmington
Mina@nso1.uhc.edu

Thomas Diekwisch

Department of Oral Biology, College of Dentistry University of Illinois at Chicago
tomdkw@uic.edu

Han-Sung Jung

Department of Oral Biology, Research Center for Orofacial Hard Tissue Regeneration
hsjung@yuhs.ac

Opposed Reviewers:



Dear Editor

27/05/11

Please find uploaded our manuscript on “New insight into the origin of the dental papilla”. This manuscript used lineage labelling to identify the origin of the dental papilla in the early tooth, and investigates the relationship of the papilla to the surrounding dental mesenchyme. We show that current ideas on how the papilla forms are inaccurate, which is important for studies where the papilla and odontoblast layer are targeted during odontogenesis. I hope you and the reviewers find it suitable for publication in *Developmental Biology*.

Yours

A handwritten signature in black ink, appearing to read "Abigail Tucker", is centered on a light blue rectangular background.

Dr Abigail Tucker

Senior Lecturer
Department of Craniofacial Development and Orthodontics
King's College London
Floor 27 Guy's Tower
Guy's Hospital
London Bridge
London
SE1 9RT

Highlights

The dental mesenchyme is a highly dynamic structure during development

The dental papilla originates from a restricted population of dental mesenchymal cells

Most of the dental mesenchymal cells at the cap stage form the layers of the dental follicle

This information is essential for targeting the future dental pulp and odontoblasts at early stages

NEW INSIGHT INTO THE ORIGIN OF THE DENTAL PAPILLA

Michaela Rothová^{1,2,3}, Renata Peterková², Abigail Tucker^{*1}

¹Department of Craniofacial Development, King's College London, Floor 27 Guy's Tower, Guy's Hospital, London Bridge, SE1 9RT, London, UK

²Department of Teratology, Institute of Experimental Medicine, Academy of Sciences of the Czech Republic, Videnska 1083, 14220, Prague, Czech Republic

³Department of Cell Biology, Faculty of Science, Charles University, Vinicna 7, 128 44, Prague, Czech Republic

rothovam@biomed.cas.cz

repete@biomed.cas.cz

abigail.tucker@kcl.ac.uk

*Corresponding author: Abigail.tucker@kcl.ac.uk

<http://www.kcl.ac.uk/schools/dentistry/research/cell/tucker>

Tel: 02071887384 Fax: 02071881674

Department of Craniofacial Development

King's College London

Floor 27 Guy's Tower

Guy's Hospital

London Bridge

SE1 9RT

Key words: Tooth, papilla, follicle, development, fate map

ABSTRACT

Tooth development has been extensively studied over the last few decades with the majority of studies concentrating on the molecular mechanisms important in embryonic odontogenesis. Our work has focused on dynamic nature of tooth morphogenesis and development of the first molar, specifically on the origin of its dental papilla, which is assumed to correspond to the portion of the condensed dental mesenchyme enfolded by rapidly growing dental epithelium. By using *in vitro* culture combined with vital cell labelling and tissue grafting, we reveal that the dental papilla originates only from a restricted population of the cells within the condensed dental mesenchyme that are adjacent to the inner dental epithelium at the cap stage. We also show that the dental papilla cells contribute to the formation of the dental follicle already from cap stage of odontogenesis. Based on our data, we propose a new model of dental papilla origin, where the restricted dental papilla mesenchyme grows in parallel with the in-growing cervical loops, while the dental mesenchyme surrounding both the dental papilla epithelium and papilla gives rise to the dental follicle. This knowledge is essential for targeting the progenitors of odontoblasts and dental papilla cells during early stages of odontogenesis.

INTRODUCTION

Teeth develop from oral epithelium and neural crest derived mesenchyme (Chai et al. 2000) with immigration of endothelial cells (Nait Lechguer et al. 2008) that have been identified as a mesoderm contribution to the dental papilla formation during the cap stage of tooth development (Rothova et al. 2011). The epithelium invaginates into the surrounding mesenchyme and forms a dental bud surrounded by condensed mesenchymal cells. Later the epithelial cervical loops grow further into the condensed mesenchyme (Fig.1C). The dental papilla is assumed to originate passively – from the condensed mesenchyme captured in between the elongating cervical loops. In other words, the condensed dental mesenchyme remains passive and is enfolded by the dental epithelium to form the dental papilla (as schematized for example in bite-it.helsinki.fi, Aberg et al. 2004, Tucker and Sharpe 2004 and Fig.1B). The dental papilla later becomes the dental pulp with its associated blood vessels and nerve supply. The condensed mesenchyme surrounding the outer dental epithelium gives rise to the dental follicle, which forms the periodontium: cementoblasts, periodontal ligament and alveolar bone (Ten Cate et al., 1971; Yoshikawa & Kollar, 1981; Palmer & Lumsden, 1987; Diep et al., 2009). At the bell stage of tooth development, the dental follicle, or dental sac, is clearly divided into 3 layers – the inner layer surrounding the enamel organ, the outer layer adjacent to the developing alveolar bone, and a less densely populated intermediate layer separating the other two. The inner layer is probably the most important part of the dental follicle for formation of cementoblast and periodontal ligament (Ten Cate et al. 1971). The outer layer later contributes to formation of the alveolar bone (Diekwisch 2002, Diep et al. 2009). When the dental papilla at the bell stage of tooth development is combined with the enamel organ, a new inner dental follicle layer forms, originating from the dental papilla cells (Yoshikawa and Kollar 1981; Palmer and Lumsden 1987). Tritiated thymidine labelling studies of the third molar at the late bell stage, also indicated a contribution of the papilla to the follicle at a stage when morphogenesis is almost complete (Osborn and Price, 1988). The capability of the early dental papilla mesenchyme to contribute to the dental follicle formation, however, has not been examined before the bell stage.

There have been many extensive studies of the molecular mechanisms that drive tooth development (for review see e.g. Thesleff and Mikkola, 2002; Cobourne and Sharpe, 2010). However a recent study has pointed out the dynamic nature of dental mesenchyme during tooth morphogenesis, with the condensed mesenchyme adjacent to the epithelial bud contributing to the dental follicle, periodontium and alveolar bone (Diep et al. 2009). The observed dynamic nature of the dental mesenchyme rises a question, whether the condensed mesenchyme (Fig. 1A) indeed plays only a passive role during papilla origin (Fig. 1B). Therefore this present study focused on the origin of the dental papilla and on the developmental relationship to the condensed dental mesenchyme and dental follicle. The dynamic nature of the dental mesenchyme was investigated by using *in vitro* slice culture, vital cell labelling and tissue grafting. In contrast to the generally accepted view on the passive role of the condensed dental mesenchyme during dental papilla origin (Fig. 1B), here we demonstrated active growth of the dental papilla. Therefore the dental papilla is not formed from the existing dental condensed mesenchymal population, but forms actively “de novo” from a restricted population of dental mesenchymal cells

adjacent to the inner dental epithelium that strongly proliferate. We also show clearly that the dental follicle starts to form from the bud stage and that the papilla cells of the first molar contribute to the formation of the dental follicle already during the cap to bell transition stage.

MATERIAL AND METHODS

Mice

All animals were killed using a schedule 1 method (cervical dislocation) as approved by the Home Office and King's College London. The females were mated overnight and noon after the detection of the vaginal plug was considered as embryonic day (E) 0.5.

Slice culture

E13.5 and E14.5 mouse mandibles of CD1 embryos were dissected out and sliced using a McIlwain tissue chopper (Mickle Laboratory Engineering Co., Ltd. UK) into frontal slices 250 μm thick (Diep *et al.* 2009, Rothova *et al.* 2011). Slices showing a clear molar tooth bud or cap were then selected and cultured. Slices were cultured on transparent nucleopore filters (VWR) supported on metal grids on medium surface. Medium consisted of Advanced DMEM F12 (Invitrogen) supplemented with 1% penicillin/streptomycin and 1% Glutamax (Invitrogen) and 10% fetal calf serum (in some experiments). Matrigel basement membrane matrix (7 μl) (BD Biosciences) was added on top of the slice. Slices were cultured at 37°C / 5% CO₂ up to 4 days, changing medium every 2 days.

DiI; DiO Labelling

DiI and DiO are lipophilic dyes, which intercalate in the cell membrane, marking groups of cells. DiI (Molecular probes cell tracker CM-DiI, C-7000) and DiO (Molecular probes, V22886) was dissolved in 100% EtOH. Small amounts of DiI were injected into the slices before culture using a mouth pipette. The slices were then placed on filters and cultured. The position of the DiI was recorded using a fluorescence Leica dissecting microscope every 24 hours.

GFP and CD1 tissue recombination

GFP (Green fluorescent protein) reporter mice were mated, at the same time as CD1 WT mice. GFP and WT mandibles were dissected out at the bud/cap stage and sliced using the tissue chopper (see above). The condensing mesenchyme from a GFP mouse was then dissected out of the tooth germ using fine tungsten needles and a small piece inserted into a WT tooth germ, where an equivalent area of condensing mesenchyme had been removed. Matrigel was then pipetted onto the slice to help fix the graft in correct position. After approximately 6 hours, once the grafted tissue had started to integrate, the culture was photographed under fluorescence to check the position of the grafted tissue. Grafts were then left to develop for several days while the tooth germ developed to the late bell stage and photographed every 24 hours.

Immuno-fluorescent staining

The double immuno-staining of Ki67 and PH3 antibody was performed on 10 µm thick sagittal and frontal frozen sections of mouse heads. The mouse embryos at E14.5 and E15.5 were weighted (according to Peterka et al. 2002), heads were dissected and frozen immediately in Cryomount (HI-00890). Frozen sections were post-fixed in 4% PFA (10 mins), blocked in 10% BSA (30 mins) and incubated at 4°C over night with primary antibody Ki67 (Rabbit polyclonal IgG to Ki67, Abcam, #Ab15570-check this) was diluted 1:1000 in 1% BSA, the primary antibody PH3 (Mouse monoclonal IgG to phosphohistone 3, Abcam, #Ab14955) was diluted 1:200 in 1% BSA and both antibodies incubated at the same time. The secondary anti-rabbit antibody (Alexa Fluor® 488 goat anti-rabbit IgG, Invitrogen, #A-11008) was diluted 1:250 in 1% BSA, the secondary anti-mouse antibody (Rhodamine TRITC sheep anti-mouse IgG, Jackson ImmunoResearch, #515025003,) was diluted 1:150 in 1% BSA and both antibodies incubated at the same time at RT for 1 hour. Nuclei were stained with Hoechst (Sigma, #B2261) and the slides mounted in Prolong® Gold anti-fade reagent with DAPI (Invitrogen, #P36935). The images were taken using inverted fluorescence microscope Leica AF6000.

Radioactive in situ hybridization

Specimens were fixed in 4% paraformaldehyde and dehydrated in methanol series. Paraffin wax sections were cut at 8 µm and prepared for radioactive 35S in situ hybridization, as previously described by Tucker et al. (1998). Mouse Syndecan-1 plasmid was a kind gift from P. Kettunen.

RESULTS

Expression of *syndecan* has been previously shown as a marker of the dental mesenchyme at various stages of tooth development (Vainio et al. 1989; 1991). At embryonic day (E) 14.5, *syndecan-1* expression is present in the condensed dental mesenchyme surrounding the forming dental cap (Fig. 1A). The developmental relationship between this condensed dental mesenchyme, dental papilla and follicle was investigated by cell fate mapping.

Fate mapping of the dental mesenchymal cells during dental papilla formation

To observe the fate of the dental mesenchymal cells during murine odontogenesis we labelled cells at various locations within the tooth germ using lipophilic dyes DiI and DiO. At first we labelled the *syndecan-1* positive condensed dental mesenchymal cells at the border of the condensing mesenchyme at E14.5 - the region of the presumptive future dental papilla (Fig. 2A,B, compare with Fig. 1). After 2 days of *in vitro* culture we found these labelled cells spread out apically (i.e. further from the oral cavity) at the base of the papilla by the early bell stage, but surprisingly these cells did not contribute to the formation of the dental papilla, which remained free of labelled cells (Fig. 2C,D).

To find out which dental mesenchymal cells at E14.5 form the dental papilla during development, we labelled the dental papilla cells in close contact with the cervical loops and inner dental epithelium (IDE) with DiO (green). In this case, to ensure that we had labelled the cells right up to the boundary with the epithelium, the DiO dot

simultaneously labelled the epithelium and the adjacent dental mesenchyme by one side of the tooth germ. A DiI dot (in red) was used as a reference point indicating the deepest part at the periphery of the mesenchymal condensation (Fig. 3A,B). After 2 days of *in vitro* culture the DiO labelled mesenchymal cells spread by the side of the expanding dental papilla, creating a light green band of labelled cells. Interestingly, the strongest DiO labelled mesenchymal cells moved with the tip of the growing cervical loop as the epithelial cells moved towards the DiI reference point at the base of the dental papilla. The DiI labelled cells spread out in a deeper dental follicle layer than the DiO labelled cells, which ended up in the apical part of the dental follicle. The labelled epithelial cells spread within the enamel organ between its stalk and IDE (Fig. 3C,D). Similar results were obtained when the papilla mesenchyme and adjacent IDE were labelled in the middle part of the tooth cap (Suppl. Fig. 1).

These results show that the cells contributing to the growth of the dental papilla are located in the dental mesenchyme in close proximity to the IDE in between the cervical loops at the cap stage. This limited mesenchymal cell population then grows together with the elongating epithelial cervical loops and fills up the space in between the cervical loops, creating the dental papilla.

To confirm that only specific cells of the condensed dental mesenchyme contribute to the dental papilla formation, we labelled two different regions of the dental mesenchyme in the same E14.5 molar tooth germ with DiI. One labelled region (a) comprised dental mesenchymal cells located adjacent to the IDE of the epithelial cervical loop. The other region (b) comprised mesenchymal cells located slightly further away at the level of the cervical loop. An unlabelled region of mesenchyme was left in between (Fig. 4A,B). After 2 days of *in vitro* culture, the labelled cells in close proximity to the IDE (a) formed a band in the enlarging dental papilla with a focal spot at the apical part of the dental follicle at the tip of cervical loop. The mesenchymal cells further from the epithelium (b) remained near to the tip of the cervical loop and did not label the papilla. Importantly, the unlabelled region of mesenchyme in between (a) and (b) expanded as the tooth enlarged during development (Fig. 4C,D).

To confirm the result produced by DiI and DiO labelling we repeated the experiments using grafts of GFP labelled cells from a GFP reporter mouse. These grafts, allowed us to follow the fate of the dental mesenchyme, without progressive losing the label as the cells divided (Suppl. Fig. 2). When the GFP tissue was grafted at the edge of the condensed dental mesenchyme (Suppl. Fig. 2A,B), the tissue did not contribute to the development of the dental papilla development (Suppl. Fig. 2C-F, compare with the DiI labelling - Fig. 2, which shows corresponding results). When the GFP dental mesenchyme was grafted closer to the dental epithelium (Suppl. Fig. 2G,H), these cells contributed to the dental papilla, while the GFP positive cells further from the epithelium contributed to formation of the dental follicle (Suppl. Fig. 2I,L), again agreeing with the DiI and DiO labelling data (Figs. 2, 3, 4; Suppl. Fig.1).

From our lineage labels at E14.5, the mesenchymal cells near to the IDE appeared to rapidly spread out to encompass the whole dental papilla within a few days *in vitro*. We therefore wanted to analyze the fate of the dental papilla cells slightly later in

development at the late cap stage, at E15.5. A large group of cells at the centre of the forming dental papilla were labelled with DiI. The labelled area was in close proximity to the IDE in between the epithelial cervical loops (Fig. 5A,B). After 2 days of *in vitro* culture the labelled cells spread as the dental papilla enlarged and elongated. In contrast to our similar labelling at E14.5 (Fig. 4; Suppl. Fig.1), the E15.5 dental papilla cells did not exhibit the distinct shift towards the apical part of the dental follicle but remained proportionally inside the dental papilla. Interestingly, some cells at the base of the dental papilla separated and spread into the apical part of dental follicle (Fig. 5C,D).

The dynamics of dental mesenchymal cells surrounding the tooth germ was even more apparent when the DiI labelling was initiated at E13.5. At E13.5 the tooth germ has reached the bud stage and we labelled the condensed dental mesenchyme at the tip of the bud in close proximity to the epithelium with DiI (Fig. 6A,B). After one day of *in vitro* culture the region of labelled mesenchymal cells elongated and some cells spread into the forming dental follicle (Fig. 6C,D). After two days of *in vitro* culture, when the tooth germ reached the cap stage, the labelled cells gave rise to the forming dental papilla but also the dental follicle surrounding the tooth germ (Fig. 6E,F).

We used GFP electroporation as a more precise cell labelling technique to follow very small populations of cells. When a small region of dental mesenchyme was electroporated further from the tip of the dental epithelial bud at E13.5 (Fig. 6G,H), we observed this small population of cells contributing to the different layers of the dental follicle but not the dental papilla (Fig. 6I-L).

Cell proliferation of the dental mesenchyme

To investigate if there are any specific proliferative domains in the dental mesenchyme which would be responsible for expansion of the dental papilla we used two markers of proliferation to precisely map the proliferation pattern. Ki67 antigen is present in cell-cycle active cells and absent from G0 resting cells, while Phosphohistone-3 (PH-3) is a mitotic marker, which is present in actively dividing cells. Together these markers show a different state of the cell to highlight any changes in proliferation within the developing tooth. Proliferation was analysed along the anterior-posterior length of the developing molar tooth on sagittal and serial frontal sections of E14.5 and E15.5 mouse embryonic heads (Fig. 7).

At E14.5 proliferation in the condensed dental mesenchyme was quite uniform and most of the cells were positive for the proliferative marker Ki67 (Fig. 7A,B). The pattern of the mitotic marker PH-3 did not show any specific region of higher proliferation but the mitotic cells were scattered throughout the condensed dental mesenchyme (Fig. 7C,D). Similar proliferative and mitotic pattern was obvious on both, sagittal and serial frontal sections. A lower intensity of cell proliferation labelling was present in anterior part of the dental epithelium and adjacent mesenchyme and in the posterior mesenchyme where the dental epithelium still exhibited a bud shape (Fig. 7A,C). At later stage E15.5 there was high intensity of mesenchymal cell proliferation in the formed dental papilla on both, sagittal and serial frontal sections by using the proliferative Ki67 marker (Fig. 7E,F) and the mitotic marker PH-3 (Fig. 7G,H), with lower intensity of cell proliferation in the periphery of the dental mesenchyme (Fig. 7E-H). The posterior dental mesenchyme

showed lower intensity of cell proliferation than the anterior (Fig. 7G) similar to the E14.5 sagittal sections (Fig. 7A).

Direction of tooth germ growth

Hypothetically, tooth germs can grow in two directions – growing deep into the surrounding tissue (Fig. 8A) or in a superficial direction - towards the oral cavity (Fig. 8B). Although it is generally assumed that tooth germs grow into the jaw, measurements of the position of the developing human tooth germs in maxilla and their surrounding tissue indicated that tooth germs might in fact grow towards the oral cavity with the deepest tip of the dental epithelium staying at a fixed position (Orban 1928) (Fig. 8B). As the slice culture *in vitro* method provides a natural environment for the tooth to grow with the tissue surrounding the tooth germ, we were searching for the direction of the lower mouse molar *in vitro*. We cultured E14.5 cap stage tooth germs on a metal grid to obtain fixed points as a scale to follow the direction of growth of the tooth germs. After 4 days of *in vitro* culture we observed the cervical loops extending into the surrounding tissue with the oral epithelium staying at a similar place during this growth (Fig. 8C). This suggests that the tooth germ is not growing towards the oral cavity (Fig. 8B) but in-growing into the surrounding tissue (Fig. 8A).

DISCUSSION

It has recently been shown that the dental mesenchymal cells around the tooth bud move apically as the tooth develops and contributes to the alveolar bone and dental follicle (Diep et al., 2009). Here we show that the fate of the dental mesenchyme is even more complex. Our present data document that there is only a small population of dental mesenchymal cells at E13.5 and E14.5 which gives rise to the dental papilla. These cells are located in close proximity to the dental epithelium and at the cap stage they are located adjacent to the inner dental epithelium in between the cervical loops. The majority of the condensed dental mesenchymal cells at this stage, together with the dental papilla cells themselves, contribute to the formation of the dental follicle. This finding supplements the previous grafting and autoradioactive studies which suggested dental papilla cells could contribute to development of the dental follicle during later stages of odontogenesis (Yoshikawa and Kollar 1981; Palmer and Lumsden 1987; Osborne and Price, 1988). We show that the dental papilla cells contribute to the dental follicle from the cap to bell transition stage of first molar development. Our labelling studies also show that the dental papilla mesenchyme from E15.5 (late cap stage) is significantly more suitable for studies aiming to target the dental papilla, and its derivatives, as the mesenchymal cell population at E15.5 is more defined, outlined and stable than during earlier stages. Targeting of the condensing mesenchyme at E14.5 could quite easily miss the future dental papilla completely.

It could be argued that the results of the present Dil labelling are caused by directional growth of the dental epithelium towards the oral cavity and the dental condensed mesenchyme is not encompassed by the in-growing epithelium but the dental mesenchyme stays at the same position and grows together with the epithelium towards

the oral cavity as it was reported in human upper jaw (Orban 1928). This hypothesis could have been an explanation of why we see bands of labelled cells in the forming dental papilla and why the main labelled dot remains by the tip of the dental epithelium in most of our fate-mapping experiments. However when we investigated the growth direction of the cultured first molar, we found significant in-growth of the epithelial cervical loops into the jaw while the oral epithelium only slightly moved towards the opposite (oral) direction. Thus the present data strongly suggest that the bands of the labelled cells result from dilution of the dye as the labelled highly proliferating dental papilla cells divide while the lower first molar in-grows into the surrounding tissue.

Our data showing that the growing cervical loop does not enfold the condensed dental mesenchyme, is supported by a study, where the growth of the mesenchymal component (papilla mesenchyme plus free dental follicle mesenchyme) was compared to that of the epithelial component (enamel organ) (Peterkova 1974). In this study the volume ratio of the two tissues remains approximately 1:1 during development from the cap to early bell stage (Peterkova 1974). This indicates that the dental mesenchyme is not a passive structure enfolded by the faster growing dental epithelium.

At E14.5 and E15.5 we were not able to detect any specific domains of high cell proliferation within the dental mesenchyme which would allow distinguishing different regions of the dental mesenchyme. High mitotic and proliferative activity was distributed throughout the dental mesenchyme. At E14.5 there were no differences between the developing dental papilla and surrounding dental mesenchyme. At E15.5 the dental papilla and surrounding dental mesenchyme was also highly proliferative, only cells at the periphery of the dental mesenchyme exhibited lower cell proliferation. These results suggest that as the tooth germ enlarges during development, not only the dental papilla expands but also the dental follicle, which is formed from the mesenchyme surrounding the dental papilla and is capable of high cell proliferation. Low cell proliferation was obvious in the very anterior part of the molar tooth germs, where the premolar rudimentary tooth germ was incorporated (Peterkova et al. 2000, Prochazka et al. 2010). Low cell proliferation also exhibited the primary enamel knot signalling center as described previously (Jernvall et al. 1994). The enamel knot is a group of epithelial cells adjacent to the dental papilla mesenchyme in the middle part of a tooth cap (for review see Butler 1956). This specific region expresses many signalling molecules and transcription factors to drive tooth development and epithelium-mesenchyme reciprocal interactions (for review see Jernvall and Thesleff 2000). We propose a model where the mesenchymal cells in close proximity to this epithelial signalling center obtain the information sent from the enamel knot and drive the dental papilla formation, while cells further away, which do not get the same molecular information, contribute to the dental follicle.

Our present work impacts on the contemporary view of the contribution of the dental mesenchyme to dental papilla development. During bud and cap stages the condensed dental mesenchyme is morphologically quite a homogenous cell population and gene expression in this region often appears quite uniform, as shown, for example, by *syndecan-1* and others (e.g. Aberg et al. 1997; Aberg et al. 2004). However the

expression of some genes suggests specific compartmentalisation of the dental mesenchyme at the cap stage. For example *Dlx* genes show some segmentation (Zhao et al. 2000) and together with *Fgf3* is expressed in a limited proportion of the dental mesenchyme (schematized in Fig. 9B, Klein et al. 2006) and *Spry4* appears specifically present only in the dental papilla mesenchyme in between the cervical loops at the cap stage (Klein et al. 2006) (schematized in Fig. 9C). *Spry4*, thus appears to be a good marker for the presumptive dental papilla at cap stage. Our fate map contradicts some claims for specific dental mesenchyme markers. For example, the Golgi protein *GoPro49* has been suggested as a specific marker of the dental follicle from the early bud stage of tooth development (Takatalo et al. 2009). The authors highlight the expression of *GoPro49* as a marker distinguishing dental follicle from dental papilla mesenchyme (schematized in Fig. 9A). However here we show that the dental mesenchyme in between the dental papilla and the dental follicle at early cap stage will not become the actual dental papilla but the dental follicle and it is necessary to distinguish these regions more precisely.

In this present study we have re-assessed the origin of the dental papilla and its relationship to the epithelial cervical loops. It has been generally assumed that the dental papilla forms passively from the majority of the condensed dental mesenchyme lying in between the forming dental papilla and follicle (bite-it.helsinki.fi; Aberg et al. 2004; Tucker and Sharpe 2004; Takatalo et al. 2009, Fig. 9A). Schemes of the dental mesenchyme distribution into dental papilla and dental follicle have also been published based on the morphology of the mesenchymal cells (Cho and Garant 2000 – Fig. 9B; Kim et al. 2007 – Fig. 9C). We show that the mesenchymal cell population giving rise to the future dental papilla is very restricted and this population is distinguishable from the cell morphological aspect, when we are able to distinguish 3 different layers of the condensed dental mesenchyme at the beginning of cap stage, at E14.5 (Fig. 9D).

Based on the present data we propose a new concept of dental papilla origin (Fig. 9E,F) where the dental mesenchymal cells adjacent to the inner dental epithelium in between the epithelial cervical loops (Fig. 9E) at early cap stage strongly proliferate and fill up the enlarging dental papilla (Fig. 9F). At the same time the condensed mesenchymal cells at a distance from the IDE also proliferate and move around the tooth germ to form the dental follicle but do not take part in papilla formation. As the tooth develops dental papilla cells move out of the papilla and into the follicle, creating the inner investing layer (Fig. 9E,F). At the same time as the papilla cells are moving out, mesodermally derived endothelial cells immigrate into the developing dental papilla as an influx of non-neural crest cells (Rothova et al., 2011). The early stages of tooth development therefore represent very dynamic population of cells, moving in and out of the tooth, something perhaps not appreciated from molecular and histological studies.

ACKNOWLEDGEMENT

We thank to Bronislava Rokytova for the graphics help on this work. Michaela Rothova and Renata Peterkova are funded by the Grant Agency of the Czech Republic (grant CZ:GACR:GA304/07/0223) and by ÚEM AV CR - AV0Z50390512. Michaela Rothova performed this work during an Erasmus exchange program with King's College London

and was funded by ESF-Functional Genomics Exchange Grant and Development Travelling fellowships.

REFERENCES

Aberg T, Wozney J, Thesleff I. (1997). Expression patterns of bone morphogenetic proteins (Bmps) in the developing mouse tooth suggest roles in morphogenesis and cell differentiation. *Dev Dyn*. 210(4):383-396.

Aberg T., Wang X.P., Kim J.H., Yamashiro T., Bei M., Rice R., Ryoo H.M., Thesleff I. (2004). Runx2 mediates FGF signaling from epithelium to mesenchyme during tooth morphogenesis. *Dev Biol* 270(1):76-93.

Bite-it.helsinki.fi

Butler P.M. (1956). The ontogeny of molar teeth. *Biol Rev*. 31:30–70.

Chai Y., Jiang X., Ito Y., Bringas P. Jr., Han J., Rowitch D.H., Soriano P., McMahon A.P., Sucov H.M. (2000). Fate of mammalian cranial neural crest during tooth and mandibular morphogenesis. *Development* 127(8):1671-1679.

Cho M.I., Garant P.R. (2000). Development and general structure of the periodontium. *Periodontol*. 24:9-27.

Cobourne M.T., Sharpe P.T. (2010). Making up the numbers: The molecular control of mammalian dental formula. *Semin Cell Dev Biol*. 21(3):314-24.

Diep L., Matalova E., Mitsiadis T.A., Tucker A.S. (2009). Contribution of the tooth bud mesenchyme to alveolar bone. *J Exp Zool B Mol Dev Evol* 312B(5): 510-517.

Diekwisch T.G.H. (2002). Pathways and fate of migratory cells during late tooth organogenesis. *Connect Tissue Res* 43: 245-256.

Jernvall J., Kettunen P., Karavanova I., Martin L.B., Thesleff I. (1994). Evidence for the role of the enamel knot as a control center in mammalian tooth cusp formation: non-dividing cells express growth stimulating Fgf-4 gene. *Int J Dev Biol*. 38(3):463-469.

Jernvall J., Thesleff I. (2000). Reiterative signaling and patterning during mammalian tooth morphogenesis. *Mech Dev*. 92(1):19-29.

Kim J.Y., Cho S.W., Hwang H.J., Lee M.J., Lee J.M., Cai J., Choi S.H., Kim C.K., Jung H.S. (2007). Evidence for expansion-based temporal BMP4/NOGGIN interactions in specifying periodontium morphogenesis. *Cell Tissue Res*. 330(1):123-132.

- Klein O.D., Minowada G., Peterkova R., Kangas A., Yu B.D., Lesot H., Peterka M., Jernvall J., Martin G.R. (2006). Sprouty genes control diastema tooth development via bidirectional antagonism of epithelial-mesenchymal FGF signaling. *Dev Cell*. 11(2):181-190.
- Nait Lechguer A., Kuchler-Bopp S., Hu B., Haïkel Y., Lesot H. (2008). Vascularization of engineered teeth. *J Dent Res*. 87(12):1138-1143.
- Orban B. (1928). Growth and movement of the tooth gemrs and teeth. *The Journal of the American Dental Association* 1004-1016.
- Osborn J.W., Price D.G. (1988). An autoradiographic study of periodontal development in the mouse. *J Dent Res* 67(2):455-461.
- Palmer R.M., Lumsden A.G. (1987). Development of periodontal ligament and alveolar bone in homografted recombinations of enamel organs and papillary, pulpal and follicular mesenchyme in the mouse. *Arch Oral Biol* 32(4):281-289.
- Peterka M., Lesot H., Peterková R. (2002). Body weight in mouse embryos specifies staging of tooth development. *Connect Tissue Res*. 43(2-3):186-190.
- Peterková R. (1974). Growth of tissue components in early development of tooth primordia in mice. *Folia Morphol (Praha)*. 22(3): 296-304.
- Peterková R., Peterka M., Viriot L., Lesot H. (2000). Dentition development and budding morphogenesis. *J Craniofac Genet Dev Biol*. 20(4):158-172.
- Prochazka J., Pantalacci S., Churava S., Rothova M., Lambert A., Lesot H., Klein O., Peterka M., Laudet V., Peterkova R. (2010). Patterning by heritage in mouse molar row development. *Proc Natl Acad Sci U S A*. 107(35): 15497-15502.
- Rothová M., Feng J., Sharpe P.T., Peterková R., Tucker A.S. (2011). Contribution of mesoderm to the developing dental papilla. *Int J Dev Biol* 55(1): 59-64.
- Takatalo M.S., Tummers M., Thesleff I., Rönholm R. (2009). Novel Golgi protein, GoPro49, is a specific dental follicle marker. *J Dent Res*. 88(6):534-538.
- Ten Cate A.R., Mills C., Solomon G. (1971). The development of the periodontium. A transplantation and autoradiographic study. *Anat Rec*. 170(3):365-379.
- Thesleff I., Mikkola M. (2002). The role of growth factors in tooth development. *Int Rev Cytol*. 217:93-135.
- Tucker A.S., Al Khamis A., Sharpe P.T. (1998). Interactions between Bmp-4 and Msx-1 act to restrict gene expression to odontogenic mesenchyme. *Dev Dyn*. 212(4):533-539.

Tucker A., Sharpe P. (2004). The cutting-edge of mammalian development; how the embryo makes teeth. *Nat Rev Genet* 5(7):499-508.

Vainio S., Jalkanen M., Thesleff I. (1989). Syndecan and tenascin expression is induced by epithelial-mesenchymal interactions in embryonic tooth mesenchyme. *J Cell Biol.* 108(5):1945-1953.

Vainio S, Jalkanen M, Vaahtokari A, Sahlberg C, Mali M, Bernfield M, Thesleff I. (1991). Expression of syndecan gene is induced early, is transient, and correlates with changes in mesenchymal cell proliferation during tooth organogenesis. *Dev Biol.* 147(2):322-333.

Yoshikawa D.K., Kollar E.J. (1981). Recombination experiments on the odontogenic roles of mouse dental papilla and dental sac tissues in ocular grafts. *Arch Oral Biol.* 26(4):303-307.

Zhao Z., Stock D., Buchanan A., Weiss K. (2000). Expression of Dlx genes during the development of the murine dentition. *Dev Genes Evol.* 2000 210(5):270-275.

FIGURE LEGENDS

Fig.1 Radioactive in situ hybridization of *syndecan-1* mRNA at E14.5 and assumed mechanism of dental papilla origin.

(A) There is a strong *syndecan-1* expression showing the dental condensed mesenchyme in black. The dental epithelium is highlighted by red dotted line. (B) A scheme showing the assumed mechanism of dental papilla origin. Outline of dental epithelium of lower tooth germ (in red) and condensed dental mesenchyme (in black). The epithelial cervical loops (in green) extend into the condensed dental mesenchyme (labelled by *syndecan-1* expression) and the enfolded mesenchymal cell population becomes the dental papilla (DP). (C) A molar tooth germ at late cap stage. Arrows pointing the tips of cervical loops. BDP – base of dental papilla, CL – cervical loop, DE – dental epithelium, DF – dental follicle, DP – dental papilla, IDE – inner dental epithelium. Scale shows 250µm

Fig. 2 Dental condensed mesenchyme cell labelling and fate-mapping at E14.5. (A) A sliced mouse mandible containing a tooth germ at the initiated cap stage at E14.5. The periphery of the condensed mesenchyme (weaker white dotted line) was labelled with DiI. (B) Outline of the same molar tooth germ under dark field. (C) The same molar tooth germ after 2 days of *in vitro* culture. The DiI labelled cells spread into the dental follicle (weaker white dotted line) at the base of dental papilla. (D) Outline of the same molar tooth under dark field.

The dental epithelium is highlighted with a white dotted line. Scale shows 250 µm.

Fig. 3: Cell labelling and fate-mapping of the dental papilla cells and epithelium at E14.5.

(A) A sliced mouse mandible containing a tooth germ at cap stage at E14.5. At day0 a single spot of DiO labelled inner dental epithelium and adjacent mesenchymal cells – in green. A cell population at the periphery of the condensed dental mesenchyme was labelled with DiI – in red. (B) Outline of the same molar tooth germ under dark field. (C) After 2 days of *in vitro* culture, the single labelled region of mesenchymal cells was spread as a band of green DiO labelled cells spanning across the dental papilla. The labelled dental mesenchyme remained in close contact with the cervical loops (white arrowheads), moving towards the red labelled cells in the forming dental follicle. The DiI labelled cells spread in a layer under the dental papilla forming the dental follicle. The labelled epithelial cells spread within the enamel organ. (D) Outline of the same molar tooth under dark field. CL – cervical loop, IDE – inner dental epithelium.

The dental epithelium is highlighted with a white dotted line. Scale shows 250µm.

Fig. 4 Cell labelling and fate-mapping of different regions of the condensed dental mesenchyme at E14.5.

(A) A sliced mouse mandible containing a tooth germ at the cap stage. Two different regions of the dental mesenchyme were labelled with DiI in red. The first DiI labelled region (a) was located in the dental mesenchyme by the IDE. The second DiI labelled region (b) was located in close proximity to the tip of the cervical loop (CL) with an unlabelled region left in the dental papilla (shown by grey dotted line). (B) Outline of the same molar tooth germ under dark field. (C) The same molar tooth germ after 2 days of *in vitro* culture. The labelled cells originally located in the dental papilla by the IDE (a) formed a band of cells with the focal labelled region staying at the level of the growing cervical loops. The other labelled cells further from the IDE (b) contributed to the dental follicle while the non-labelled region expanded as the dental papilla grew (shown by grey dotted line). (D) Outline of the same molar tooth germ under dark field. CL – cervical loop, IDE – inner dental epithelium.

The dental epithelium is highlighted with a white dotted line. Scale shows 250µm.

Fig. 5. Fate-mapping of the dental papilla cells at E15.5.

(A) A sliced mouse mandible containing a tooth germ at late cap stage, E15.5. Dental papilla cells labelled with DiI in red. (B) Outline of the same molar tooth germ under dark field. (C) After 2 days of *in vitro* culture the labelled cells spread in length as the dental papilla enlarged and elongated. Some cells separated and spread into the apical part of the dental follicle (schematized with white arrow). (D) Outline of the same molar tooth germ under dark field.

The dental epithelium is highlighted with a white dotted line. Scale shows 250 µm.

Fig.6 Cell labelling and fate-mapping of early condensed dental mesenchyme at the bud stage.

(A) A sliced mouse mandible containing a tooth germ at bud stage at E13.5. Mesenchymal cells in close proximity to the tip of the epithelial bud were labelled with Dil in red. (C) The same tooth germ after one day of *in vitro* culture. The red labelled mesenchymal cells elongated and some cells started to spread into the forming dental follicle. (E) The same tooth germ after 2 days of *in vitro* culture. The labelled mesenchymal cells contributed to the dental papilla and spread further into the dental follicle around the enamel organ. (B, D, F) Outlines of the corresponding molar tooth germs under dark field (A,B) day0, (C,D) day1, (E,F) day2.

(G) A sliced mouse mandible containing a tooth germ at bud stage at E13.5. Dental mesenchymal cells electroporated with a GFP expression construct (white arrow) are located close to the tip of the dental epithelium but they are not directly adjacent to the epithelium. (I) The same tooth germ after one day of *in vitro* culture. The cells expressing GFP divided into 3 layers of the forming dental follicle (white arrows). (K) The same tooth germ after two days of *in vitro* culture. The GFP cells contribute to the dental follicle (white arrows). (H, J, L) Outlines of the corresponding molar tooth germs under dark field at (H) day0, (J) day1, (L) day2. At the site of electroporation a patch of auto-fluorescence develops. The white arrows indicate and distinguish GFP positive cells from auto-fluorescent tissue.

The dental epithelium is highlighted with a white dotted line. Scale shows 250µm.

Fig. 7 Detection of cell proliferation on sagittal and frontal sections by using Ki67 and PH-3 antibodies.

Immunohistochemistry of Ki67 antibody – the proliferative marker (in green) and Phosphohistone-3 antibody – the mitotic marker (in red), nuclei (in blue). (A,C) Sagittal section of E14.5 tooth germ (embryonic weight 260 mg). There is very high cell proliferation in the condensed dental mesenchyme. The posterior and very anterior mesenchyme exhibits much lower cell proliferation. (B,D) Frontal section of E14.5 tooth germ (embryonic weight 260 mg, the same litter). (E,G) Sagittal section of E15.5 tooth germ (embryonic weight 390-400 mg). There is high cell proliferation in the anterior part of the dental papilla. The white arrows point out the periphery of the dental mesenchyme which exhibits low cell proliferation. (F,H) Frontal section of E15.5 tooth germ (embryonic weight 390-400 mg, the same litter). The white arrows point out the periphery of the dental mesenchyme which exhibits low cell proliferation. (A, B, E,F) Ki67 immuno-staining. (C,D,G,H) PH-3 immuno-staining. Ant – anterior, epi – epithelium, mes – mesenchyme, post – posterior. Scale shows 100µm.

Fig. 8 Study of directional growth of tooth germs.

(A,B) A scheme of two possible directions of tooth germ growth. Adjusted from Orban 1928. (A) Generally assumed direction of tooth germ growth – epithelium invaginating into the surrounding tissue (dashed line) while the oral cavity surface stays at the same level (full line). (B) The growth of tooth germ of human maxilla according to Orban 1928. The tip of the dental epithelium stays at the same level (dashed line) during the odontogenesis and the tooth germ elongates and grows towards the oral cavity surface (full line). (C) A sliced mouse mandible containing a tooth germ at cap stage. The molar tooth germs at E14.5 were placed on a metal grid used as a scale. (D) The same molar tooth germ after 1 day of *in vitro* culture. The tissue slice slightly moved down but the epithelium started to ingrow into the surrounding tissue. (E) The same molar tooth germ after 4 days of *in vitro* culture. The epithelial cervical loops (CL) grew further into the surrounding tissue (red dashed line) while the oral epithelium stayed at similar position (red full line) during the culture period. CL – cervical loop.

Fig. 9 Schemes of dental mesenchyme contribution to the dental papilla and follicle formation.

(A,B,C,E,F) Dental follicle mesenchyme in purple, dental papilla mesenchyme in blue. (A) A scheme, where the majority of the dental mesenchyme represents the dental papilla (characterized by *syndecan-1* expression) and the follicle mesenchyme constitutes from only a small population of cells lining the enamel organ and presumptive dental papilla (bite-it.helsinki.fi; Aberg et al. 2004; Tucker and Sharpe 2004; Takatalo et al. 2009). (B) A scheme, where the dental papilla cells are defined to a smaller population of cells of the dental mesenchyme (Cho and Garant 2000) and which area is characterized by *Fgf3* expression (Klein et al. 2006) or by *Dlx2* expression (Zhao et al. 2000). (C) A scheme, where the dental papilla cells are limited to the region of dental mesenchyme in between cervical loops (Kim et al. 2007), which is characterized by *Spry4* expression (Klein et al. 2006). (D) Histological section of E14.5 molar tooth germ

at cap stage. Already at this stage, there are distinguishable 3 layers of dental mesenchyme separating dental papilla and follicle (black lines), with higher magnification for better resolution of the layers. **(E)** Our present concept of dental papilla origin. The dental papilla comprises only a limited mesenchymal cell population located next to the IDE in between the cervical loops (in blue). The rest of the dental mesenchyme forms the dental follicle with 2 layers distinguishable at the cap stage (in purple). These outer layers of the dental follicle region contain mesodermally derived endothelial cells (Rothova et al., 2011). **(F)** A model of a bell staged dental papilla where the blue mesenchymal papilla cells have filled up the space in between the cervical loops and the mesodermally derived endothelial cells immigrate into this region. Purple mesenchymal follicle cells spread around the enamel organ with some dental papilla cells from the cap staged tooth germ (*) contributing to the inner layer of the dental follicle (*).

Fig. 1

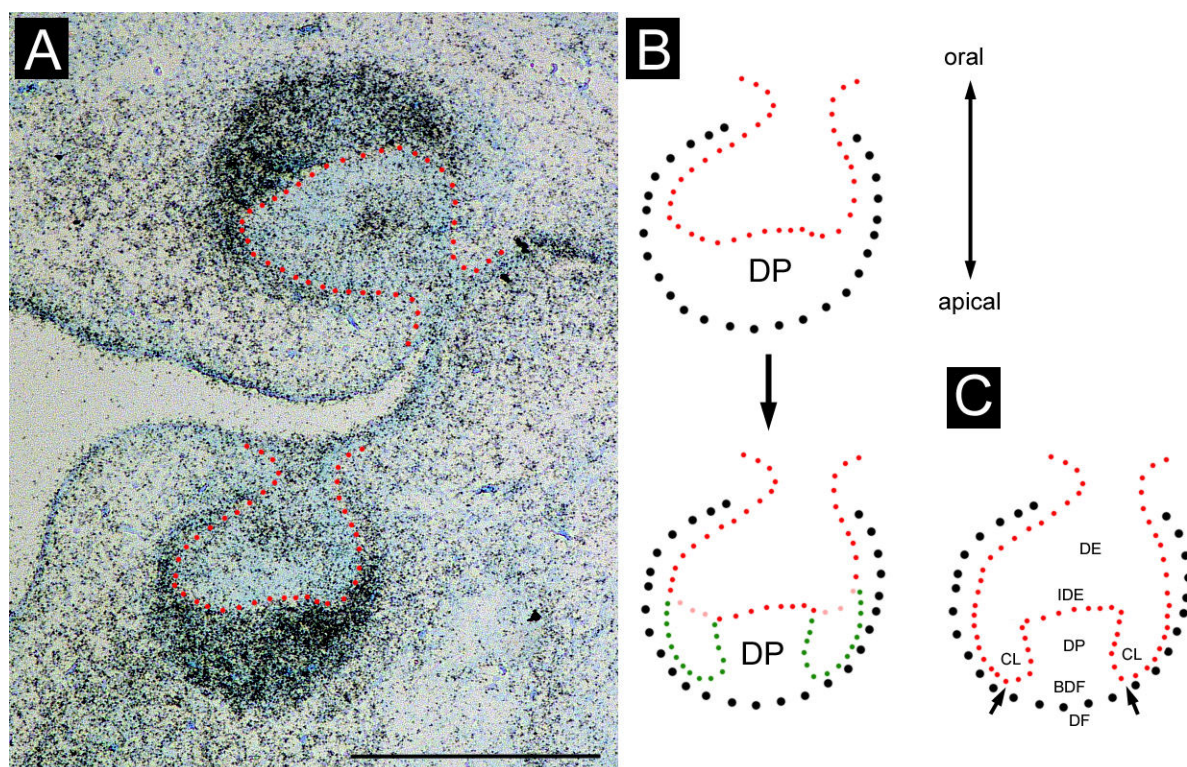


Fig. 2

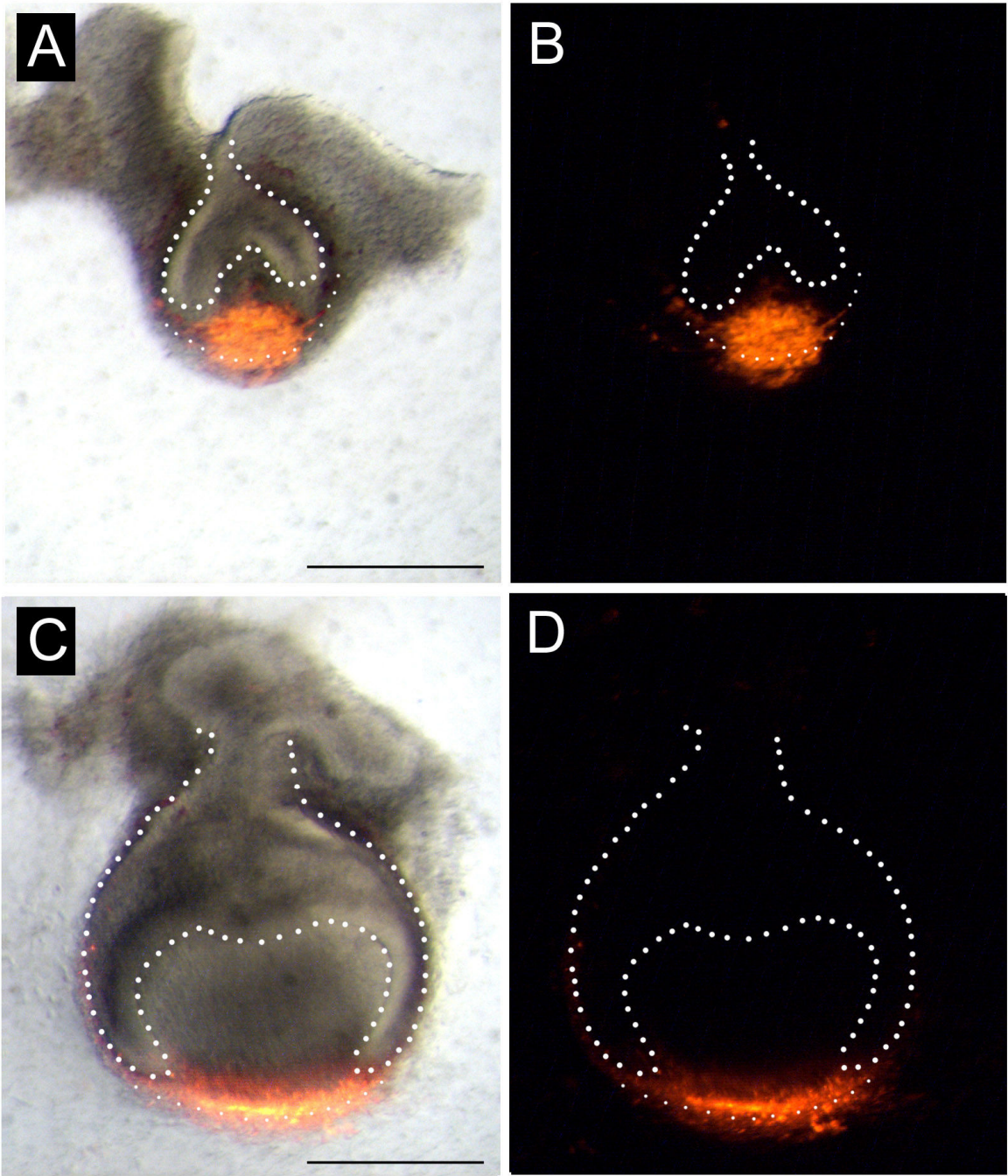


Fig. 3

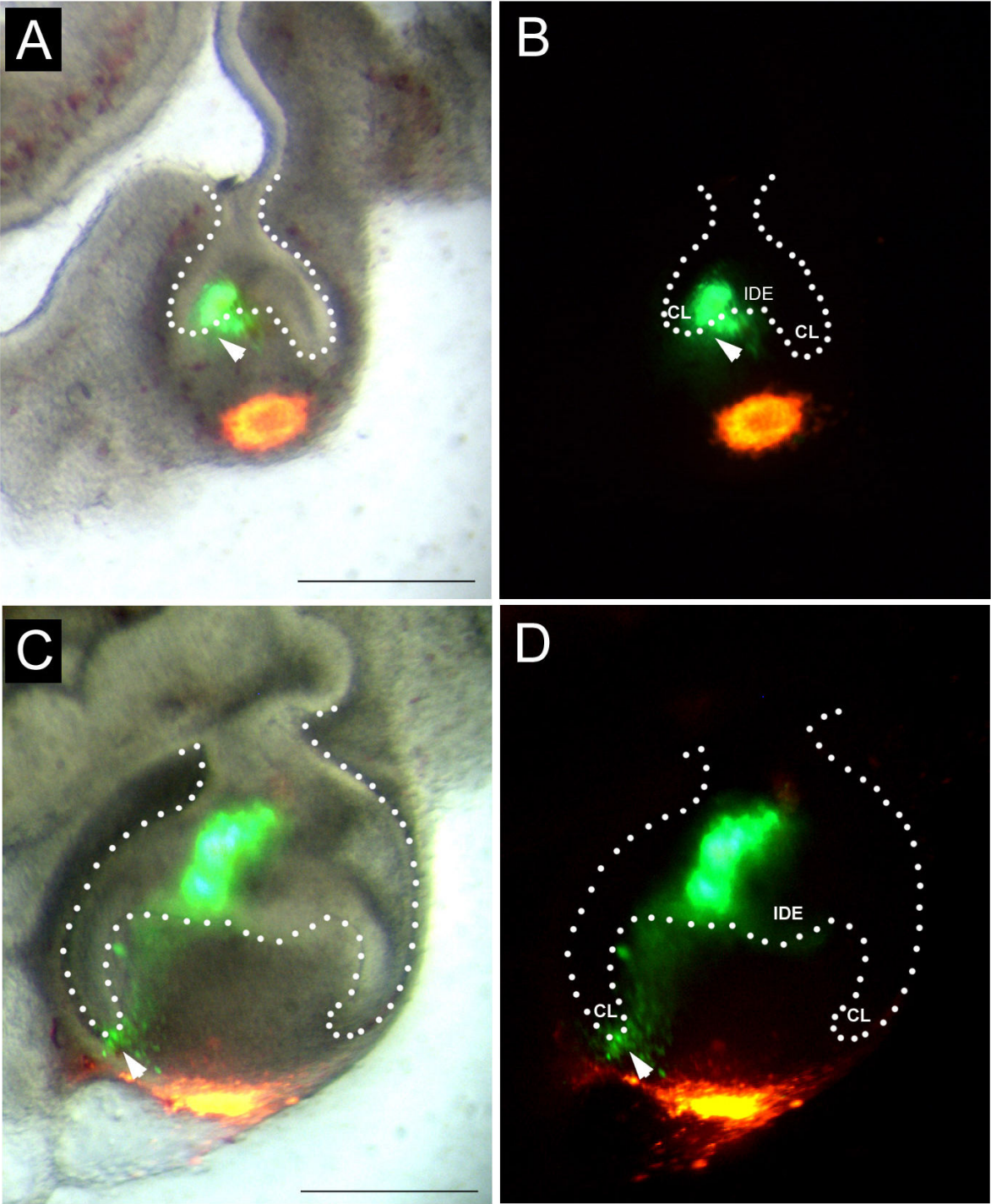


Fig. 4

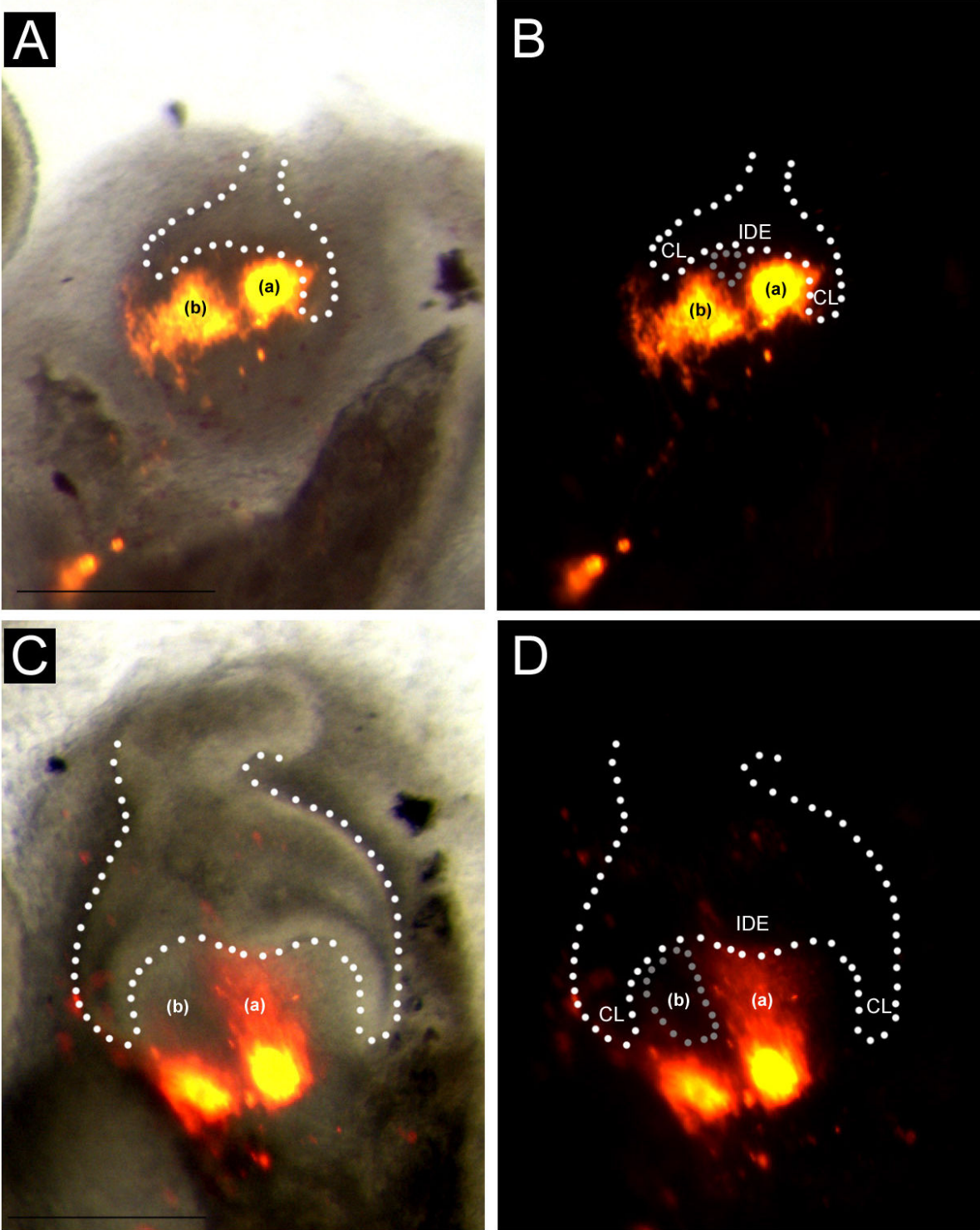


Fig. 5

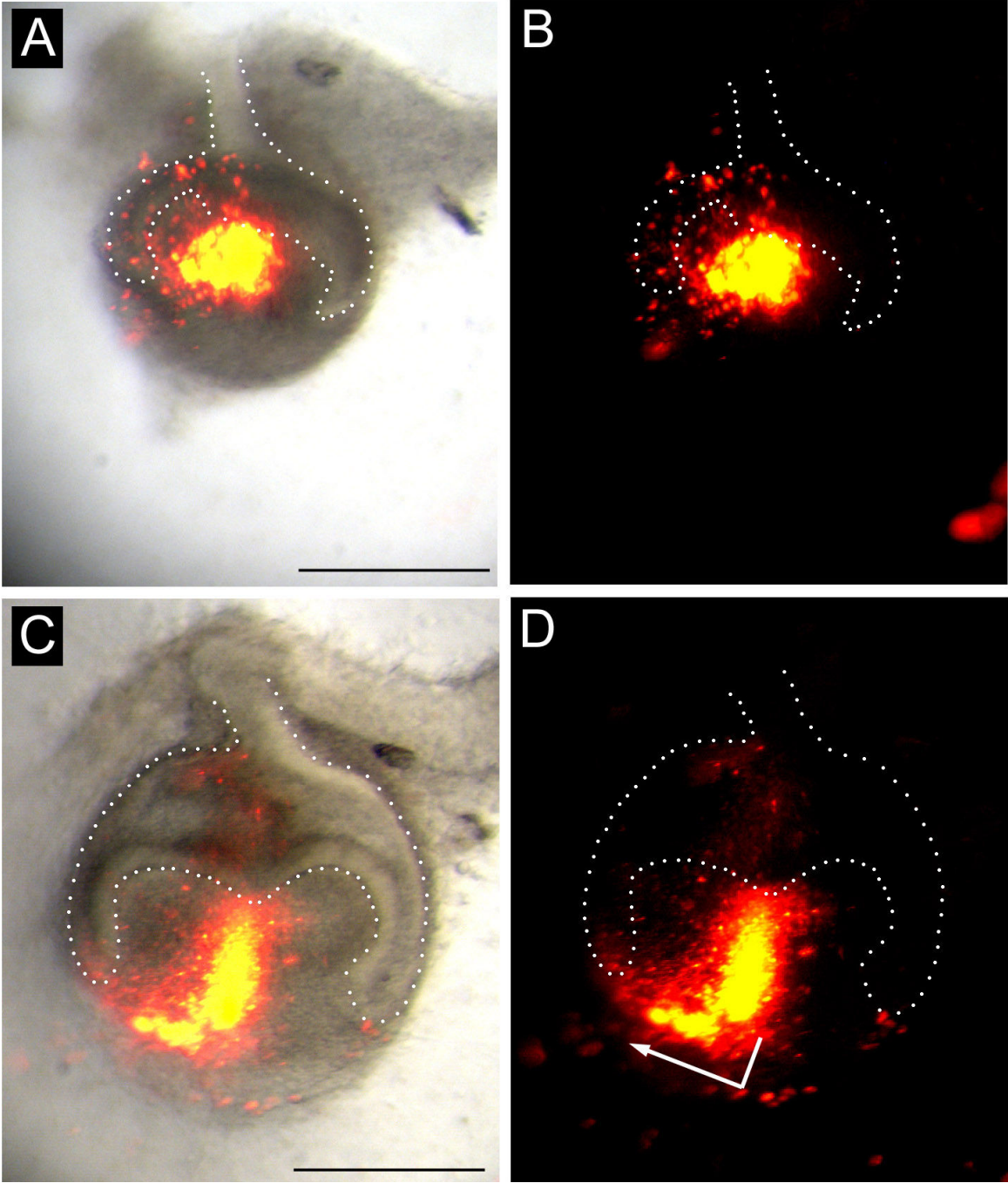


Fig. 6

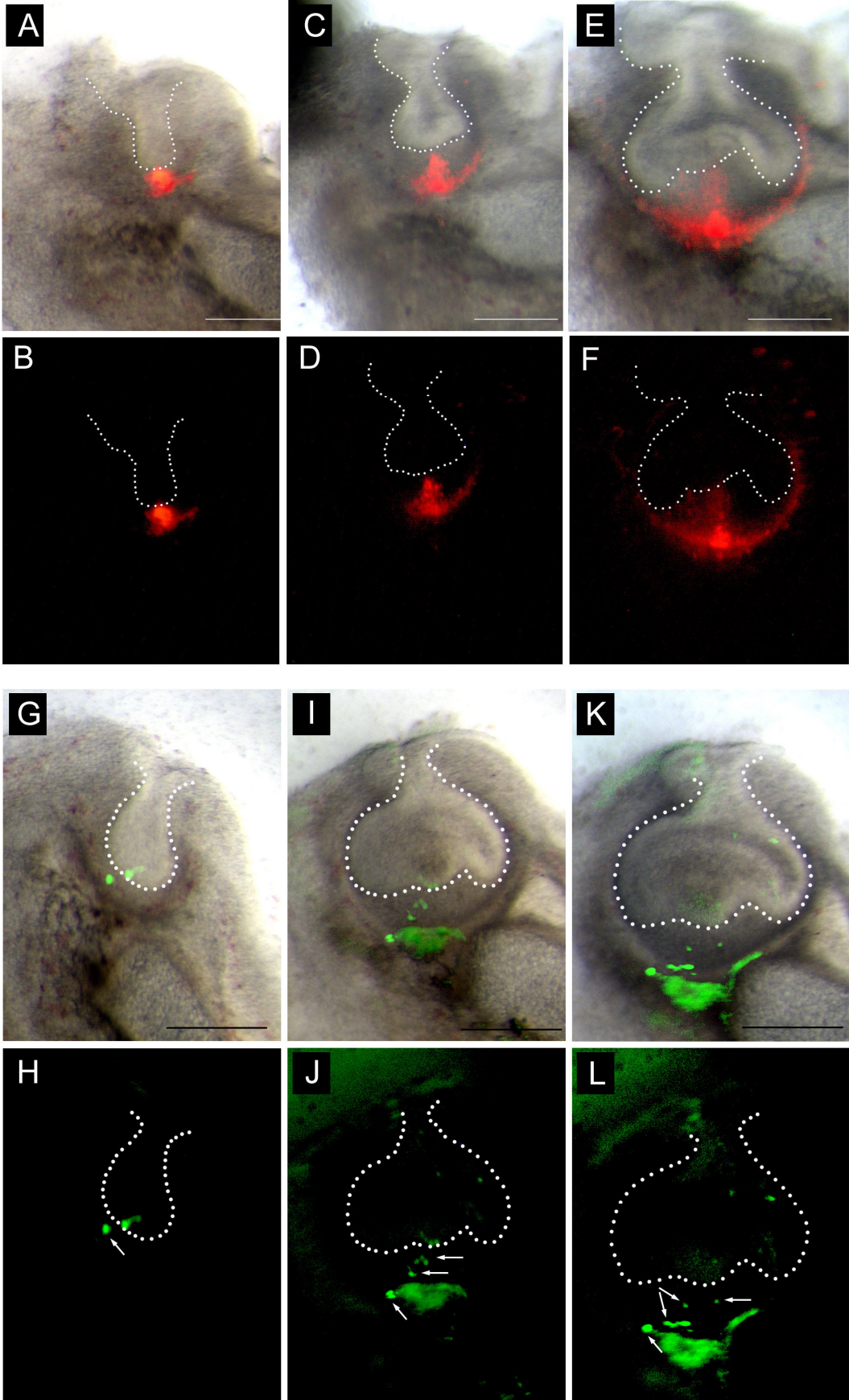


Fig. 7

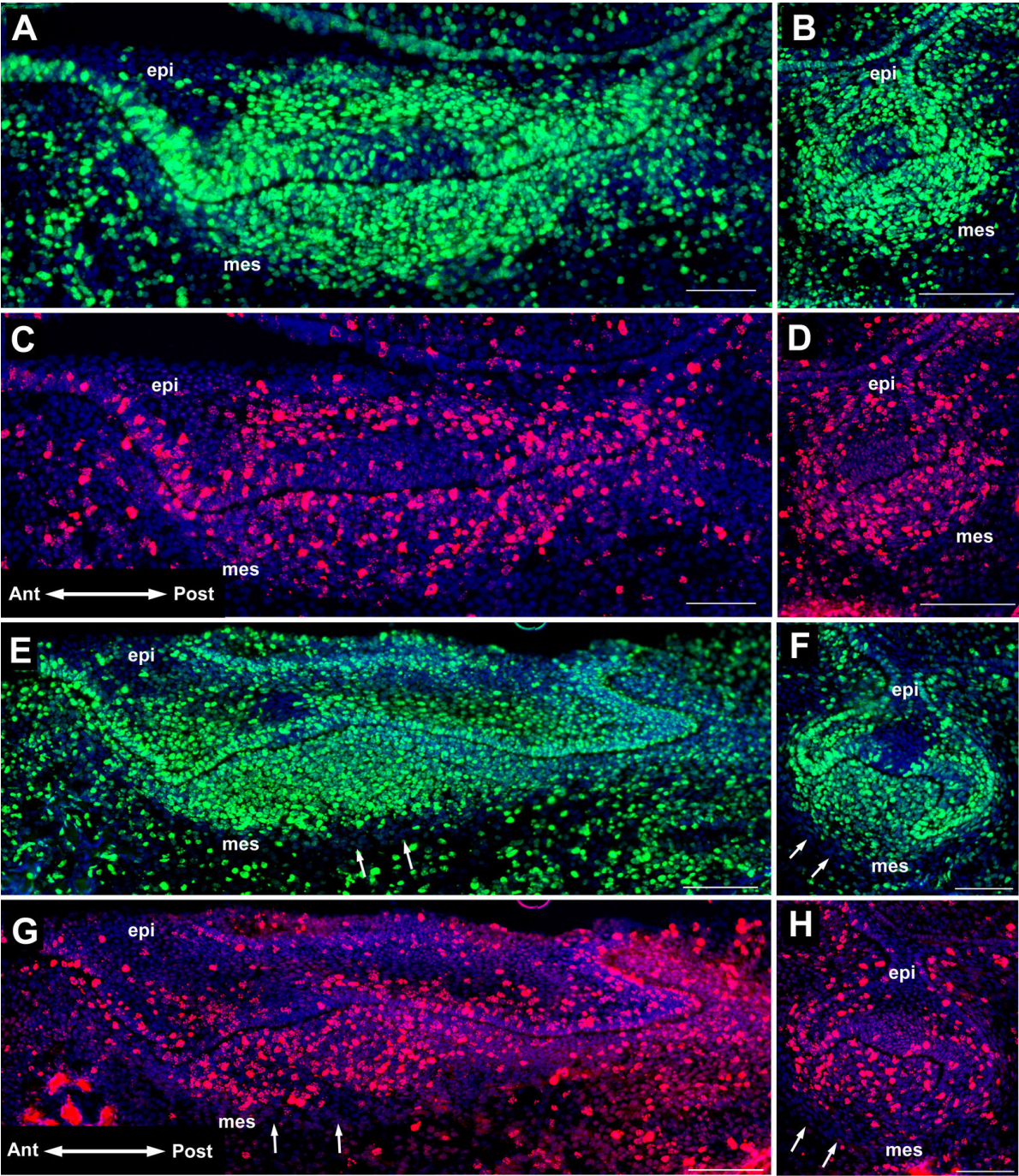


Fig. 8

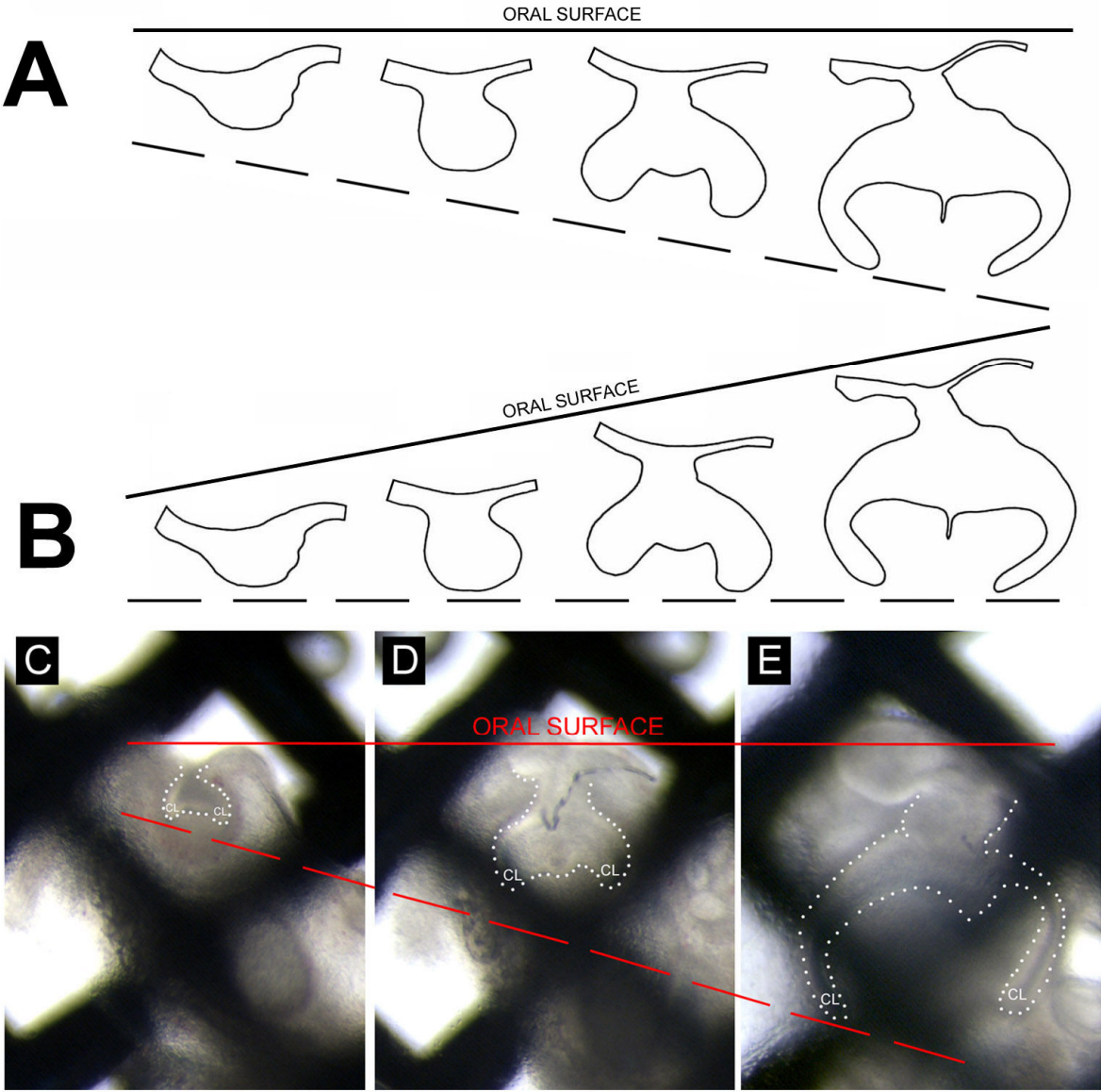
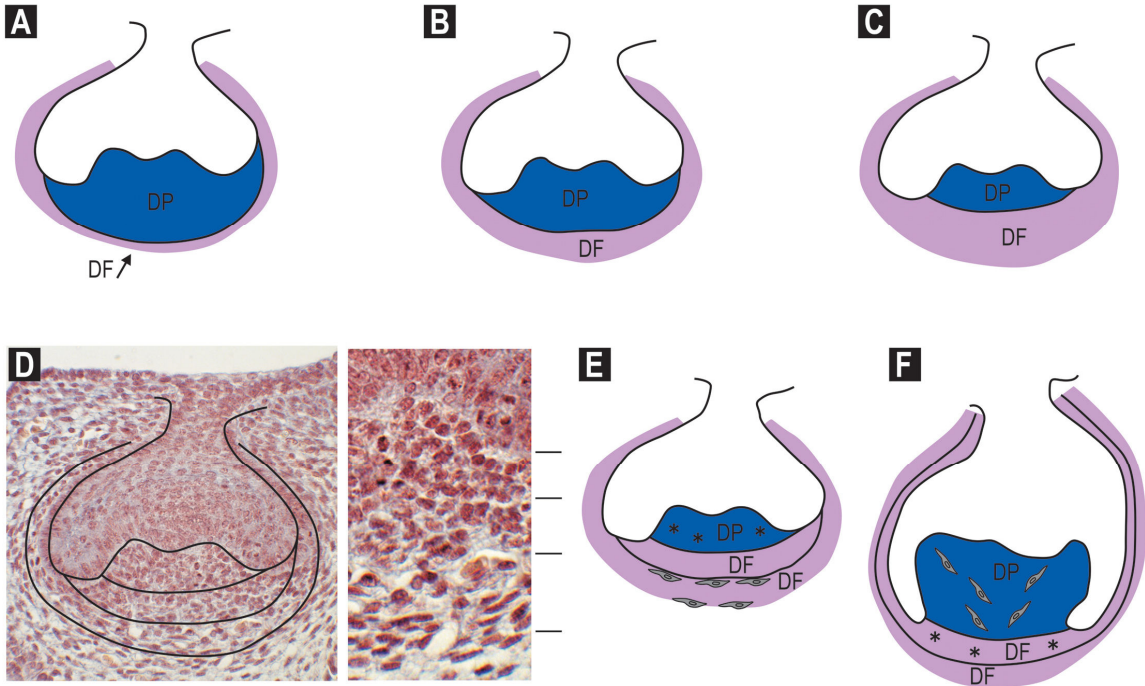
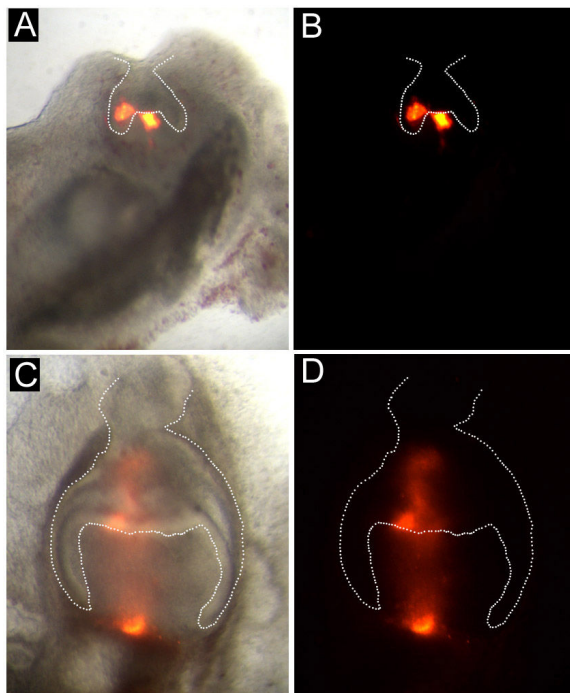


Fig. 9



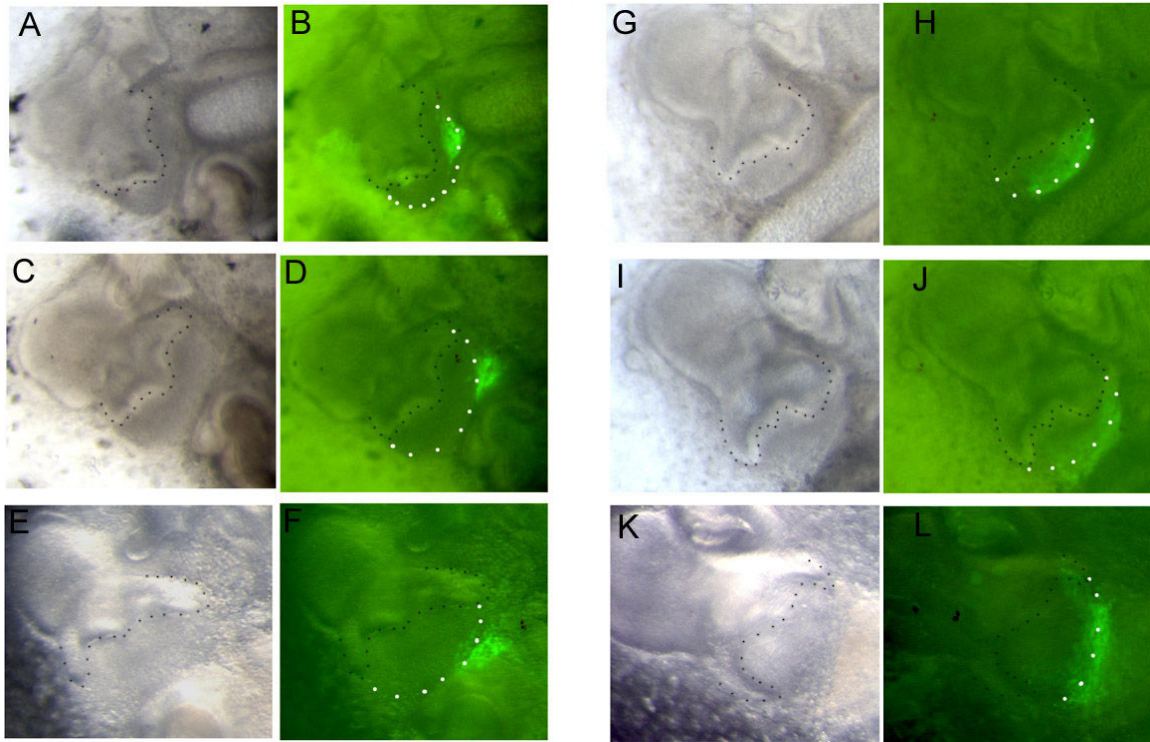
SUPPLEMENTARY DATA



Suppl. Fig. 1: The central part of dental papilla cells under the IDE form a band of cells filling the dental papilla.

(A) A sliced mouse mandible containing a tooth germ at the early cap stage, E14.5. At day0 there DiI labelled (red) epithelial cells in the IDE layer and mesenchymal cells in the middle proportion of the dental papilla by the IDE. (B) Outline of the same molar tooth germ under dark field. (C) After 2 days of *in vitro* culture, the labelled mesenchymal cells form a band of red DiI labelled cells in the centre of the dental papilla. A stronger labelled area of cells was separated from the epithelium and shifted towards the apical part of the forming dental follicle at the base of the dental papilla. The labelled epithelial cells spread within the enamel organ. (D) Outline of the same molar tooth germ under dark field.

The dental epithelium is highlighted with a white dotted line.



Suppl. Fig. 2: Grafting of GFP mesenchyme into a WT tooth slice to fate map the condensed dental mesenchyme at the cap stage.

GFP positive dental mesenchyme was grafted into CD1 sliced tooth germs into different regions of the CD1 condensed dental mesenchyme at E14.5

(A-F) GFP tissue grafted at the border of the condensing mesenchyme. **(A,C,E)** Light Field. **(B,D,F)** Combined light and dark field to visualize the GFP grafted tissue in green. **(A,B)** Day 0. **(C,D)** Day 1, **(E,F)** Day 3. The GFP labeled mesenchyme moves from the condensing mesenchyme to the edge of the forming dental papilla and ends up in the dental follicle at the apical end of the bell stage tooth germ.

(G-L) GFP tissue grafted within the condensing mesenchyme. **(G,I,K)** Light Field. **(H,J,L)** Combined light and dark field to visualize the GFP grafted tissue in green. **(G,H)** Day 0. **(I,J)** Day 1, **(K,L)** Day 3.

The GFP labeled mesenchyme moves from the condensing mesenchyme towards the edge of the forming dental papilla. In this case GFP cells from the graft are found both within the dental papilla at its most apical end, and in the adjacent dental follicle.